

UC San Diego

UC San Diego Electronic Theses and Dissertations

Title

Design Considerations for Seismically Isolated Structures under Extreme Loading

Permalink

<https://escholarship.org/uc/item/3n8468k8>

Author

Bustamante, Ricardo

Publication Date

2024

Peer reviewed|Thesis/dissertation

UNIVERSITY OF CALIFORNIA SAN DIEGO

DESIGN CONSIDERATIONS FOR SEISMICALLY ISOLATED STRUCTURES UNDER
EXTREME LOADING

A Dissertation submitted in partial satisfaction of the requirements
for the degree Doctor of Philosophy

in

Structural Engineering

by

Ricardo Bustamante

Committee in charge:

Professor Gilberto Mosqueda, Chair
Professor Kenneth J. Elwood
Professor Shabnam Jandaghi Semnani
Professor Peter M. Shearer
Professor Pui-Shum Benson Shing
Professor Georgios Tsampras

2024

Copyright

Ricardo Bustamante 2024

All rights reserved.

The Dissertation of Ricardo Bustamante is approved, and it is acceptable in quality and form for publication on microfilm and electronically.

University of California San Diego

2024

DEDICATION

To Valentina and Max

TABLE OF CONTENTS

DISSERTATION APPROVAL PAGE	iii
DEDICATION	iv
TABLE OF CONTENTS	v
LIST OF FIGURES	ix
LIST OF TABLES	xii
ACKNOWLEDGEMENTS	xiii
VITA.....	xv
ABSTRACT OF THE DISSERTATION.....	xvii
Chapter 1 INTRODUCTION	1
General	1
Research Objective and Scope	3
Overview of Dissertation.....	3
Chapter 2 SIMPLIFIED MODEL TO CHARACTERIZE SUPERSTRUCTURE RESPONSE FOR BEYOND DESIGN LOADING OF BASE-ISOLATION SYSTEM.....	6
Abstract.....	6
Introduction	7
Seismic Hazard and Ground Motions.....	10
Structural Models: full model and 2DOF.....	11
Full prototype model.....	11
2DOF model	13
Structural capacity	14
Limitations on the 2DOF model.....	15
Results	18
Quantification of higher mode contributions	23
Moat wall pounding.....	26

Impact velocity dependency on pounding effects	29
Discussion.....	32
Conclusions	33
Acknowledgements.....	35
Chapter 3 EVALUATION OF BASE-ISOLATED ARCHETYPES BUILDINGS UNDER BEYOND DESIGN LOADING.....	37
Abstract.....	37
Introduction	37
Analysis Model.....	39
Isolation System Level	39
Superstructure characterization	39
Seismic Hazard and Incremental Dynamic Analysis.....	43
Incremental Dynamic Analysis	44
Backbone curve parametric analysis	46
Moat wall pounding.....	52
Conclusions	55
Acknowledgements.....	56
Chapter 4 EVALUATION OF SEISMIC ISOLATION RETROFIT FOLLOWING EARLY DESIGN STANDARDS: A CASE STUDY	58
Abstract.....	58
Introduction	58
Evolving standards for seismic isolation.....	60
Description of Building	63
Development of simplified models	65
Model of seismic isolation system.....	65
6DOF model of superstructure	66

Reduction to 2DOF model.....	68
Performance Evaluation	69
Simplified models.....	69
Comparison of the 2DOF model with the full 6DOF model.....	71
Feasible Domain Analysis for the 6DOF Model.....	74
Moat wall pounding.....	76
Consideration of property modification factors.....	77
Influence of the tower on the feasible domain.....	80
Supplemental damping	81
Conclusions	85
Acknowledgements.....	87
Chapter 5 ENHANCED SEISMIC PROTECTION SYSTEM FOR AN EMERGENCY DIESEL GENERATOR UNIT.....	88
Abstract.....	88
Introduction	88
Seismic hazard and expected seismic performance.....	91
Results	99
Response for target seismic hazard intensity.....	100
Scaled ground motion records	103
Incremental Dynamic Analysis.....	105
Fragility Curves	107
Discussion.....	112
Conclusions	113
Acknowledgements.....	114
Chapter 6 SUMMARY AND CONCLUSIONS	115
Summary.....	115

Discussion of Results	118
Limitations and future research work.....	121
REFERENCES	123

LIST OF FIGURES

Figure 2.1: Target response spectra and ground motions	11
Figure 2.2: Numerical model of the reference building	12
Figure 2.3: Simplified 2DOF model.....	13
Figure 2.4: Static Pushover curves comparison	14
Figure 2.5: Periods and mode shapes comparison between models.....	16
Figure 2.6: Seismic Isolation Theory (a) Linear elastic range (b) Isolation system yielded with linear superstructure (c) Yielding of both DOFs	17
Figure 2.7: Comparison of the isolation system lateral displacement (a) beyond-design intensity (b) IDA analysis.....	20
Figure 2.8: Comparison of the Superstructure Base Shear (a) beyond design intensity (b) IDA analysis	21
Figure 2.9: Comparison of the superstructure drift (a) beyond-design intensity (b) IDA analysis	22
Figure 2.10: Comparison of the acceleration superstructure drift (a) beyond-design intensity (b) IDA analysis	23
Figure 2.11: Acceleration Time Histories for (a) Record 3 (b) Record 7	24
Figure 2.12: Spectrogram for (a) Record 4 (b) Record 7	25
Figure 2.13: Maximum roof acceleration for the 2DOF model, full model, and full model filtered signal.	26
Figure 2.14: a) IDR with pounding model comparison b) Superstructure drift with pounding model comparison	27
Figure 2.15: IDR profile per record without (dashed line) and with (solid line) pounding effects.	28
Figure 2.16: IDR amplification factor over impact velocity	29
Figure 2.17: IDR dependency impact velocity for a) Story 1 with all records and b) all stories with average responses	30
Figure 2.18: IDR profile dependency on moat wall clearance	31
Figure 3.1: Normalized pushover comparison between all four models.....	42
Figure 3.2: Seismic hazard and scaled ground motions for base-isolated systems.	43
Figure 3.3: Incremental Dynamic Analysis results for all models	45
Figure 3.4: RCSW2 parametric analysis	48
Figure 3.5: SMF parametric analysis.....	49
Figure 3.6: RCSW1 parametric analysis	49
Figure 3.7: RCSW1 strength comparison.....	50

Figure 3.8: SCBF parametric analysis	51
Figure 3.9: Moat wall pounding analysis for a) RCSW1 b) RCSW2 c) SCBF d) SMF	53
Figure 3.10: Seismic assessment with and without moat wall pounding for different superstructure strengths	54
Figure 4.1: Isometric view of full building model	64
Figure 4.2: Models for the isolation level	65
Figure 4.3: Backbone curves for (a) shear walls (b) frames.....	67
Figure 4.4: 6DOF model.....	67
Figure 4.5: Superstructure capacity estimation: computed, bilinear, degrading	68
Figure 4.6: Model Comparison Utilizing Isolation System Lower Bound Properties with BSE- 1E and BSE-2E Hazard using Lower Bound Properties	70
Figure 4.7: Isolation system lateral displacement using 6DOF and 2DOF model.....	72
Figure 4.8: Interstory Drift using 6DOF and 2DOF model.....	73
Figure 4.9: Superstructure shear coefficient using 6DOF and 2DOF model	74
Figure 4.10: Feasible domain surface per EDP (a) Isolation System Lateral Displacement (b) Tower Drift.....	75
Figure 4.11: Design feasible domain for isolation system nominal properties	76
Figure 4.12: Design feasible domain for isolation system nominal properties	77
Figure 4.13: Feasible domain design for the isolation system using lower and upper bound properties considering IDR at various levels.....	78
Figure 4.14: Feasible domain per EDP (a) moat wall clearance (b) IDR Stories 1 & 3 (c) IDR Story 2 (d) IDR Tower and (e) overall feasible domain.....	79
Figure 4.15: Feasible domain design assuming a linear Tower for (a) Story 1 (b) Story 2 (c) Story 3 and (d) Tower.....	80
Figure 4.16: Feasible domain with superstructure as is adding viscous damping a) 5% b) 10% c) 15% d) 20%	82
Figure 4.17: Feasible domain with linear tower adding viscous damping for a) 5% b) 10% c) 15% d) 20%	83
Figure 4.18: Feasible domain for a) superstructure with nonlinear tower, b) superstructure with the linear tower.....	84
Figure 4.19: Effective damping using Lower Bound Properties with and without adding viscous damping for a) superstructure with nonlinear tower, b) superstructure with a linear tower	85
Figure 5.1: Ground motion pseudo spectral acceleration.....	91
Figure 5.2: Proposed seismic protection configuration; (a) side elevation view; (b) front elevation view. Dimensions in millimeters	95

Figure 5.3: FEMA P-751 equivalent lateral force procedure results.....	97
Figure 5.4: Horizontal acceleration time history results for non-scaled Record 4 – Direction ‘X’ (a) Record and EDG response comparison (b) System response by isolation level.....	100
Figure 5.5: Vertical acceleration time history results for non-scaled Record 4 – Direction ‘Z’ (a) Record and EDG response comparison (b) System response by isolation level	101
Figure 5.6: Spectral acceleration results for non-scaled record 4 (a) horizontal direction ‘X’ (b) vertical direction ‘Z’	102
Figure 5.7: Horizontal acceleration time history results for the Record 4 with PGA = 0.925g – Direction ‘X’ (a) Record and EDG response comparison (b) System response by isolation level	103
Figure 5.8: Vertical acceleration time history results for the Record 4 with PGA = 0.925g – Direction ‘Z’ (a) Record and EDG response comparison (b) System response by isolation level	103
Figure 5.9: PSA results for scaled Record 4 (a) horizontal direction ‘X’ (b) vertical direction ‘Z’	104
Figure 5.10: Force-displacement hysteresis for the Scaled Record 4 (a) IsoV horizontal direction ‘X’ response (b) IsoV vertical direction ‘Z’ response (c) IsoH horizontal direction ‘X’ response (d) IsoH vertical direction ‘Z’ response.....	105
Figure 5.11: IDA for Lateral Displacement EDP.....	106
Figure 5.12: IDA for EDG Acceleration EDP.....	107
Figure 5.13: Fragility curve for (a) Pipeline LS1 (b) Bearing LS2 – LatDisp=320mm (c) Bearing LS3 – LatDisp=576mm	109
Figure 5.14: Fragility curve for EDG LS1 – Acc=0.40g.....	110
Figure 5.15: Fragility Curves results for both Limit States.....	111

LIST OF TABLES

Table 2.1: Superstructure backbone	14
Table 2.2: Peak roof acceleration values for Records 3 and 7	25
Table 3.1: PGAYield factors for different limit states	46
Table 4.1: Changes within the code over the years	61
Table 4.2: Property modification factors for an existing system.....	66
Table 5.1: Limit States and HCLPF values per EDP	93
Table 5.2: Frequencies dependent properties of both isolation levels.....	96
Table 5.3: Properties of LRB and resulting isolation system properties	97
Table 5.4: IsoV properties.....	99
Table 5.5: IDA results for the Lateral Displacement EDP	106
Table 5.6: IDA results for the EDG acceleration EDP	107

ACKNOWLEDGEMENTS

It would not have been possible without the unwavering support, patience, and encouragement of many individuals who have contributed to both my personal and academic life. Among these invaluable contributors, I reserve a unique, special gratitude to Valentina, whose role transcends the mere support expected from a partner.

This is a path I have not walked alone; the support, encouragement, and companionship of numerous friend, whose roles have been indispensable in both my academic and especially personal life throughout this journey: Koorosh, Rodrigo, Kayla, Lucho, Fito, Antonio, Allan, Mayorga, CSM, Cristian, Claudio, Rodolfo, Felipe, Eric, Cora, Bruno, Lindsay, Franco, Adrielly, Iza, Lucas, Rodrigo, Pastor, Ary, Carlos, among others.

I would like to acknowledge my mother, whose influence extends far beyond the confines of moral support. Her boundless optimism and unconditional love have provided me with a sanctuary of peace and positivity.

For my father, whose memory I hold dear. The pain of his loss was magnified by the circumstances that prevented me from being at his side to bid a final farewell.

A special acknowledgment is reserved for my son, Max, whose existence has been both a source of joy and a profound inspiration. The journey through doctoral research is often depicted as a solitary voyage, but Max's presence in my life has added a rich tapestry of motivation, perspective, and purpose to this endeavor.

I would like to acknowledge Professor Gilberto Mosqueda for his support and insight throughout my research journey. Beyond his professional excellence, I deeply appreciate his compassionate demeanor and genuine attentiveness to the personal concerns of his students, which have made my experience both enriching and rewarding.

Chapter 2 contains unpublished material coauthored with Elwood, Kenneth J. and Mosqueda, Gilberto. The dissertation author was the primary author of this chapter.

Chapter 3 contains unpublished material coauthored with Elwood, Kenneth J. and Mosqueda, Gilberto. The dissertation author was the primary author of this chapter.

Chapter 4 is currently being prepared for submission for publication, coauthored with Erler, Kayla; Sepulveda, Claudio; Mosqueda, Gilberto; Del Carpio, Maikol; Lopez, Joshua; and Elwood, Kenneth, J. The dissertation author was the primary researcher and author of this material.

Chapter 5, in full, is a reprint of the material as it appears in *Energies*, MDPI, 2022. The dissertation author was the primary investigator and author of this paper.

VITA

- 2009 Bachelor in Civil Engineering. Technical University Federico Santa Maria, Valparaiso, Chile
- 2010 Civil Engineer. Technical University Federico Santa Maria, Valparaiso, Chile
- 2010-2014 Design Engineer. Fluor, Santiago, Chile
- 2014-2017 Project Engineer. Ruben Boroschek and Associates, Santiago, Chile
- 2016 Master in Structural and Geotechnical Engineering. Pontifical Catholic University of Chile, Santiago, Chile
- 2020 Master of Science, University of California San Diego
- 2024 Doctor of Philosophy, University of California San Diego

PUBLICATIONS

Van Den Einde L, Conte JP, Restrepo JI, **Bustamante R**, Halvorson M, Hutchinson TC, Lai C-T, Lotfizadeh K, Luco JE, Morrison ML, Mosqueda G, Nemeth M, Ozelik O, Restrepo S, Rodriguez A, Shing PB, Thoen B, and Tsampras G (2021) NHERI@UC San Diego 6-DOF Large High-Performance Outdoor Shake Table Facility. *Front. Built Environ.* 6:580333. doi: 10.3389/fbuil.2020.580333

Bustamante R, Mosqueda G, Elwood K.J. (2021) Moat Wall Pounding Analysis for a Prototype Base-Isolated Building in Wellington New Zealand. *Struct. Eng. Soc. New Zeal.* 2021

Bustamante R, Mosqueda G, Kim M. (2022) Enhanced Seismic Protection System for an Emergency Diesel Generator Unit. *Energies.* 2022; 15(5):1728. <https://doi.org/10.3390/en15051728>

Bustamante R, Mosqueda G, Elwood K.J. (2022) Inelastic superstructure response of base-isolated systems using nonlinear response spectra under extreme loading. 12th National Conference on Earthquake Engineering - 12NCEE 2022, Utah, Salt Lake City.

Bustamante R, Mosqueda G, Elwood K.J. (2022) Moat wall pounding for a prototype base-isolated building in Wellington, New Zealand 12th National Conference on Earthquake Engineering - 12NCEE 2022, Utah, Salt Lake City.

Bustamante R, Erler K, Sepulveda C, Mosqueda G, Del Carpio M, Hershberg M, Lopez J, Elwood K J. (2022) Evaluation of Seismically Isolated Structures Designed to Early Standards

Sepulveda C, **Bustamante R**, Mosqueda G (2022) Seismic Performance of Isolated Bridges under Extreme Shaking. XVII Anti-Seismic Systems International Society Conference

Bustamante R, Mosqueda G (2022) Seismic Isolation of an Emergency Diesel Generator System for Nuclear Power Plants, SMiRT-26 Conference, Berlin, Germany

Sepulveda C, **Bustamante R**, Mosqueda G (2024) Performance of Seismically Isolated Bridge Considering Abutment Pounding. 18th World Conference on Earthquake Engineering, Milan, Italy

Kwon, T.H, Erler, K, **Bustamante R**, Mosqueda G (2024) Seismic Protection of Electric Cabinets in Nuclear Facilities. 18th World Conference on Earthquake Engineering, Milan, Italy

Bustamante R, Erler K, Sepulveda C, Mosqueda G, Del Carpio M, Lopez J, Elwood K J. (2024) Evaluation of Seismic Isolation Retrofit Following Early Design Standards. 18th World Conference on Earthquake Engineering, Milan, Italy

FIELD OF STUDY

Major Field: Structural Engineering

Studies in Seismically Isolated Buildings under Extreme Loading Events

Professor Gilberto Mosqueda

ABSTRACT OF THE DISSERTATION

DESIGN CONSIDERATIONS FOR SEISMICALLY ISOLATED STRUCTURES UNDER
EXTREME LOADING

by

Ricardo Bustamante

Doctor of Philosophy in Structural Engineering

University of California San Diego, 2024

Professor Gilberto Mosqueda, Chair

Seismic isolation is an established effective strategy to protect building structures from earthquake-induced damage by reducing accelerations and drifts within the superstructure. Current design codes primarily focus on ensuring operational resilience under design-level earthquakes with the building structure designed to remain essentially elastic. However, there is limited guidance for assessing the nonlinear behavior of the superstructure for beyond-design seismic events, which can be of concern since the structural performance can degrade rapidly

from this point. This research investigates the performance of seismically isolated structures under extreme loading conditions, with emphasis on the response of the superstructure. The motivation for this research is to expand rapid assessment tool for the seismic performance evaluation of seismically isolated buildings. This expansion aims to enhance the understanding of limit state behaviors for beyond-design basis events.

Utilizing a two-degree-of-freedom (2DOF) model, this study explores the dynamic interactions between the isolation system and the superstructure, highlighting the limitations and reliability of simplified models compared to full nonlinear analyses. Through Incremental Dynamic Analysis (IDA), the study evaluates various archetype buildings with different lateral force-resisting systems, examining the effects of parameters such as yield strength, ductility capacity, strength degradation, and moat wall pounding on the overall performance. The results indicate that while 2DOF models can provide a rapid assessment of the isolation system lateral displacements and superstructure drifts, they tend to underestimate roof accelerations and overestimate interstory drifts. Furthermore, the occurrence of moat wall impacts is shown to significantly affect the structural response, emphasizing the critical need for design strategies that mitigate or avoid such impacts. The research contributes to the broader understanding of seismic isolation, offering valuable insights into the performance of isolation systems under extreme seismic loading conditions.

Chapter 1 INTRODUCTION

General

Over the past four decades, seismic design guidelines have evolved, leading to a significant increase in the required displacement capacity for base isolation systems [1]. A review of seismic isolation applications reveals that modern buildings are designed to accommodate larger displacement capacities [2], reflecting an enhanced understanding of seismic hazards and structural behavior. Consequently, the existing building stock of isolated structures exhibits varying levels of displacement capacity, with some potentially yielding during severe seismic events. Additionally, under beyond-design-basis seismic events, moat wall pounding becomes a significant concern if the displacements from analysis exceed the moat wall clearance [3].

The design criteria for base-isolated structures aim to achieve functional recovery by ensuring an essentially elastic performance of the superstructure during seismic events [1]. However, under beyond-design-basis seismic events, the superstructure could yield due to increased base shear transmitted through the isolation level. While most current code standards for base isolation effectively safeguard the superstructure under design-level events, they do not contain explicit provisions for limit states beyond the design basis. The inaugural version of New Zealand Guideline for the Design of Seismic Isolation Systems for Buildings [4] addresses the potential nonlinear response of the superstructure by providing guidelines to evaluate and limit this response. Additionally, this design code requires estimating the potential for moat wall pounding and including contact elements around the perimeter of the isolation plane to capture the effects when pounding is expected.

Extensive research has been conducted on the inelastic behavior of base-isolated structures using reduced-order models, such as the simplified two-degree-of-freedom (2DOF) model [5–11]. However, these studies often characterize the inelastic response of the superstructure using a bilinear model with unlimited deformation capacity. Furthermore, the 2DOF results have not been compared with comprehensive nonlinear models of yielding superstructures. The validity of the 2DOF model results is crucial for its adoption in common practice, especially when addressing extreme seismic events.

These reduced-order models offer a promising approach for rapid assessment of the isolation system and the superstructure behavior. For design practitioners, the 2DOF model is particularly beneficial due to its ability to streamline the design process, allowing engineers to quickly explore various scenarios without the extensive computational resources required for more detailed models. In contrast, a full nonlinear superstructure model, while providing a more comprehensive analysis, demands significant effort, time, and cost. The complexity and resource intensity of these detailed models make them less feasible for preliminary design stages or iterative design checks.

This dissertation aims to provide a comprehensive analysis of the 2DOF model capabilities to capture the nonlinear behavior of the superstructure, ensuring it can serve as a robust tool for the seismic assessment of base-isolated structures. The findings of this research do not include the wall flexibility and soil models to characterize their influence on the superstructure response, while assuming a simplified bearing models. Future work should incorporate more detailed bearing models that can simulate a wider range of failure mechanisms.

Research Objective and Scope

The goal of this study is to provide a comprehensive investigation of the performance of seismically isolated structures under extreme loading conditions. Specifically, the main objective of this research includes the evaluation and validation of simplified two-degree-of-freedom (2DOF) models in predicting the dynamic response of isolated structures under beyond design loads using parameters such as isolation system lateral displacement, the superstructure interstory and roof drifts, and roof accelerations.

The specific objectives of this research are:

- Investigate moat wall pounding effects on the superstructure response. Quantify how varying moat wall clearance and superstructure parameters influence the response under impacts.
- Application to a case study, where an isolated building designed using early design standards requires to be retrofitted, with a non-ductile superstructure and insufficient moat wall clearance.
- Design a customizable seismic protection system for an Emergency Diesel Generator (EDG) located at a Nuclear Power Plant using existing seismic isolation devices.

Overview of Dissertation

This work has been divided into four chapters with the following content:

Chapter 2 explores the effectiveness and limitations of the simplified 2DOF model in assessing the seismic response of a base-isolated building under beyond design basis seismic events. The chapter describes the development and analysis of a full nonlinear base-isolated frame model, which is analyzed in parallel with the 2DOF model. The performance between both models is evaluated using an Incremental Dynamic Analysis (IDA) under increasing seismic

intensities and moat wall pounding. This chapter suggests that while simplified models are useful for initial assessments, they must be carefully validated against more detailed models to ensure accuracy in engineering applications.

Chapter 3 discusses a simplified model to characterize superstructure responses beyond design demands on base-isolated systems. It presents a two-degree-of-freedom (2DOF) model to capture the dynamic interaction between the superstructure and the isolation system, emphasizing the impact of beyond-design seismic events that challenge the conventional design limitations. The chapter evaluates the performance of four superstructure archetypes under extreme seismic events, analyzing the importance of the superstructure deformation capacity to achieve a resilient performance.

Chapter 4 presents a case study on seismic isolation retrofit following early design standards. An evaluation of a building retrofitted with base isolation in the early 1990s is conducted, analyzing the performance of the existing isolation system against current standards. Through model comparisons and performance evaluations, the chapter emphasizes the critical balance required in retrofitting existing structures to ensure effective seismic isolation while achieving a desired performance objective.

Chapter 5 focuses on enhancing seismic protection systems for an Emergency Diesel Generator unit. This chapter examines the application of seismic isolation technologies to critical infrastructure components, evaluating their performance through Incremental Dynamic Analysis and fragility curves. The research underscores the role of tailored seismic isolation strategies in safeguarding essential services during earthquakes, using existing and proven technology.

Chapter 6 provides insights on how the dissertation results could assist designers and practitioners to approach how base isolated structures could include the influence of

superstructure yielding, moat wall impact or bearing capacity into their seismic assessment evaluation.

Finally, Chapter 7 summarizes the main contribution and findings of this study.

Conclusions and recommendations for future work is shown herein

Together, these chapters contribute to the broader understanding of seismic isolation as a robust strategy for enhancing the earthquake resilience of structures under extreme loading conditions.

Chapter 2 SIMPLIFIED MODEL TO CHARACTERIZE SUPERSTRUCTURE RESPONSE FOR BEYOND DESIGN LOADING OF BASE-ISOLATION SYSTEM

Abstract

Base isolation has been shown to be an effective seismic protection strategy for buildings. Accelerations and drifts in the superstructure can be reduced; therefore, increased protection is achieved for structural and nonstructural elements. Code criteria for base isolation design produces a structure with enhanced functional recovery by stipulating an essentially elastic performance of the superstructure through design-level considerations. As base isolation code standards are not geared towards assessing nonlinear behavior of the superstructure, explicit provisions are not provided for limit states of beyond design basis seismic events. These rare events can trigger an inelastic response in the superstructure from increased base shear in the isolation level. Reduced order nonlinear analysis models are desirable to inform a rapid assessment with increased detail over a prescriptive procedure found in code standards. A reduced order model prominently used for isolation studies is a simplified 2-degree-of-freedom (2DOF) system. To investigate the reliability and limitations of this model under beyond design events, a full nonlinear base-isolated frame model is developed and analyzed in parallel. An Incremental Dynamic Analysis (IDA) is conducted to compare predictions under increasing seismic intensities. A case in which the presence of a moat wall induces pounding is considered. This study indicates that a 2DOF model can be a useful rapid assessment analysis tool for isolated structures subject to beyond-design basis events with several key limitations. The 2DOF model is shown to provide a reliable estimate of the isolation system lateral displacement and superstructure drift through yielding of the superstructure. Inadequacies in the estimation of the simplified system are noted, including underestimation in roof acceleration and overestimation of roof drift, and a conservative estimate of conditions when moat wall pounding occurs.

Introduction

Base isolation is a verified approach to reduce the seismic response of building structures, showing significant advantages when compared to fixed-base structures. For seismic isolation to function effectively, the superstructure must be designed with sufficient stiffness and strength to limit deformation and remain essentially elastic. The superstructure performance comes at the expense of large deformation demands on the bearing devices. The required displacement capacity for the isolation system is a key design parameter that has notably increased with evolving seismic design guidelines. A review of applications of seismic isolation over the last four decades showed more modern buildings being designed for a larger displacement capacity [2]. Consequently, the current building stock of isolated buildings has varying levels of displacement capacities with different limit-state exceedance levels, potentially reaching beyond-elastic superstructure behavior.

This inelastic behavior in base-isolated structures has been the subject of extensive research using simplified 2-degree-of-freedom (2DOF) models [6–9,11,29]. These studies have defined critical design parameters influencing the performance and design of base-isolated structures. Kikuchi et al. [6] conducted a comprehensive study of the inelastic behavior of superstructures on isolation systems using a 2DOF model. They found notable differences in the effect of stiffness deterioration on the nonlinear response between fixed-base and isolated structures, with self-propagating damage in base-isolated structures resulting in larger deformations. Vassiliou et al. [8] extended the analysis of 2DOF models to examine the dynamic response of inelastic structures under pulse ground motions. The study highlights the relationship between yield strength, displacement ductility demand, and the fundamental vibration period of the structure. They show that for a relatively stiff seismically isolated structure designed to yield under the expected seismic base shear, the displacement ductility demand increases quickly as

the yield strength decreases (while maintaining the same period) and as the stiffness increases (while maintaining the same yield strength). Building upon Vassiliou et al., Tsiavos et al. [16] expanded the study to include unidirectional ground motions, emphasizing the large ductility experienced by inelastic base-isolated structures compared to a fixed-base structures designed using the same strength reduction factor. They concluded that the strength of the isolation system is a critical factor affecting the inelastic behavior. The study shows that weaker isolation systems may activate early in an earthquake, leading to larger but safer inelastic deformations that help dissipate energy. In contrast, stronger isolation systems may activate later, exposing the superstructure to higher forces before effectively reducing them. These studies, however, did not provide information on how the inelastic superstructure behavior of the superstructure was characterized nor did they compare the inelastic response to a detailed non-linear model of a yielding superstructure. The extent of validity for the 2DOF model results is a critical factor for its use in common practice.

Extending beyond the simplified 2DOF system, studies on detailed building models have provided similar trends on the superstructure nonlinear behavior [6]. Recent investigations by Kitayama and Constantinou [26] on a 6-story archetypical steel building indicate that base-isolated buildings designed by the minimum criteria of ASCE7-10 [30] or 16 [31] may not have an adequate probability of collapse under Maximum Considered Earthquake (MCE) shaking. They show that to improve the collapse performance, a Response Modification Factor (R_1) equal to 1.0 for the design response spectrum is needed, increasing the strength of the superstructure, and delaying the inelastic action. While previous research has explored the performance of detailed seismically isolated superstructures and simplified models separately, the comparison of two equivalent models under extreme seismic conditions has not been fully explored. This gap

provides a strong basis for this paper, which uses a comprehensive detailed model (referred to as the full model) and reduces this to an equivalent single-degree-of-freedom (SDOF) system for inclusion in a 2DOF model. The resulting analysis is compared to evaluate differences and comment on practical use.

This study considers two scenarios: the first with sufficient moat wall clearance, such that the increased base shear at large isolator displacements could yield the superstructure. Yielding of the superstructure reduces the effectiveness of the isolation system, while transferring large forces to the superstructure. Kikuchi et al [6] showed that once the building yields, damage self-propagates and leads to large inelastic demands. As design standards specify essentially elastic performance of the superstructure for isolated buildings, nonlinear behavior is not generally considered and is understood in a limited capacity.

The second scenario considers the provision of an insufficient moat wall clearance and subsequent pounding and transfer of impact forces into the base-isolated system. Depending on the impact velocity, pounding could further increase the ductility demand on the superstructure, for which the superstructure stiffness and ductility demand play a critical role [8]. Thiravechyan et al. [7] investigated the effects of yielding on base isolated buildings, focusing on the strength of the superstructure and the moat wall clearance under MCE and DBE level ground motions. Their findings suggest that adjusting the superstructure strength and clearance can mitigate ductility demands or reduce the possibility of pounding. Design codes for new buildings prescribe a required clearance to avoid pounding, while for existing buildings subjected to beyond-basis events, adjusting the clearance or the superstructure strength might not be feasible. Although the matter of inelastic actions in base-isolated structures has been explored through full models and two degrees of freedom models, this paper aims to concurrently address these

aspects by comparing the capability of reduced order models to characterize the inelastic actions of more detailed models. The objective is to provide an integrated analysis, thereby offering insights on the validity of the 2DOF model as a practical tool when inelastic behavior is exhibited by base-isolated structures. The responses are compared with the aim of characterizing a validity range for the 2DOF model when inelastic superstructure behavior occurs. The comparison is performed using four Engineering Demand Parameters (EDPs): (i) maximum isolation level displacement, (ii) maximum interstory drift ratio, (iii) maximum superstructure drift ratio, and (iv) maximum roof acceleration.

The study results show that a simplified 2DOF model is suitable as an analysis model for both scenarios when pounding and superstructure nonlinearity are expected at demands around and slightly above beyond design intensity level. Particularly, the simplified 2DOF model can represent an upper bound of the superstructure drift of the detailed model, with an explicit limitation on its capability to provide an interstory drift ratio profile. Also, this 2DOF model provides a slightly lower boundary for lateral displacement of the isolation system and a poor estimation of roof acceleration. These results and analysis are derived from a single structure with specific properties within the scope of the parameters; hence this study could be expanded for insights on trends for a broader range of structural configurations.

Seismic Hazard and Ground Motions

For this study, the subject building (see Section Structural Models) is assumed to be located in the Los Angeles, California, area, for which ASCE7-22 [1] defines the following parameters for the design spectrum for Soil Type C: $S_{MS}=2.28$ g, $S_{M1}=1.42$ g, and $T_L=8.0$ sec. Eleven unidirectional ground motions are scaled for an average response spectra matching or exceeding the design spectrum between 2.0 sec and 4.0 sec, henceforth referred as beyond-design-basis records, as shown in Figure 2.1.

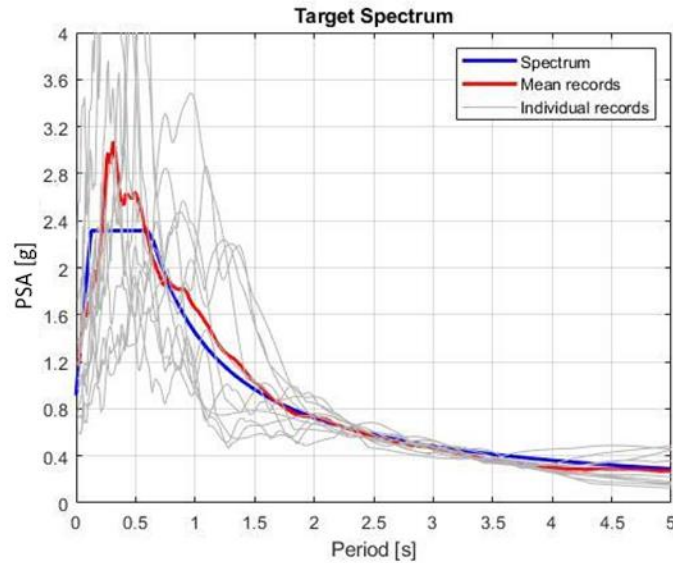


Figure 2.1: Target response spectra and ground motions

Structural Models: full model and 2DOF

The study focuses on the analysis of a 5-story Steel Special Moment Resisting Frame (SMRF) prototype building design by Guan et al [32] per ASCE7-16 specifications. The structural framing layout of the building was sourced from the ATC-123 Project [33].

Time-history analyses of the base-isolated prototype building are performed using both a detailed model for the superstructure and a two-degree-of-freedom model, which lumps the superstructure into a single degree of freedom. The following sections describe each model in detail.

Full prototype model

The prototype building by Guan et al. is modeled in two dimensions using OpenSees [34] with concentrated plasticity capturing the nonlinear response of beams and columns. The hinges are based on zero-length rotational springs using the modified Ibarra-Medina-Krawinkler material model [35]. The model includes a panel zone using elastic elements and a trilinear backbone curve embedded in a zero-length rotational spring. The numerical model includes a

leaning column supporting all gravity loads connected to the frame to account for P- Δ effects, as shown in Figure 2.2.

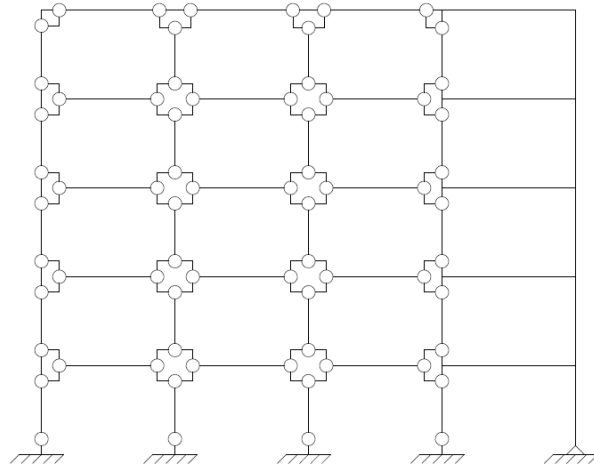


Figure 2.2: Numerical model of the reference building

An extra level is added to the fixed full model to seismically isolate the building, incorporating elastomeric bearings below each column and a rigid elastic beam to represent the isolation slab. A Bouc-Wen model [18] is used to represent the isolation bearings with parameters determined by the desired characteristic strength (Q_d) and corresponding post-yield period (T_d), which can be used to characterize the isolation level independently of lateral deformation. A focus is placed on the superstructure performance; therefore, it is assumed that the bearings can withstand the combined axial load and lateral deformation. The characteristic values used for the isolation system are based on referenced values used by York and Ryan [20], with $T_d=3.5$ sec and $Q_d=0.09W_T$. Using the seismic hazard shown in Figure 1, the maximum displacement (D_m) is found to be 650 mm, provided that the weight of the system including the isolation level is 20,406 kN, with an effective damping of 18% and a seismic coefficient (V_s/W_s) equal to $C_s=0.30$.

2DOF model

For the simplified formulation, the isolation system is represented by the combined aggregate model of the elastomeric bearings used in the full prototype (see previous section), while the superstructure is specified by a trilinear backbone curve, which can better quantify the peak deformations at the superstructure level compared to the bilinear curve commonly used in practice for the same purpose, see Figure 2.3.

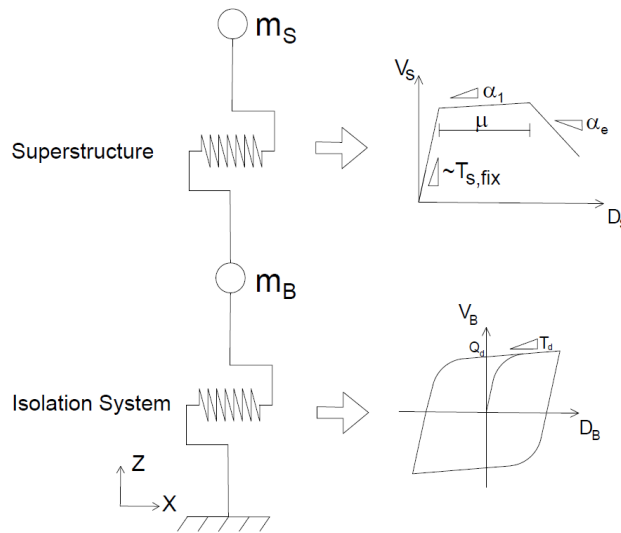


Figure 2.3: Simplified 2DOF model

The trilinear characterization of the superstructure follows an idealized force-displacement relationship using five parameters: the natural period of the superstructure under a fixed-base period condition ($T_{s,fix}$), the yield strength (V_y), the ductility (μ), the positive post-yield slope (α_1) and the negative post-yield slope (α_e). The force-displacement curve of the superstructure is estimated using a nonlinear static pushover analysis of the full base-isolated prototype model, with the base shear distributed on each level per the specifications of Chapter 17 on ASCE7-22. The load distribution is based on that provided in York and Ryan, that considers linear superstructure behavior. Figure 2.4 compares the force-deformation curves recommended for the fixed-base structure configuration using the load pattern specified in

Chapter 12 of ASCE7-22 showing a more gradual degradation in strength and more ductile behavior. The parameters required to linearize the superstructure capacity into a multilinear backbone curve are listed in Table 2.1:

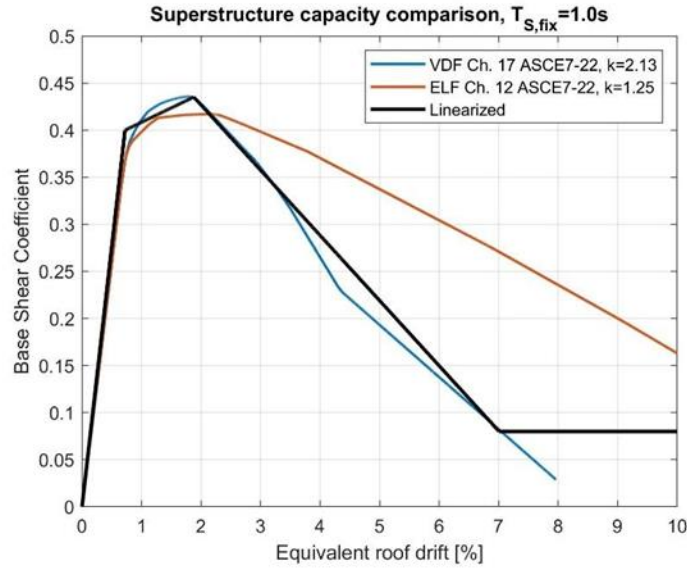


Figure 2.4: Static Pushover curves comparison

Table 2.1: Superstructure backbone

Parameter	Value
$T_{s,fix}$ [sec]	1.0
V_y / W	0.40
μ	2.6
α_1	0.055
α_e	0.125

Structural capacity

The yield strength of the superstructure can be tied to the isolation system lateral displacement using the equations 17.5-6 and 17.5-7 from ASCE7-22:

$$V_s = \frac{V_{st}}{R_I} = V_b \left(\frac{W_S}{W} \right)^{1-2.5\beta_m} \quad \text{Eq. (1)}$$

Where V_s and V_{st} are the total and unreduced lateral seismic design force on elements above the base level, respectively, with R_I representing the numerical coefficient related to the type of seismic force-resisting system above the isolation system.

The total lateral seismic design force on elements of the isolation system or elements below the isolation system, V_b , is defined per equation 17.5-5 as:

$$V_b = k_M \cdot D_M \quad \text{Eq. (2)}$$

The effective stiffness (k_M) can be written in terms of the characteristic strength (Q_d) and the post-yield stiffness expressed here in terms of period (T_d):

$$k_M = \frac{Q_d}{D_M} + \frac{W}{g} \left(\frac{2\pi}{T_d} \right)^2 \quad \text{Eq. (3)}$$

By equating the total lateral seismic design shear on elements above the base level (V_s) to the yield strength and using Equations (1), (2), and (3), gives:

$$V_y = \left(\frac{Q_d}{D_M} + \frac{W}{g} \left(\frac{2\pi}{T_d} \right)^2 \right) \cdot D_M \left(\frac{W_s}{W} \right)^{1-2.5 \cdot \beta_m} \quad \text{Eq. (4)}$$

Given that the pushover analysis provided a value for the yield onset of the superstructure at $V_y=0.40W_s$, equation (4) can be solved for D_{my} . The result provides an isolation system lateral displacement that yields the superstructure and is equal to $D_{my}=864$ mm, 1.34 times larger than D_m .

Limitations on the 2DOF model

The response predicted by the 2DOF model when the superstructure undergoes nonlinear deformations under beyond-basis shaking is expected to have a limited accuracy compared to the full model, due to three main factors: (i) the influence of higher modes, (ii) the changing dynamic characteristics of the superstructure post-yield and (iii) the linearized characterization of the superstructure obtained from a pushover analysis.

(i) Influence of higher modes and their variation upon yielding of the superstructure

The absence of higher modes in the predicted response limits the accuracy that can be achieved. The 2DOF model can capture the interaction between the superstructure and the base isolation system limited to two fundamental periods. Figure 2.5 shows the first three mode shapes for the full nonlinear model and the two mode shapes for the 2DOF model.

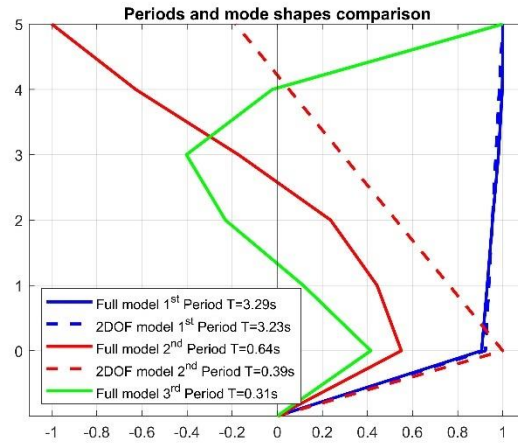


Figure 2.5: Periods and mode shapes comparison between models

(ii) the changing dynamic characteristics of the superstructure post-yield

The theory of linear seismically isolated systems [2] can be used to highlight the modal participation variation upon yielding based on the ratio between the superstructure period and the base isolation period, defined as epsilon (ϵ) in Eq. 5.

$$\epsilon = \left(\frac{\omega_{iso}}{\omega_{ss}} \right)^2 = \left(\frac{T_{ss}}{T_{iso}} \right)^2 \quad \text{Eq. (5)}$$

Epsilon near zero ($\epsilon \approx 0$) typically are referred as the first mode representing a rigid superstructure on a flexible base isolation system. The almost rigid movement of the superstructure implies that the higher modes of vibration may not significantly contribute to the overall base shear demand [2]. The parameter epsilon varies given that both the isolation system and the superstructure undergo changes in stiffness in response to the deformations they experience. Figure 2.6 illustrates three distinct stages of a two-degree-of-freedom (2DOF) base

isolation system model. The first stage depicts both degrees of freedom within the linear elastic deformation range. The second stage represents a scenario where the isolation system is activated and exhibits effective stiffness while the superstructure remains in the linear elastic range. The final stage shows the condition in which the isolation system retains its effective stiffness while the superstructure has yielded, indicated by the effective stiffness of the superstructure.

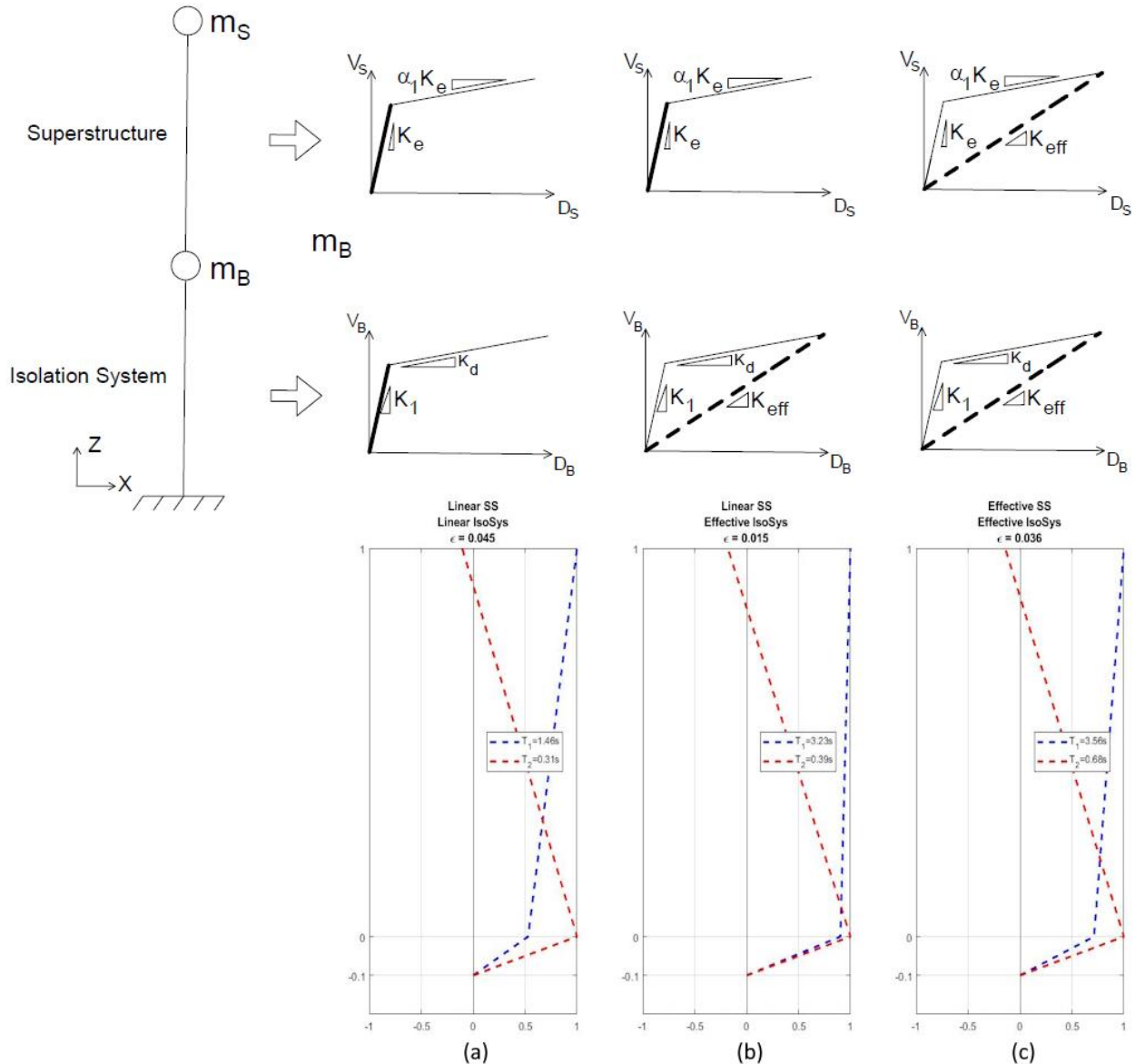


Figure 2.6: Seismic Isolation Theory (a) Linear elastic range (b) Isolation system yielded with linear superstructure (c) Yielding of both DOFs

These stages highlight the progressive behavioral changes in the system under varying levels of seismic demand. Before the isolation system activation (Figure 2.6a) epsilon equals 0.045, while gets reduced to 0.015 after the activation of the isolation system (Figure 2.6b). Once the superstructure yields (Figure 2.6c), the tangent stiffness of the superstructure is reduced, elongating the natural period, thereby increasing the parameter epsilon to 0.036. A larger epsilon value implies larger demands on the yielded superstructure potentially leads to further deformations. It should be noted that the well-defined yield point in the bilinear superstructure backbone leads to the rapid change in modal properties, while for a full model this transition has a more gradual progression.

(ii) the characterization of the superstructure starting from a pushover analysis

When characterizing the superstructure into a single lumped mass, the fundamental question is how the linearization of the pushover affects the superstructure characterization. The behavior obtained for the full model shows a progressive incursion into the nonlinear range, while the 2DOF backbone curve has single, sharp transitions. This sudden stiffness change modifies the dynamic properties of the superstructure and represents a characterization limitation when compared to the smooth, gradual transition exhibited by the pushover curve. Additionally, once the superstructure reaches the ultimate strength, the negative slope is engaged, leading to a superstructure with a reduced strength with an isolation system still capable of transferring large forces into the superstructure. This paper intends to quantify these differences using the EDPs and establish a range for which a simplified 2DOF model could be used for beyond-basis analysis.

Results

The time history analyses results from the full prototype and the simplified 2DOF model are compared. The results for two kinds of analysis are shown for each model: one shows the

maximum values for each beyond-design and MCE intensity levels; the other shows the results of an Incremental Dynamic Analysis (IDA) [25] with scaling factors from 0.1 to 2.0 times for the beyond-design basis intensity, discretized in increments of 0.1. For the first type of analysis, the plot shows a normalized EDP of interest on the y-axis for each record number. For the IDA plot, the x-axis shows the average EDP value from the 2DOF model, while the y-axis shows the average EDP value from the full model.

Figure 2.7a displays the maximum lateral displacement of the isolation system for both models, normalized by the maximum displacement $D_m=650$ mm. Under the MCE demand, the 2DOF model and the full model give nearly identical average displacements equal to D_m . For the beyond-basis design demand, at which the yielding of the superstructure is expected, the 2DOF model averages 125% of D_m while the full model averages 129%. Regarding the MCE demand, the 2DOF model averages 98% of D_m , compared to the full model, which averages 99% of D_m . Particularly for Record 7, the maximum displacement of each model is similar for both intensities with no evident yielding of the superstructure for the MCE level. For all other records, the 2DOF model has a yielding superstructure, which limits additional lateral displacement, also noted by Thiravechyan et al [7].

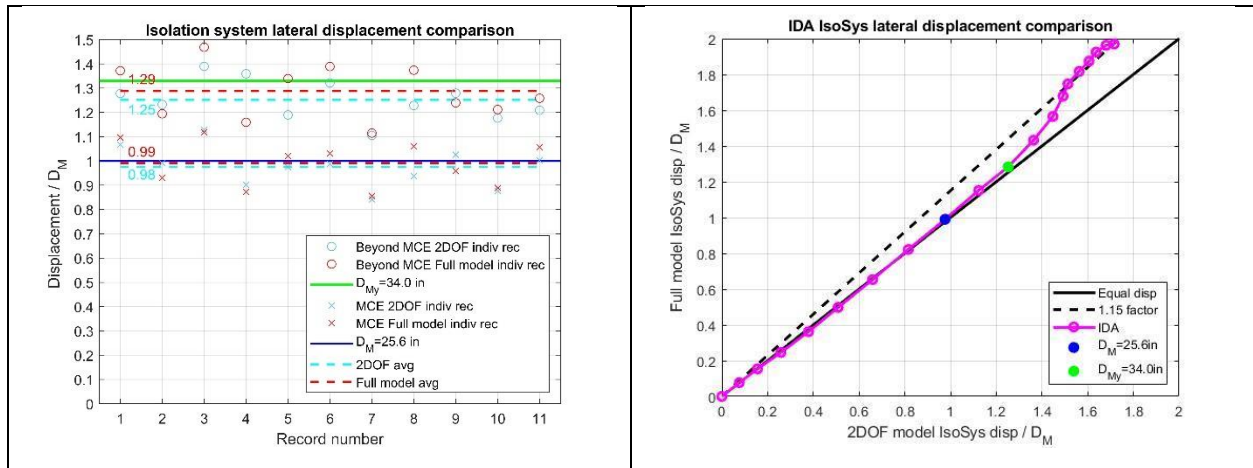


Figure 2.7: Comparison of the isolation system lateral displacement (a) beyond-design intensity (b) IDA analysis

The responses from the 2DOF model and full model are compared under increasing seismic intensity in Figure 2.7b, showing the IDA analysis results of the average lateral displacement of the isolation system normalized by D_m . The blue and green marker represents the corresponding average values of Figure 2.7a for the MCE and beyond MCE scaled motions. For ground motion sets scaled below the beyond-basis design, both models provide the same isolation lateral displacement. For higher intensity motions, the 2DOF model underpredicts the response of the full model that has up to 15% larger displacements.

The underestimation of lateral displacement by the 2DOF model can be explained by how the dynamics of the base isolation system are influenced by the abrupt shift in superstructure stiffness compared to the full model. Once the superstructure in the 2DOF model yields, its stiffness slope decreases by a factor of 18. This sudden slope change adjusts the ratio of the isolation period to the fixed-base period ($T_d/T_{s,fix}$) from 3.50 to 0.82. Nevertheless, the differences between the models are minimal (3%) at beyond-design basis intensity levels but expand to 15% at higher intensities, still providing a good estimate of the isolation system lateral displacement.

Figure 2.8a shows the superstructure base shear force coefficient (V_s/W_s) for each record scaled to the two intensities. For the 2DOF and full model under the beyond basis-demand, the average base shear on the superstructure equals $0.42W_s$ and $0.44W_s$, respectively, both exceeding the yield strength of $0.40W_s$.

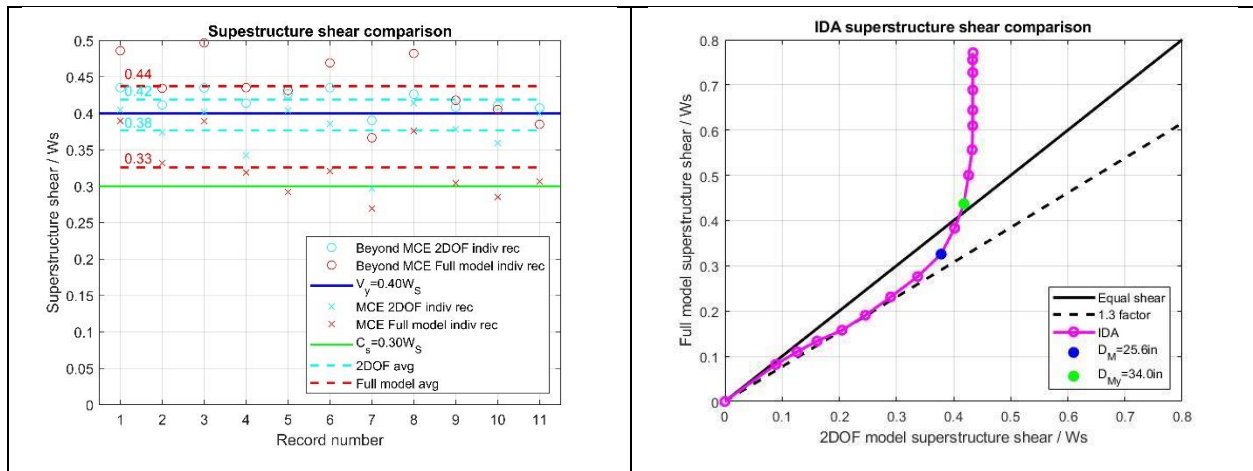


Figure 2.8: Comparison of the Superstructure Base Shear (a) beyond design intensity (b) IDA analysis

Figure 2.8b shows the IDA results with two clear trends. First, before the superstructure yields, the base shear predicted by the 2DOF model exceeds that of the full model by up to a factor of 1.3. This indicates that the 2DOF model provides a conservative estimate before yielding occurs. Following the onset of yield in the superstructure, the backbone curve in the 2DOF model limits the base shear. This leads to an underestimation of the predicted force demand compared to the results from the full model. These results show a conservative estimation of the superstructure shear force using the 2DOF model for MCE demands.

An EDP that can be used to predict structural and nonstructural of a structure is the superstructure drift. Figure 2.9a shows that the 2DOF model on average overestimates superstructure drifts of the full model by 22% at the beyond-design basis intensity, while for the design demand the 2DOF model underestimates the drift by a narrow margin of 9%. Figure 2.9b shows the superstructure drift results under the IDA, with a change of trend around the yielding

point of the superstructure. Before yielding, the 2DOF model underestimates the superstructure drift by up to a factor of 1.5, while after yielding, the superstructure drift is largely overestimated. The overestimation can be explained by the inability of the 2DOF model to redistribute forces after yielding.

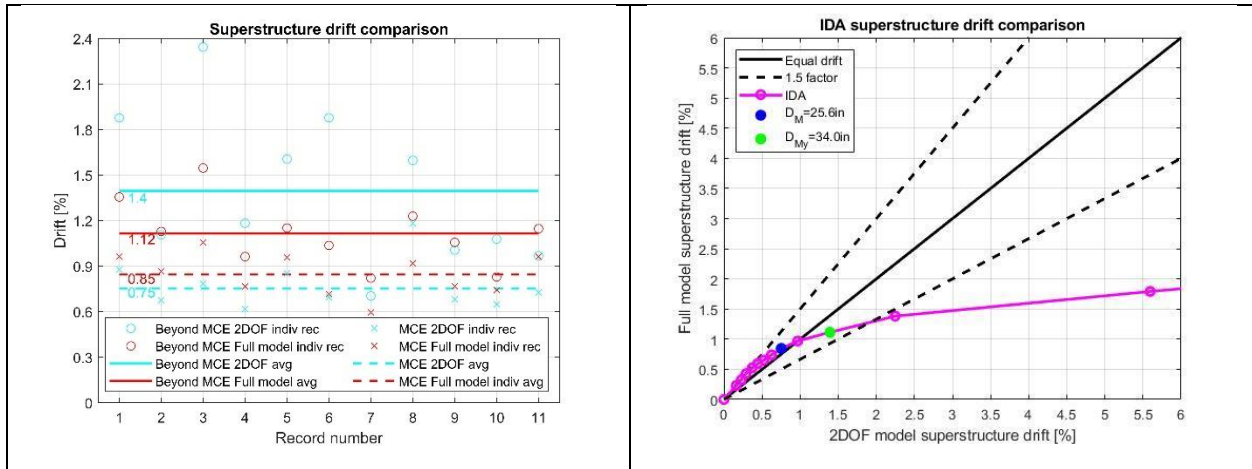


Figure 2.9: Comparison of the superstructure drift (a) beyond-design intensity (b) IDA analysis

Finally, the roof acceleration is compared. Figure 2.10a shows a 62% difference under the beyond-basis design demand between the average acceleration estimated by the 2DOF and the full model, with the latter exhibiting larger accelerations. This trend continues for all the intensities considered in the IDA, as shown in Figure 2.10b, with an average difference of around 60% between models. The 2DOF model roof acceleration estimation is greatly underpredicted for the MCE demand.

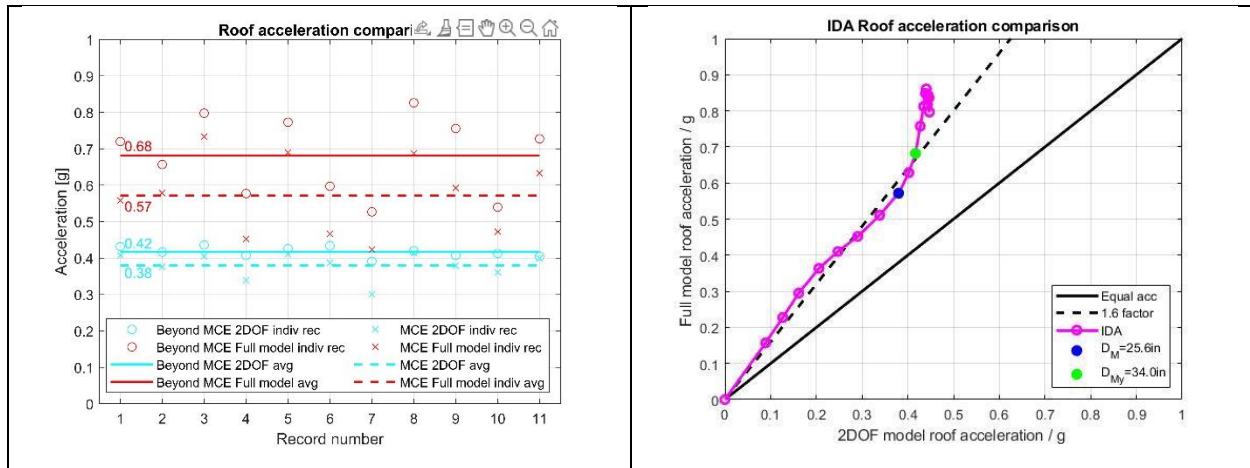


Figure 2.10: Comparison of the acceleration superstructure drift (a) beyond-design intensity (b) IDA analysis

The roof acceleration differences can be attributed to the number of modes each model considers. The full model accounts for more degrees of freedom than the 2DOF model can represent, limited to only DOF for the superstructure. The influence of those higher modes in the response is analyzed in the next section to quantify their contribution to this disparity.

Quantification of higher mode contributions

The three predominant frequencies of the full model are 0.3 Hz, 1.6 Hz, and 3.2 Hz. The 2DOF model is limited to two fundamental frequencies and is unable to capture higher frequency responses. A spectrogram analysis is performed to quantify the effects of the frequencies not captured by the 2DOF model using the roof acceleration obtained from the full model under the beyond-basis ground motions.

Records 3 and 7 are considered for frequency analysis since they provide the highest and lowest roof accelerations. Additionally, under Record 3 the superstructure yields, while for Record 7 it does not, providing a wide behavior range. Figure 2.11 shows the acceleration time history for both records for the ground and roof level. For both records the roof level accelerations in the full model exceed those of the 2DOF model, which is attributed to the

contribution of higher modes of the superstructure, independently to the yielding of the superstructure.

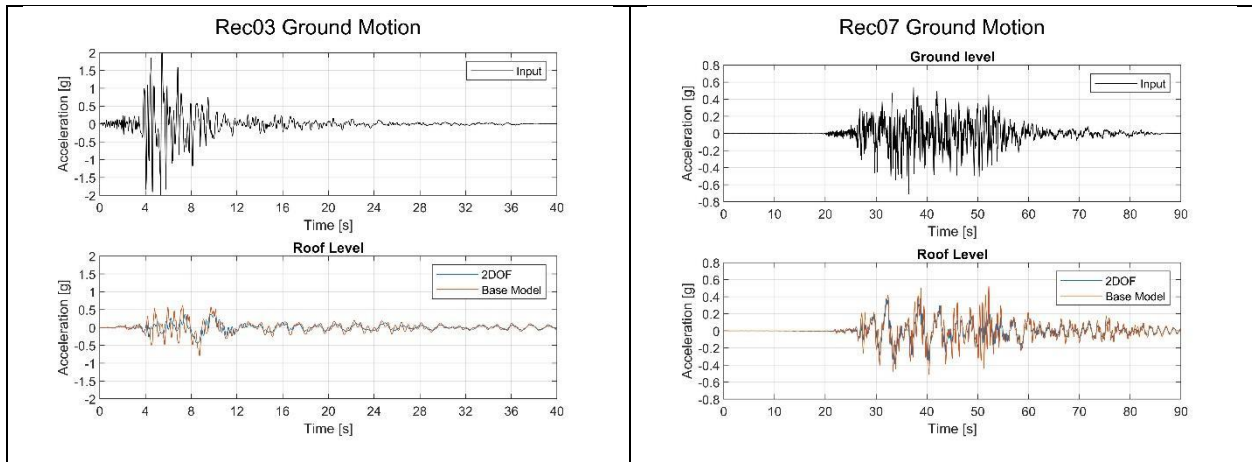


Figure 2.11: Acceleration Time Histories for (a) Record 3 (b) Record 7

Figure 2.12 shows a frequency domain analysis of the two roof acceleration records from the full model to explore the higher mode contributions. The plot at the top shows the roof acceleration time history, while the left side shows the Fast-Fourier-Transform (FFT) of the same record. The center plot shows the spectrogram, which displays the frequency content of the signal over time, essential for understanding how different vibration modes are excited, using color to symbolize signal strength, from warm for strong and cold for weak. Particularly, this plot shows the contribution of frequencies up to 10 Hz to the roof acceleration. The results for these two records show the predominant frequency excited over time oscillates between the first and second frequencies. Nevertheless, the spectrograms show that higher modes (above the first two frequencies) contribute to the roof acceleration, predominantly during the strong motion phase of the record.

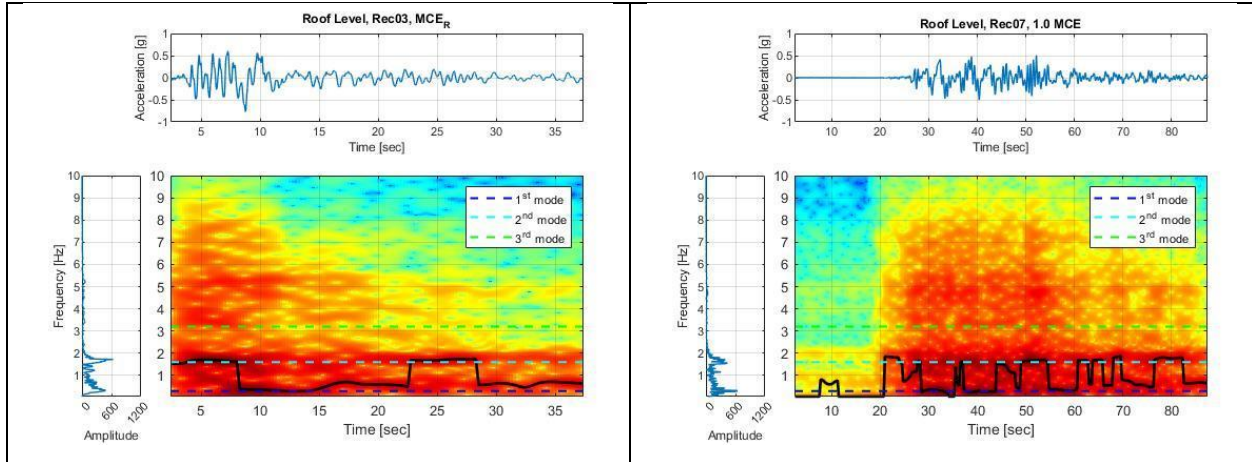


Figure 2.12: Spectrogram for (a) Record 4 (b) Record 7

A 4th order low-pass Butterworth filter with a cutting frequency of 3 Hz is considered to remove the third frequency and any other higher frequencies of these two records, with the results shown in Table 2.2, with higher frequencies contributing around 21% to 25% of the peak roof acceleration.

Table 2.2: Peak roof acceleration values for Records 3 and 7

Record	Original full model response [g]	Filtered full model response [g]	Difference [%]
3	0.80	0.63	-21
7	0.53	0.40	-25

The analysis results for the complete set of ground motions are shown in Figure 2.13. There is a 30% average reduction in the acceleration from the full model when comparing the results with and without the high-frequency content.

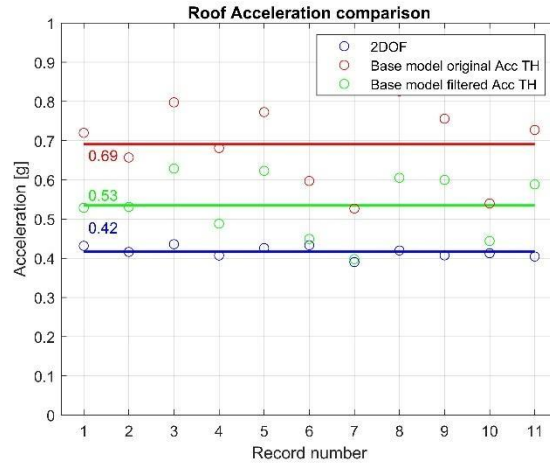


Figure 2.13: Maximum roof acceleration for the 2DOF model, full model, and full model filtered signal.

The 2DOF model estimates are based on the first two predominant frequencies, underpredicting the response provided by the full model, with values bounded and little dispersion around the average superstructure strength of $0.42W_s$, which is related to reaching the yield strength at $0.40W_s$. This result shows i) the contribution of the higher modes to the response, which the 2DOF model cannot capture, thus underpredicting the response, and ii) how critical the backbone curve characterization is to define the acceleration response.

Moat wall pounding

Larger than expected ground motions could displace the isolation system beyond the moat wall clearance, leading to pounding. Previous studies [3] have shown pounding of the moat wall transfers large forces into the building, affecting critical EDPs, such as the peak interstory drift ratio (IDR). Since the IDR is a parameter related to expected damage, it is used herein to quantify the effects of pounding. A uniaxial Hertz contact element [28] is added to each model at the isolation level to account for the moat wall pounding effects, assuming a coefficient of restitution equal to 0.7 and a Hertz nonlinear stiffness assuming a colliding sphere of radius equal to the isolation slab depth and a massive plane surface.

The contact element is placed on both models to compare the estimation of the peak IDR after pounding with a moat wall clearance of D_m . Figure 2.14a shows the average response of the eleven beyond-basis ground motions applied to both models, with a dashed line representing the original models without the pounding effects and with a continuous line when pounding is considered.

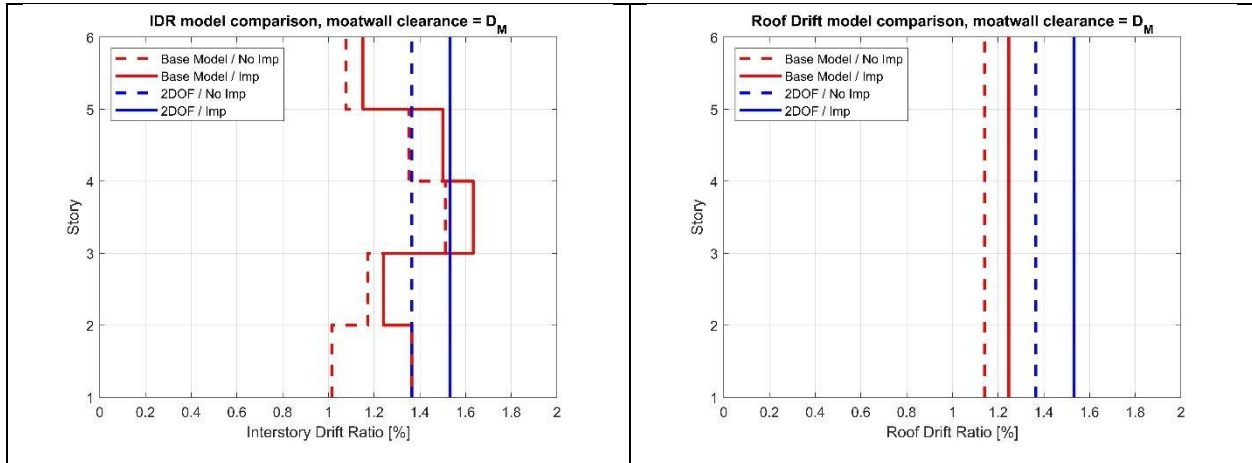


Figure 2.14: a) IDR with pounding model comparison b) Superstructure drift with pounding model comparison

The 2DOF model lumps the superstructure into a single DOF; therefore, it cannot provide an interstory drift profile but rather a superstructure drift estimation. Figure 2.14b compares the superstructure drift, showing that the 2DOF model estimation accounting for pounding effects is conservative and useful for analysis or design purposes.

Figure 2.15 shows the peak IDR response of the full model, with and without accounting for moat wall pounding, for each beyond-design basis record. For five records at least one impact was recorded, and the highest impact velocity is shown.

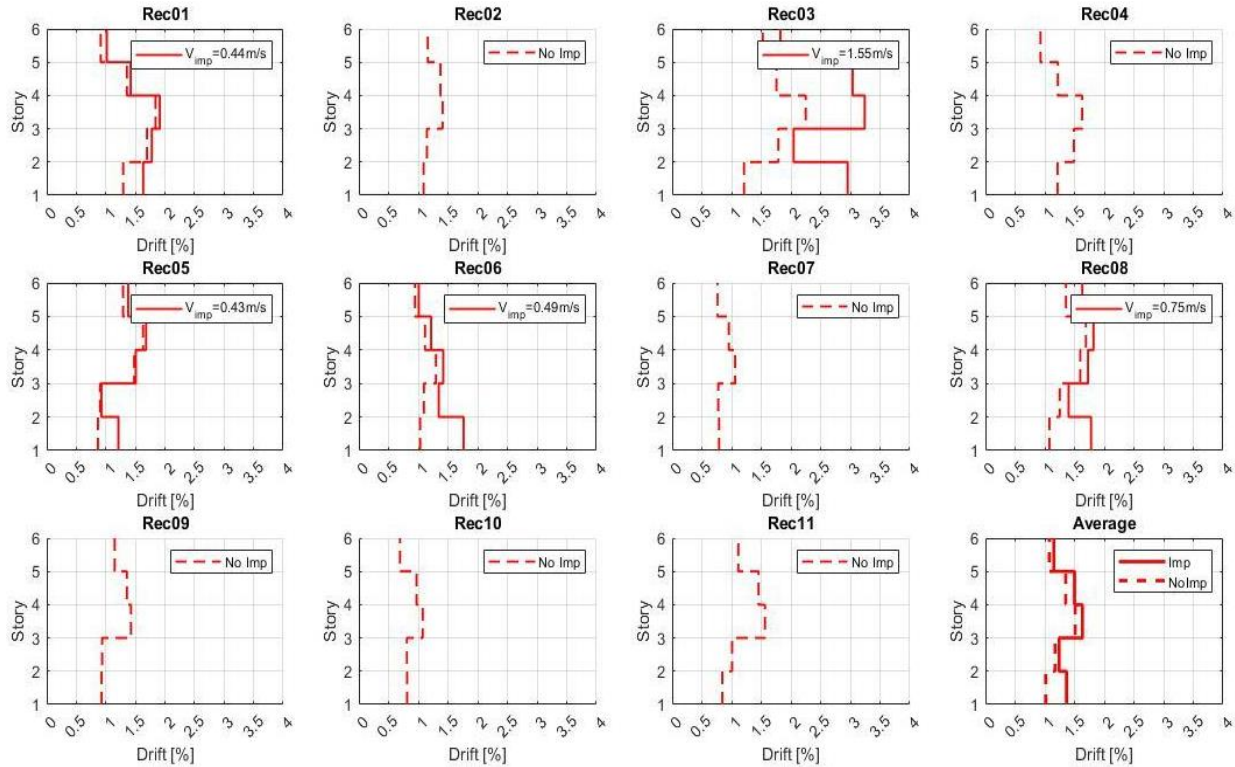


Figure 2.15: IDR profile per record without (dashed line) and with (solid line) pounding effects.

The IDR profile analysis provide insight on:

- In all cases the highest effect on pounding occurs at the 1st level.
- For relatively low impact velocity, around 0.5 m/s, the effect of pounding is minor at higher levels.
- For intermediate impact velocities the effect at higher levels is larger (25% on average of the higher floors on record 8).
- For high velocity impact the pounding significantly increases the IDR at all levels (270% at 1st floor and an average of 100% on higher floors for record 3).

These results highlight that the parameter that most influences the pounding effects is the impact velocity, which tends to increase upon reducing the moat wall clearance [27].

Impact velocity dependency on pounding effects

Previous studies [27] showed the influence between the moat wall clearance and the impact velocity on the interstory drifts. A sensitivity analysis on the moat wall clearance was performed to relate the impact velocity to the IDR increment. Record 4 was chosen since at a lateral displacement D_m , it does not register pounding. If the clearance is reduced by 1%, there is pounding, with an impact velocity of 0.32 m/s. Figure 2.16 shows the IDR sensitivity over different moat wall clearances (i.e., different impact velocities) expressed as an amplification factor of the interstory drift with respect to the case without pounding.

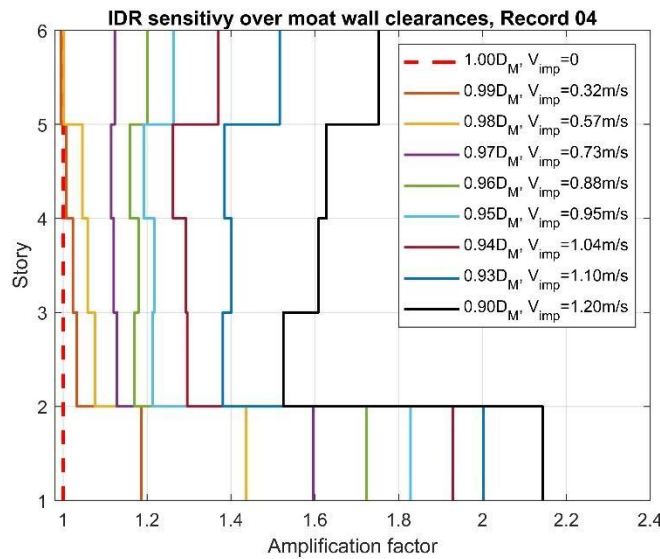


Figure 2.16: IDR amplification factor over impact velocity

Figure 2.16 shows two distinct IDR profiles, one that has a reduction of the amplification over height above the first story and one that amplifies it. For Record 4, this threshold happens around an impact velocity of 0.73 m/s.

Small changes in moat wall clearance show a significant difference in the impact velocities. To explore the trend for all records, Figure 2.17a shows the highest impact velocity for each ground motion relative to the moat wall clearance distance, where in the x-axis, a distance of 1 reflects the non-impact case. This result shows that if there is an impact, relying on

reducing the impact velocity below a threshold seems not feasible, given the rapid evolution of the impact velocity magnitude at small distances.

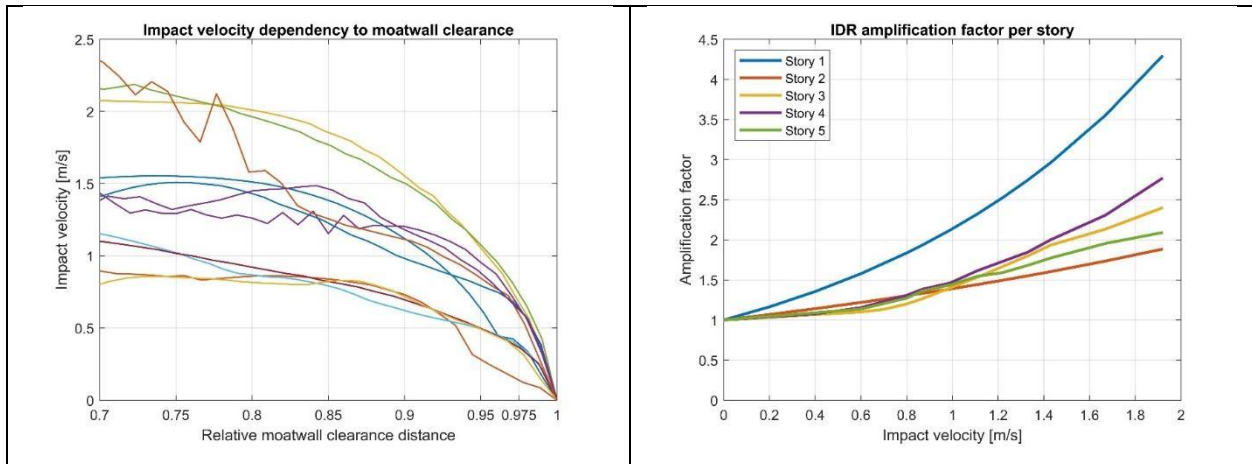


Figure 2.17: IDR dependency impact velocity for a) Story 1 with all records and b) all stories with average responses

Figure 2.17b shows the IDR for each story normalized by its non-impact IDR in terms of the impact velocity. For an impact velocity of 0.5 m/s, which happens within a relative distance of 2.5%, the Story 1 IDR is amplified by 1.5, while for all other levels, the amplification factor is, on average, 1.15. The rapid onset of the moat wall pounding effects on a small distance and the large dispersion of the velocity-distance path show that the clearance increment required to avoid impact should be large.

Figure 2.18 explores how the IDR profile relates to the moat wall distance. Two cases without impact are depicted to compare the moat wall pounding effects on the IDR profile: one using a seismic hazard intensity equivalent to D_m and one intensity using scaled-up to the displacement that yields the superstructure (D_{my}). Five moat wall clearances are considered using the latter seismic intensity: i) 1.15 times D_m , equivalent to the minimum total maximum displacement allowed by the ASCE7-22 code, ii) 1.20 times D_m , iii) 1.26 times D_m , iv) 1.32

times D_m , equivalent to D_{my} , and v) 1.40 times D_m , equivalent to a single record experiencing pounding.

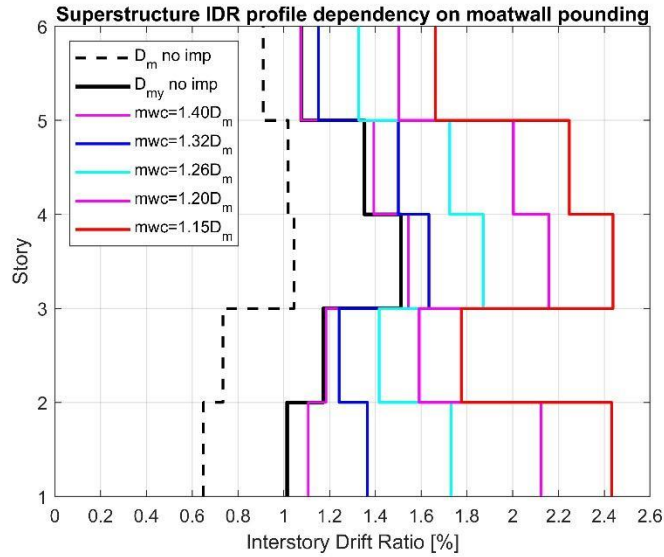


Figure 2.18: IDR profile dependency on moat wall clearance

For the cases without impact, the results show that an increase of 1.32 times the demand (D_{my} no imp) increases the drift up to a factor of 1.6, which is related to the nonlinear behavior of the superstructure. For the cases with impact, the reference IDR profile (D_{my} no imp) is compared to different clearances, with the minimum clearance amplifying the IDR profile ranging from 1.5 on the roof level to 2.4 times at the 1st story. Under this clearance, the superstructure does not reach yielding levels, and all records but one record at least one impact instance. Increasing clearances reduces the pounding effects on the IDR profile, primarily by reducing the impact velocity and engaging nonlinear behavior. If the moat wall clearance equals the displacement that yields the superstructure, five records experienced at least one impact instance but with significantly lesser effects on the IDR profile, highlighting how critical the impact velocity is. The IDR profile does not show a significant variation from the non-impact case for the case with a clearance located at a distance such as only one record pounds with an

impact velocity equal to 1.08 m/s. The results highlight that if moat wall impact is inevitable, avoiding acceleration and drift-sensitive equipment at the first story could lessen the pounding effects on nonstructural components.

Discussion

A main assumption of base-isolated systems is that the superstructure remains essentially elastic. Upon subjection to beyond design basis events, the assumption may not provide a realistic representation. Triggering a nonlinear response in the superstructure changes the dynamics of the system, transferring larger demands to a superstructure that is not required by code to be analyzed or detailed accordingly. Nevertheless, in the early stages of analyzing a base-isolated building, simplified models are used to explore potential alternatives. Given the assumption that the superstructure remains essentially elastic, a linear SDOF model is commonly used, which can potentially misrepresent key EDPs.

The characterization of the superstructure influences the 2DOF model results to different degrees. The isolation system lateral displacement is less sensitive to the superstructure characterization, primarily due to dependency on the first mode response. Regarding the roof acceleration and superstructure drift, the 2DOF model underpredicts both EDPs, which is related to both the backbone curve shape and the superstructure strength. As discussed, the sudden and sharp change of the superstructure stiffness at yielding modifies the dynamic properties of the system, increasing the deformation transferred to the superstructure. Further breaks of the backbone curve shape could be provided to transition to a multi-linear characterization, aiming to depict a more accurate force-displacement relationship. Nevertheless, results show an underestimation of the superstructure strength, which defines the onset of yielding, caps the force experienced by the superstructure, and increases the deformation in lieu of lesser force. Hence the capacity estimation of the superstructure is critical towards a better estimation of the EDPs.

A capacity estimation was obtained using a load pattern to distribute the design forces over the height. This force distribution, derived for linear elastic superstructures, is highly influenced by the k factor. The same superstructure with a fixed-base condition has a factor of 1.25, while when placed on an isolation system with an effective damping of 18%, the factor increases to 2.13. The load distribution changes from a triangular to a parabolic load pattern, which, if used to estimate the capacity of the superstructure, provides a lower deformation capacity to the fixed-base counterpart.

Finally, some concerns arise about the moat wall pounding effects on the superstructure. Codes such as ASCE7-22 or ASCE41-17 do not explicitly provide guidelines to capture its effects. For existing base-isolated structures with a non-modifiable moat wall clearance, pounding might be inevitable. In 2019, the New Zealand Society for Earthquake Engineering (NZSEE) introduced the inaugural version of the "Guideline for the Design of Seismic Isolation Systems for Buildings," for pilot implementation [4]. The establishment of the guidelines aims to standardize the design of base isolation systems throughout the nation, addressing the lack of formal documentation for base isolation within the Building Code. The code provides criteria to help designers recognize that superstructure capacity reductions must be closely controlled, while local plastic rotations are required to be explicitly evaluated and limited. The code introduces the occurrence of pounding for new and existing buildings, providing guidelines for the designer. The merit of this guideline lies in its proactive recognition and strategic response to the significant, albeit low probability, impacts of unforeseen seismic events.

Conclusions

This study explores the dynamic behavior of a detailed nonlinear model and its equivalent simplified 2DOF model version under conditions exceeding design-basis seismic shaking. Employing time-history analysis on eleven ground motions scaled to a beyond-design

basis intensity, the research focuses on assessing four critical Engineering Demand Parameters (EDPs): isolation system lateral displacement, interstory drift ratio, superstructure drift, and roof acceleration. At the design intensity level, the 2DOF model demonstrates proficiency in estimating two of the four EDPs, with unrealistic estimation for the interstory drift ratio and roof accelerations. The structural simplification to a 2DOF representation lowers its ability to represent inter-story drifts accurately and to account for the influence of higher modes on roof accelerations.

Using an Incremental Dynamic Analysis (IDA) to assess both models under increasing seismic demands, the results show the divergence in response between the 2DOF model and a fully nonlinear model, particularly once the superstructure begins yielding. This yielding instigates a stark change in stiffness, fundamentally altering the dynamics of the structure. Pre-yield, the 2DOF model reasonably estimates the full model in predicting isolation system lateral displacement and superstructure drift, while the roof acceleration is significantly underestimated. For post-yield conditions in the superstructure, the isolation system lateral displacement is the only EDP that can be accurately estimated, underpredicting its average value by 15%.

This research also delves into the discrepancies between the 2DOF and the full model. The primary of which is contributed to the inability to incorporate higher mode effects for the reduced order model and the limitations in accurately estimating the superstructure capacity therein. The characterization of the superstructure as a single-degree-of-freedom system restricts its capacity to involve higher modes, significantly influencing the accelerations estimated by the model. Moreover, the capacity estimation methods used, involving two pushover load patterns, seem to underestimate the yield and maximum strengths exhibited by the full model during the dynamic analysis, thus constricting the 2DOF model predictive accuracy.

A notable aspect of the study is its exploration of moat wall pounding effects, revealing a correlation between these impacts and peak interstory drifts. The analysis shows that the correlation between the velocity and trajectory of the isolation system exhibits substantial variability across different ground motions. Notably, there is a pronounced deceleration of velocity occurring at approximately 95% of the maximum displacement. This finding shows that relying on small increases in moat wall clearances to prevent pounding is inherently risky. Furthermore, the results show that even minor impact velocities should not be disregarded. As for the 2DOF model as a rapid assessment tool to analyze pounding effects, it is shown to provide conservative estimates of superstructure drifts.

To conclude the research findings from this study, it is recommended that additional validation steps are taken to enhance the reliability and applicability of the 2DOF model. A broader performance comparison between the full model and the 2DOF model across various superstructure characteristics, such as fundamental periods and post-yield slopes, is necessary to refine the understanding of EDP trends upon yielding. Similarly, a comprehensive study on the lateral load pattern is required to examine base isolated system with nonlinear superstructures. Experimental testing, subjecting structures to their yield points and subsequent moat wall impacts, is crucial for validating the theoretical predictions and enhancing the design of base-isolated structures to withstand beyond-design basis seismic events effectively.

Acknowledgements

Chapter 2 contains unpublished material coauthored with Elwood, Kenneth J. and Mosqueda, Gilberto. The dissertation author was the primary author of this chapter. I am profoundly grateful to Kenneth J. Elwood and Gilberto Mosqueda for their invaluable guidance and support, which significantly enriched the quality and depth of this dissertation. Their

expertise, mentorship, and encouragement have been instrumental in shaping the direction and outcomes of this research endeavor.

Chapter 3 EVALUATION OF BASE-ISOLATED ARCHETYPES BUILDINGS UNDER BEYOND DESIGN LOADING

Abstract

Base-isolated buildings are designed for operational resilience under design-level earthquakes, but their performance under more severe seismic events remains uncertain. Current design codes aim for essentially elastic superstructure response by requiring adequate stiffness and strength, yet beyond-design seismic events can induce yielding that modifies the dynamic response reducing the effectiveness of the isolation system with increased ductility demands. Moreover, large isolator displacements can cause moat wall pounding, exacerbating inertial force transmission and potential damage. This study employs a two-degree-of-freedom (2DOF) model to understand the damage progression in isolated buildings, considering beyond-design limit states. By examining representative nonlinear frame models for different archetype building lateral resisting systems, we examine the superstructure performance post-yielding and during moat wall impacts to delineate the seismic performance governing parameters. The findings highlight the performance of in base-isolated structures under beyond-design loading, emphasizing the interplay between yielding thresholds, strength variations, moat wall clearances, and seismic intensity in shaping structural resilience.

Introduction

Base-isolated structures are designed to enhance resilience when subjected to seismic events. While their efficacy under design-level earthquakes is well-documented [12–14], their response to more severe seismic forces warrants further investigation. Current design standards [1] focus on avoiding inelastic behavior in the superstructure by enforcing specific stiffness and strength requirements. However, extreme seismic events can induce yielding and subsequent

dynamic response changes with the reduced stiffness, leading to increased ductility demands [6–8]. Additionally, large displacements in the isolation system can cause moat wall pounding, which exacerbates the transfer of inertial forces, potentially leading to structural and nonstructural damage [3].

To address this gap, this study employs nonlinear two-degree-of-freedom (2DOF) models representative of archetype lateral force resisting systems to analyze the damage progression in isolated buildings under beyond design shaking. The effectiveness of 2DOF models in capturing the key dynamics of base-isolated structures has been demonstrated in previous studies [6–11,15,16]. These models have provided a better understanding of the dynamic interplay between the structure and the isolation system, extending beyond the traditional rigid superstructure assumption. Notable past analytical studies have leveraged simplified 2DOF models to explore inelastic superstructure demands, including, yielding and ductility, under various design parameters like superstructure stiffness and strength [9,10,13], post-yield stiffness ratio [10,11], natural frequency [10], and ground motion characteristics [9–12]. Experimental investigations on 2DOF models have further revealed distinct response modes of base-isolated structures, contingent on superstructure strength, and highlighted the potential for high ductility demands and concentration of damage post-yield.

In this study, representative nonlinear frame models with designs compliant with building codes [17] are used to assess the superstructure behavior post-yielding and with moat wall impacts. The parameters used to characterize the base isolation system are kept constant throughout all archetypes to enable comparison across all models. The analysis aims to identify key parameters governing the seismic performance of the archetypes. The findings underscore the need for refined design strategies in base-isolated structures, particularly considering the

balance between yielding thresholds, moat wall clearances, and seismic intensity. Such insights contribute significantly to the ongoing discourse on the seismic resilience of base-isolated systems, as they reveal the critical interdependencies that shape structural responses under extreme seismic conditions.

Analysis Model

The 2DOF model utilized in this study represents the superstructure as a SDOF on a base isolation system. This model captures the dynamic interaction between the superstructure and the isolation level, considering to some extent the inherent flexibility of the structure. Nonlinear models with different levels of complexity can be used for both the superstructure and the isolation system behavior. To estimate the structural response for beyond design shaking, the superstructure is characterized using a trilinear backbone curve with capacity derived from the pushover curve of the full frame structure.

Isolation System Level

In this study, the isolation level is represented by a smooth bilinear Bouc-Wen model [18], with characteristic strength (Q_d) and the post-yield stiffness described in terms of the corresponding period (T_d). The isolation properties remain constant in the simulations that follow to focus on the response of different structural systems under the same ground motions and isolation system. The isolation level post-yield period (T_d) is set to 3.5 sec, aiming to provide a period sufficiently larger than the effective period of the structures examined. The weight of the isolation level is 853 kN, and the characteristic strength is set to be 5% of the total weight (W_T) above the isolation layer.

Superstructure characterization

This study investigates the performance of the isolated superstructure before and after yielding using models representative of different types of lateral load resisting systems. To

explore different system behaviors, four capacity curves shown in Figure 1 aim to include a large range of initial and post-yield characteristics. The nonlinear force-deformation capacity of the superstructures is characterized using the results from a comprehensive study to evaluate the FEMA P-695 [19] methodology using detailed nonlinear models with explicit simulation of collapse modes. It is assumed that the capacity of the base-isolated superstructure can be estimated in the fixed-base configuration. ASCE7-22 [1] provides the vertical force distribution using an Equivalent Lateral Force (ELF) procedure specific to base isolation. The lateral load pattern is based on York and Ryan [20] and can be used for a pushover analysis, though the method is intended primarily for linear behavior of the superstructure.

Ordinary Reinforced Concrete Shear Wall Structures

Capacity curves were obtained for two four-story Ordinary Reinforced Concrete Shear Wall (RCSW) designed based on ACI318-08 [21] and ASCE7-05 [22] subjected to different axial loads. The high axial load system RCSW1 defines the concrete crushing failure at a roof drift equal to 1.3% and steel buckling failure at 4%. The low axial load system RCSW2 models the concrete crushing failure at a roof drift equal to 3.0% and 5.0% for the steel buckling failure. Both archetypes have an elastic period equal to 0.53 sec and were designed considering a Response Modification Factor (R) equal to 5. The difference in axial loads carried by the two archetypes significantly influences the negative post-yield slope, which can potentially lead to P-delta induced collapse. When these P-delta effects are combined with large inelastic displacements, they can accelerate the progression towards collapse.

Steel Braced Frame Structure

The capacity curve was obtained from a three-story special steel concentrically braced frame (SCBF) system designed following the ELF procedure of ANSI/AISC 341-05 [23] and ASCE7-05. The structure shows a significant negative tangent stiffness post-yield primarily

caused by P-Delta effects with collapse assumed at 7% drift. The SCBF elastic period is equal to 0.49 sec and an R=6 is assumed for design.

The overall expectation is that SCBFs will sustain significant inelastic deformations and damage to braces while preserving the integrity of the overall structural system and preventing collapse. A Special SCBF is designed to provide a reliable seismic performance by yielding in a controlled manner during significant seismic events. The bracing members in SCBFs are expected to act as the primary energy dissipating elements by yielding under compression and tension. SCBFs are designed with strict detailing requirements to ensure that braces can buckle in a stable manner and that connections remain intact and robust during and after seismic events.

Steel Moment Frame Structure

The capacity curve was obtained from a four-story special steel moment frame (SMF) system designed following the ELF procedure of ASCE 7-05. The collapse roof drift ratio was not explicitly defined, so a 10% roof drift limit for collapse. The SMF elastic period is equal to 0.83 sec and was designed for an R=8.

The expected seismic performance of a SMF is designed to be highly ductile, allowing it to undergo significant inelastic deformation during severe seismic events. The design principles behind SMFs focus on ensuring that the frame can bend and sway under earthquake forces, dissipating energy and preventing the accumulation of damage that could lead to structural failure. This is achieved through detailed design provisions that promote ductile behavior in beam-to-column connections and other critical regions of the frame.

Strength normalization

The later force resisting systems considered are normalized to have the same initial yield strength for comparison purposes using the same isolation system. All capacity curves are scaled to a yield strength of 20% of the superstructure weight equal to 4,246 kN, while maintaining the

yield drift and initial elastic properties of the structure. The capacities are characterized using a trilinear backbone curve with three parameters defining the nonlinear behavior following the notation used by ASCE41-17 [24]: i) the displacement ductility (μ), ii) the post-yielding stiffness ratio (α_1), and iii) the failure slope ratio (α_e). The four normalized pushover curves in Figure 3.1 show the range of behavior considered, with the RCSW2 system exhibiting the largest ultimate strength.

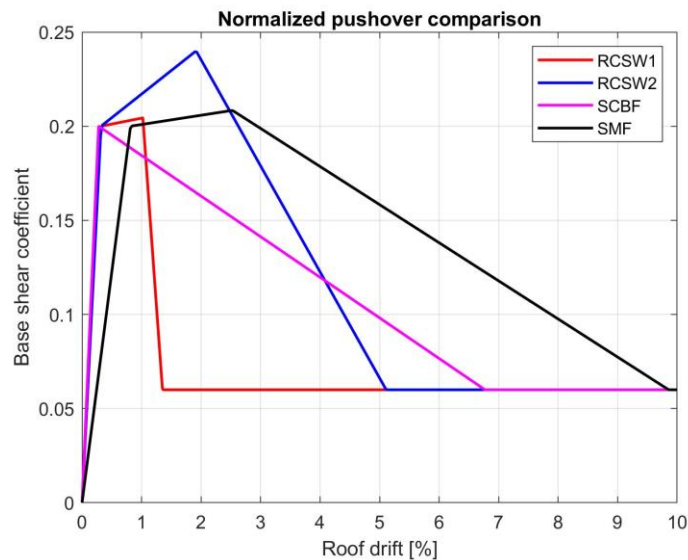


Figure 3.1: Normalized pushover comparison between all four models

Both RCSW models have the same linear stiffness and yield at a roof drift equal to 0.35%, however the nonlinear behavior after yielding is different. The RCSW1 model has less deformation capacity compared to the RCSW2 model, with a flatter post-yielding stiffness ratio and a larger failure slope ratio due to the high axial load. Given that they share initial linear properties, their performances can be contrasted to quantify the influence of the ultimate strength and deformation capacity. A more flexible model, the SMF model with a yield roof drift equal to 0.82%, has post-yielding stiffness ratio and ductility values that are in between those from the RCSW models. The SCBF model is considered to quantify the performance of brittle system

without deformation capacity nor a larger ultimate strength, with a roof drift yield equal to 0.28%. The initial stiffness and the resulting fixed-base periods of the four archetypes are different, ranging from 0.48 sec to 0.95 sec. Variations in initial stiffness within the same base isolation system influence the dynamic analysis, resulting in slight differences in the forces transmitted to the superstructure prior to yielding.

Seismic Hazard and Incremental Dynamic Analysis

The seismic hazard is defined using the ASCE7-22 for a site in Los Angeles, California, with $S_{DS}=1.52$ g, $S_{D1}=0.95$ g, and $T_L=8.0$ sec. Two sets of eleven unidirectional ground motions are scaled to the response spectra, using a range for the soil shear wave velocity for the first 30 meters ($V_{S,30}$) between 250 [m/s] and 450 [m/s]. One set is scaled for the average response of the ground motion to match the target response spectra in the period range between 1.0 sec and 3.8 sec, as shown in Figure 3.2, for a 5% damping.

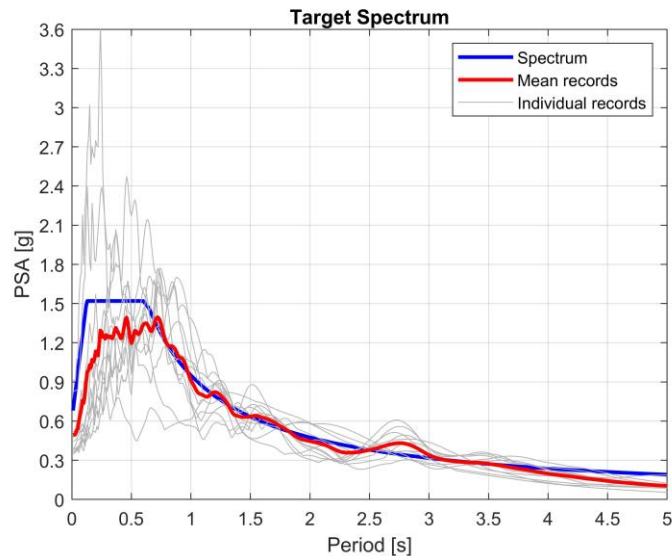


Figure 3.2: Seismic hazard and scaled ground motions for base-isolated systems.

The target spectrum was scaled such that the ground excitation transfers sufficient base shear force to yield the superstructure, defined as $0.20 W_T$. An Incremental Dynamic Analysis

(IDA) [25] approach is applied by scaling the base motions from 0.1 to 1.4 in discrete increment intervals of 0.1. The scale factor of 1.0 is labeled as PGA_{yield} for normalization purposes, with a SA value at $T_{eff}=3.10$ sec equal to 0.31 g. At this intensity, the displacement demand in the isolation system provides an average shear force equal to the base shear capacity of the superstructure. The IDA analysis is conducted up to 1.4 PGA_{yield} since another limit state like the moat wall clearance could be exceeded at this magnitude. It is important to note that the base motions are scaled by a factor of 1.15 above Maximum Considered Earthquake (MCE_R) since the superstructure is not expected to yield for this level of shaking.

Incremental Dynamic Analysis

The IDA is applied to evaluate the sensitivity of the response of the building models to increasing seismic intensity. The response of the four base-isolated systems is shown in Figure 3.3 in terms of the superstructure drift ratio. The models exhibit a low drift ratio for PGA_{yield} values below one, indicating the effectiveness of the isolation system. However, beyond yield, the superstructure drift increases at a rapid rate for the four models, with the two models with limited ductility (archetypes RCSW1 and SCBF) having a more pronounced effect. These results are in agreement with past studies including full detailed frame models on isolation that indicate the potential for collapse [8, 23] following the onset of yielding. The results also demonstrate the importance of ductile response and sustained strength to limit superstructure deformations for beyond design demands.

The two archetypes with ductile behavior, RCSW2 and SMF, show controlled roof drifts up to 1.4 PGA_{yield} and do not reach the assumed collapse failure limit state of 10% roof drift for the SMF and 5.6% for the RCSW2 model. This enhanced performance of the SMF model occurs despite possessing 30% less displacement ductility, 14% lower ultimate strength, and a 50%

smaller post-yielding stiffness ratio, as indicated by the backbone curves. The difference in performance can be explained by their fixed-base period, with the SMF having an 83% larger period and a 2.5 times larger yield drift.

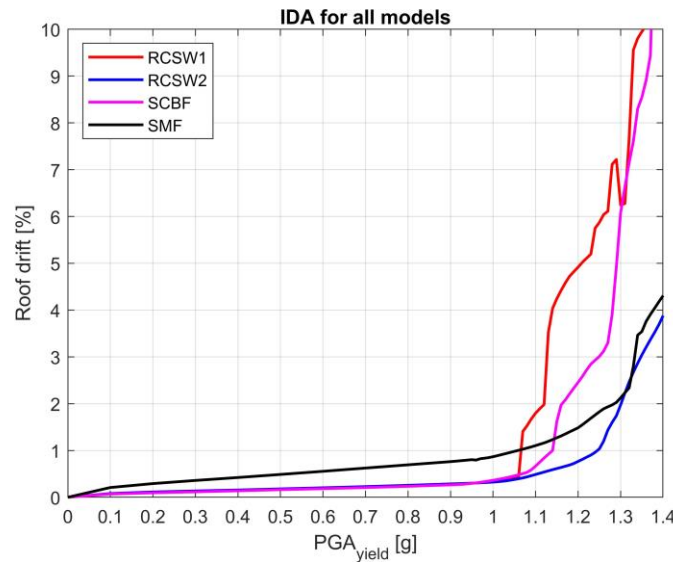


Figure 3.3: Incremental Dynamic Analysis results for all models

The comparison between the limited ductility models shows similar behavior with the SCBF having more favorable behavior immediately after yield. This is interesting considering the SCBF backbone begins to exhibit strength degradation immediately after yield. However, its failure slope is significantly less steep, maintaining a higher strength capacity for most of the nonlinear range compared to RCSW1. Both models exhibit sudden increase in drift after reaching yielding, resulting in a rapid onset of uncontrollable deformation, skewing the average represented by each line. A more detailed analysis of limit states is displayed in Table 3.1, covering all the archetype models.

Table 3.1: PGA_{yield} factors for different limit states

Archetype	Yield Drift [%]	PGA_{yield} factor to yield strength	PGA_{yield} factor to ultimate strength	PGA_{yield} factor to 50% yield strength
RCSW1	0.33	1.00	1.06	1.07
RCSW2	0.33	1.00	1.30	>1.40
SCBF	0.27	1.00	1.00	1.20
SMF	0.82	1.00	1.32	>1.40

Table 3.1 illustrates that the RCSW1 model experiences a significant strength reduction, with a 50% decrease in strength occurring immediately after reaching maximum strength. In contrast, the other limited ductility archetype, SCBF, requires a 20% increase in PGA_{yield} to go over the same limit states. Notably, the RCSW2 and SMF archetypes do not reach 50% strength degradation even with a 40% increment of PGA_{yield} . These findings prompt an important inquiry regarding which backbone parameter is the most critical for achieving a superior seismic performance during beyond-basis events. To better understand the influence of the backbone parameters, a sensitivity analysis is performed in the next section.

Backbone curve parametric analysis

The parametric analysis considers the variation of three parameters: i) the displacement ductility (μ), ii) the post-yielding stiffness ratio (α_1), and iii) the failure slope ratio (α_e). Each parameter is varied by +/- 50% to quantify its influence on the seismic performance of the system post-yielding. The variation aims to account for uncertainties in characterizing the capacity curve, which is highly dependent on the lateral load pattern. Beyond the material and structural system, the focus is on the shape of the backbone curve and its interaction with the

isolation system once it yields. The analysis is presented from the more ductile systems to the more brittle ones.

RCSW2 archetype

The RCSW2 archetype exhibits the largest ductility capacity and ultimate strength among the systems analyzed. The parametric analysis of each backbone parameter is shown in Figure 3.4, adding the original backbone curve to serve as a baseline for comparisons. Regarding the parametric variation of the displacement ductility, it has the largest change in performance compared to the other two parameters considered. The curve with 0.50μ shows that halving the ductility parameter results in a steeper rise in the roof drift. The structure experiences much larger drifts at lower levels of seismic intensity. In contrast, the variations in the post-yielding stiffness ratio and failure slope show modest sway on performance. For the post-yielding stiffness ratio (α_1), a 50% reduction leads to larger roof drifts post-yield. The adjustment of α_1 alters the dynamic characteristics of the superstructure post-yield, increasing its period. This results in a more flexible system that, upon yielding, exhibits increased deformability and, therefore, experiences greater roof drifts. The 50% increment of α_1 results in a stiffer superstructure after yielding, although this condition seems to produce a roof drift behavior that remains closer to the original curve.

Reducing the failure slope ratio by 50% slows the rate of degradation and provides a better performance compared to the original structure, as the roof drift increases more gradually. Increasing to $1.50\alpha_c$ shows a similar effect to reducing α_1 by 50%, worsening the performance overall when compared to the baseline case.

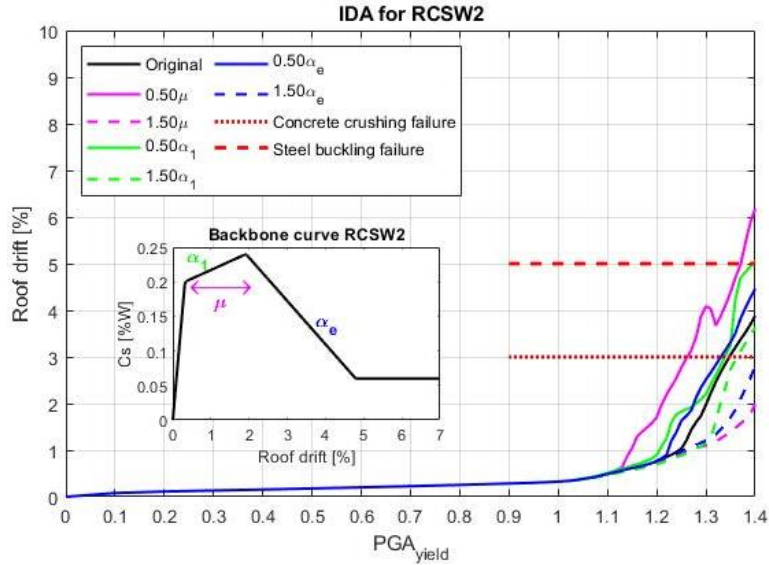


Figure 3.4: RCSW2 parametric analysis

Steel Moment Frame Structures

The steel moment frame archetype shows minor variations in performance after yielding for all the parameter variations considered, as shown in Figure 3.5. The responses begin to deviate approaching $1.2 \text{ PGA}_{\text{yield}}$, which is about when the capping strength is reached. Similar to the RCSW2, reducing the ductility has the largest change in performance when compared to the baseline, while increasing the ductility further extends the limit at which the drift begins to increase. Given that the original post-yielding stiffness ratio (α_1) is as low as 2%, adjustments of plus or minus 50% have a negligible impact on performance, rendering the influence of these changes relatively insignificant. Regarding the failure slope ratio (α_e), the parametric analysis reveals that the performance of the superstructure closely aligns with the outcomes observed in the ductility parametric analysis.

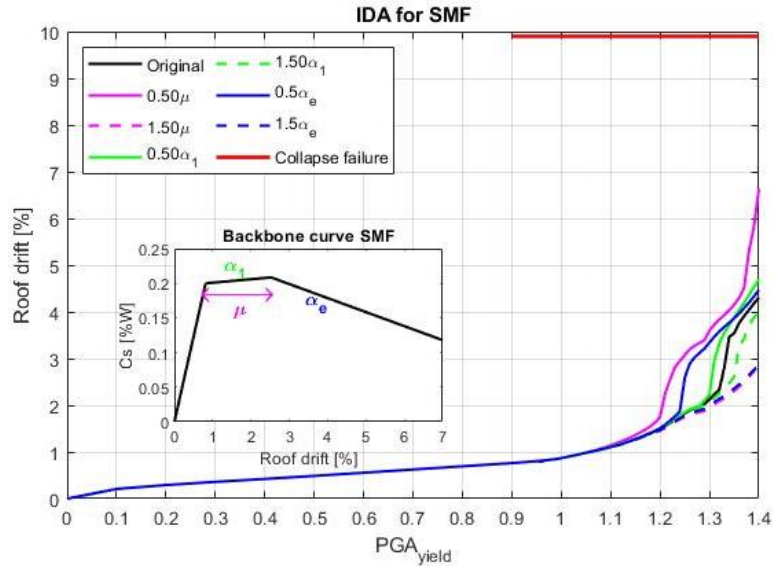


Figure 3.5: SMF parametric analysis

Ordinary RCSW1

The RCSW1 system differs from RCSW2 by the axial load they are subjected to, which partially conditions the ductility capacity (μ) and the failure slope ratio (α_e). Figure 3.6 shows the parametric analysis on the RCSW1 system, showing no significant differences in the performance at any intensity above yielding. The parametric analysis shows that the limited ductility puts the structure at risk of rapid degradation once the yield force is exceeded.

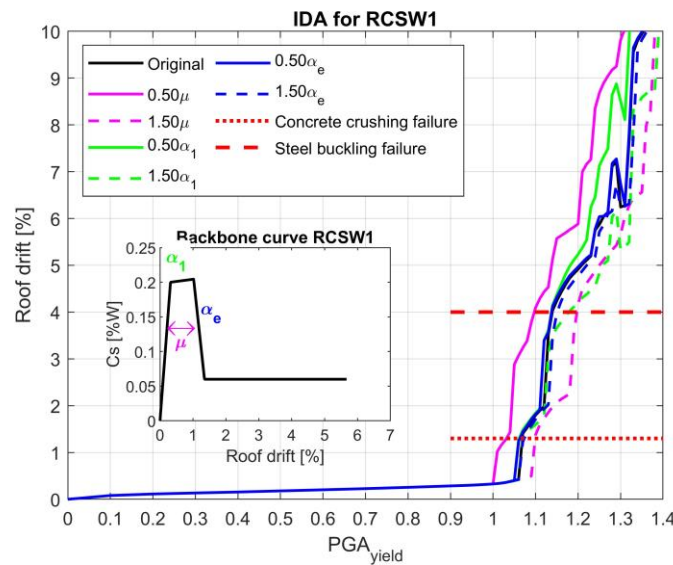


Figure 3.6: RCSW1 parametric analysis

A 50% increase in ductility allows for larger deformations prior to structural failure, suggesting that the structure can absorb more seismic energy before reaching critical deformation limit. Conversely, a 50% ductility reduction leads to an earlier onset of increased drifts. Despite these effects, the overall change in deformation capacity remains limited with a 10% variation observed between the lower and upper bounds of the ductility scenarios presented.

Variations in the factors α_1 and α_e , which represent the post-yield stiffness and failure slope, exhibit a negligible impact on the seismic performance. This outcome points to the dominance of initial stiffness and yield strength in dictating the response over ductility or post-yield behavior when limited deformation capacity is provided. The results indicate that for structural systems with a brittle behavior and rapid strength degradation, could have large drift demands at the onset of yielding. For retrofit purposes, these insights suggest a shift in focus towards enhancing the strength in the pre-yield phase. For example, if the linear strength would be increased by 25%, keeping the same nonlinear backbone curve parameters, the performance would be significantly enhanced, delaying the onset of yielding up to a demand of 1.3 PGA_{yield} , as shown in Figure 3.7.

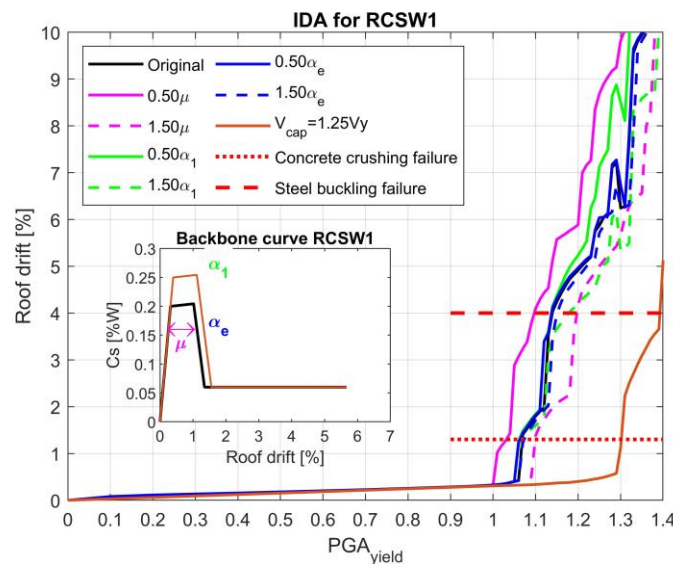


Figure 3.7: RCSW1 strength comparison

Steel Braced Frame Structures

The SCBF model is limited to a single parameter, the failure slope ratio (α_e). The drift rapidly increases at the onset of yield, reaching the assumed collapse failure limit of 5% roof drift at 1.3 PGA_{yield} for the baseline case. For the parametric analyses, that limit oscillates between 1.22 PGA_{yield} for the 50% steeper failure slope and 1.42 PGA_{yield} for a 50% less steep failure slope, as shown in Figure 3.8.

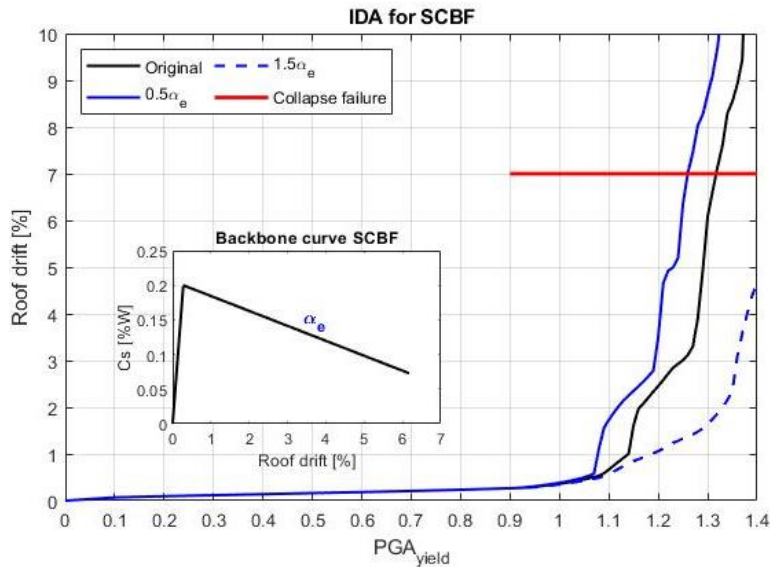


Figure 3.8: SCBF parametric analysis

The absence of a ductility plateau in the backbone curve suggests that the SCBF system is expected to behave in a more brittle manner, which has significant implications for design strategies. The ability to delay the onset of a sharp drop in strength post-yield can contribute to the overall robustness of the structure under seismic loads, potentially compensating for the lack of significant ductility and post-yield stiffness. This principle aligns with the concept that by carefully managing the post-yield degradation, even a system with limited ductility can be made to perform satisfactorily under beyond-design seismic conditions.

Moat wall pounding

In the event that ground motions increase beyond expected thresholds, they hold the potential to displace the isolation system beyond the specified moat wall clearance, resulting in moat wall pounding. Prior research [3,10,26,27] has shown that such impacts transfer significant forces to the structure, affecting accelerations and peak interstory drift ratios (IDR). The superstructure roof drift is used in this study for evaluating the effects of pounding with the understanding that moat wall impact is likely to excite higher modes not captured by the 2DOF model. To simulate pounding at the isolation interface, a uniaxial Hertz contact element, as described by Hughes and Mosqueda [28], is employed. This element is modeled with a restitution coefficient of 0.7 and a Hertzian nonlinear stiffness based on the assumption of a sphere, with a radius equating to the depth of the isolation slab, colliding with an extensive planar surface.

The analysis assesses the effects of moat wall pounding across various clearances, evaluating how increasing seismic intensities affect each of the four archetypes, as shown in Figure 3.9. The results show that the roof drift ratios increase in the presence of moat wall pounding, relative to the non-impact scenario defined as baseline. This upward shift highlights the moat wall pounding effects on the deformations induced by the moat wall impact. The gradations of moat wall clearance, spanning from 0.8 to 1.2 times the displacement equivalent to $PGA_{yield} (D_{m,y})$, show that smaller clearances correspond with larger roof drift ratios. The aim is to quantify the effects of pounding both before and after the superstructure yields and any differences in response.

At the individual performance of each archetype, the RCSW1 model exhibits the least favorable performance among the four archetypes analyzed, experiencing the greatest amplifications in roof drift due to pounding. In all but one instance, the structures reach the

concrete crushing limit state, with no noticeable difference in performance whether pounding occurs before or after yielding. The roof drift amplification varies significantly with clearance across archetypes, with the RCSW1 model showing the largest increments. The RCSW2 and SCBF archetypes display comparable performances, with roof drift amplifications due to pounding approximately six times that of the non-pounding scenario, while sustaining non-collapse up to a demand of 1.1 PGA_{yield} . These results show considerable resilience from both archetypes, as they are able to withstand a demand of 1.1 PGA_{yield} using a clearance set for 0.80 PGA_{yield} without collapsing.

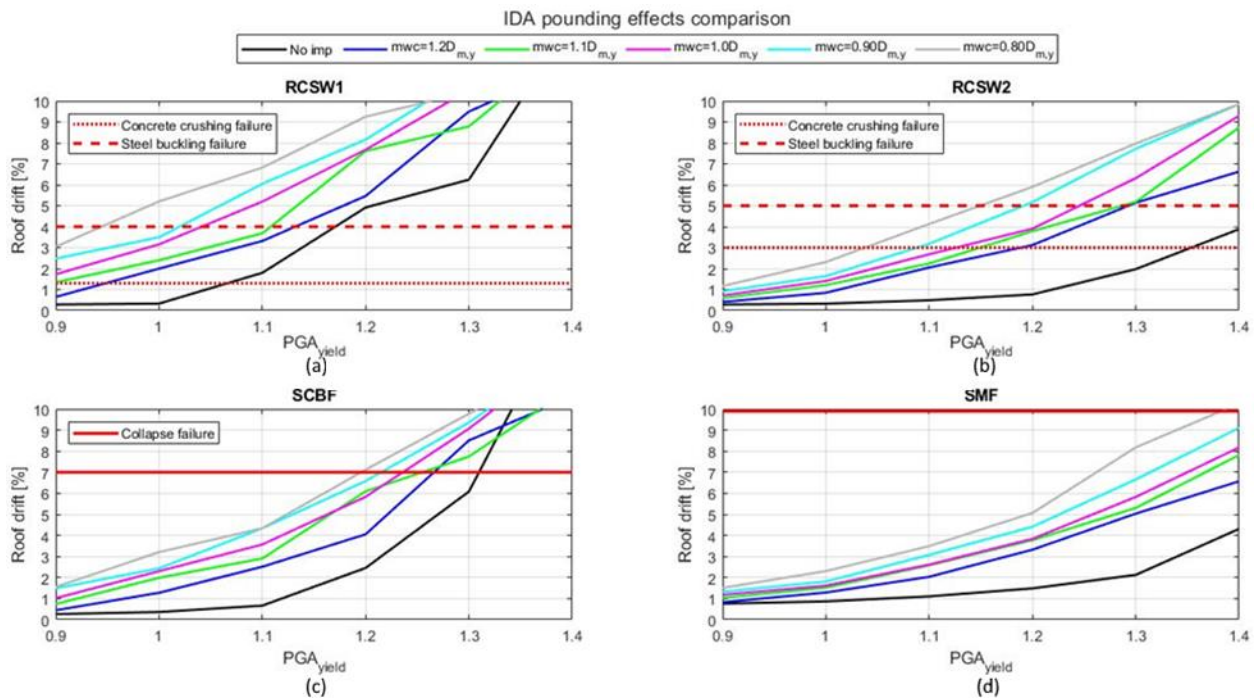


Figure 3.9: Moat wall pounding analysis for a) RCSW1 b) RCSW2 c) SCBF d) SMF

To account for variations of the superstructure strength, the inherent overstrength of the seismic force-resisting system, Ω , is used following ASCE7-22 in Eq. 6.

$$\Omega = \frac{V_y}{V_s} \quad (\text{Eq 6})$$

Where V_y represents the yield strength and V_s is the design force. Given that the superstructure is characterized by V_y , the analysis considers values of Ω between 1 and 2 to

reduce the superstructure strength. The analysis evaluates the effects of reduced superstructure strength with and without moat wall pounding to examine the response with yielding before pounding and with pounding before yielding.

Figure 3.10 presents an analysis of the seismic performance of the four structural archetypes and examines the variations in roof drift ratios with and without moat wall pounding. Continuous lines depict scenarios without pounding effects while dotted lines represent the pounding. The location of the moat wall is 20% larger than the isolation displacement at which the superstructure is expected to yield ($D_{m,y}$).

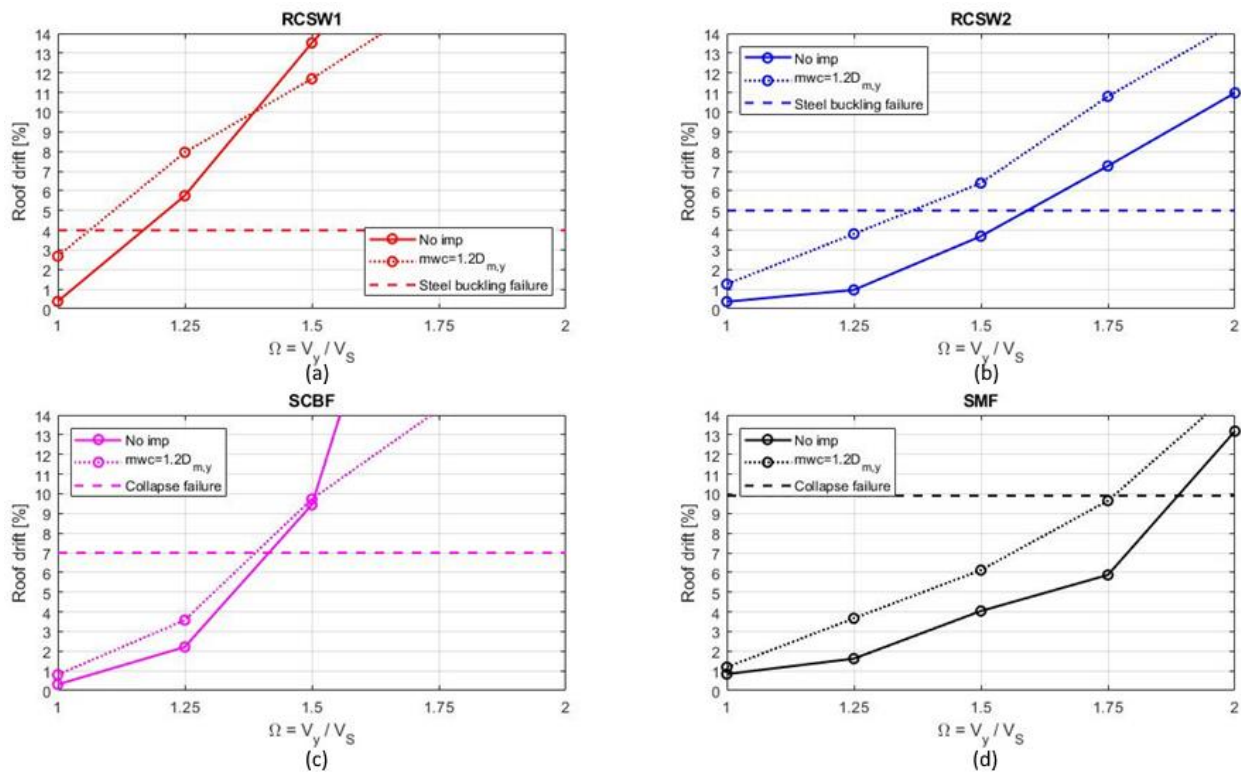


Figure 3.10: Seismic assessment with and without moat wall pounding for different superstructure strengths

Across all archetypes, a reduction in strength is associated with increased roof drifts, both in scenarios without and with pounding effects, with the cases experiencing pounding displaying the largest roof drifts. The pounding effects significantly influence the performance at Ω values

between 1 and 1.5. The RCSW1 and SCBF archetypes with reduced strengths show a pronounced susceptibility to pounding effects with a poor performance. In contrast, the RCSW2 and SMF archetypes exhibit a good performance, with roof drift increments due to pounding between 1.4 to 2 times the baseline scenario.

Above $\Omega=1.5$, two distinct behaviors emerge: for the RCSW1 and SCBF archetypes, excessive yielding driven by the reduced strength dominates the nonlinear response of the superstructure. In these cases, pounding has a minimal effect as the superstructure reaches a collapse state prior to pounding occurs. Conversely, for the RCSW2 and SMF archetypes, the superstructure does not reach collapse state limits, with pounding causing the most substantial increases in roof drifts.

Conclusions

This paper studies the performance of base-isolated structural systems subjected to beyond-design basis earthquake loading, with a focus on the nonlinear performance of the superstructure. The superstructures were characterized using the results of a comprehensive study to evaluate the FEMA P-695 methodology for quantifying seismic performance factors. Four distinct archetypes were used, ranging from ductile to non-ductile behavior, thus characterizing a wide range of structural systems typically used in practice.

The Incremental Dynamic Analysis results show that all base-isolated systems perform as intended in the design-basis demand range. After yielding, the more ductile systems exhibit better performance with controlled roof drift increments compared to the more brittle systems. Ductile systems exhibit a satisfactory performance up to 1.4 times the demand level expected to yield superstructure, while the limited ductility system show a rapid increase in drifts beyond collapse limit states.

A parametric analysis was conducted to determine the sensitivity of the backbone curve parameters, with the ductility capacity having the most significant impact on performance after yielding when compared to the post-yielding stiffness ratio and the failure slope ratio. Although there is no clear trend on what the minimum requirement is for these three parameters given that the linear period of the superstructure and the roof drift yield also influence the nonlinear behavior. No single parameter can significantly change the performance trend of the system, especially if it lacks deformation capacity. To improve the seismic performance of a non-ductile system, the results show that avoiding or postponing the onset of yielding by providing a larger yield strength significantly improves the seismic performance.

Furthermore, the study addresses moat wall pounding given the use of beyond-basis design ground motions, which may lead to large displacement that could surpass the clearance provided. The pounding effects comparison suggests that yielding of the superstructure followed by pounding increases the drift ratios by at least 1.5 times across all archetypes. Reductions in superstructure strength are linked to increased roof drifts in scenarios both with and without pounding, doubling the roof drift when pounding occurs. However, in more brittle systems with reduced strength, excessive yielding dominates the nonlinear response. In these cases, pounding is irrelevant because the superstructure reaches a collapse limit before pounding occurs.

Overall, this study contributes towards better understanding the seismic performance of base-isolated structures, particularly their behavior beyond design-level ground shaking. It demonstrates the importance of ductility in improving the collapse capacity of structures, a factor not considered in current building design code provisions.

Acknowledgements

Chapter 3 contains unpublished material coauthored with Elwood, Kenneth J. and Mosqueda, Gilberto. The dissertation author was the primary author of this chapter. I am

profoundly grateful to Kenneth J. Elwood and Gilberto Mosqueda for their invaluable guidance and support, which significantly enriched the quality and depth of this dissertation. Their expertise, mentorship, and encouragement have been instrumental in shaping the direction and outcomes of this research endeavor.

Chapter 4 EVALUATION OF SEISMIC ISOLATION RETROFIT FOLLOWING EARLY DESIGN STANDARDS: A CASE STUDY

Abstract

Seismic isolation has been widely applied for the design of new structures and for retrofit applications, especially of historical structures. The isolated building superstructure is designed to remain essentially elastic for the considered seismic hazard, with development in design standards evolving towards stricter requirements over the last decades. To further examine early retrofit applications of seismic isolation, a seismic performance assessment is conducted on a building retrofitted with base isolation in the early 1990s. The building structure is evaluated considering current seismic evaluation and design requirements for the isolation system and design constraints imposed by the existing non-ductile superstructure and available moat wall clearance. A feasible domain of the isolation system properties that provide adequate performance are identified, considering the effects of moat wall pounding and isolation system property modification factors. Increasing the effective isolation period combined with supplemental damping is shown to reduce demands on the superstructure while maintaining reasonable isolation system displacements. Importantly, supplemental linear viscous damping beyond 15 percent of critical was shown to have limited benefit causing increasing shear forces on the superstructure. This study demonstrates that the retrofit of existing base-isolated buildings can be a balance between the superstructure base shear and the isolation system displacement capacity and provides a framework for evaluating design alternatives.

Introduction

Seismic isolation is considered one of the most effective earthquake protection strategies for the design of new buildings or for seismic retrofit, especially historical structures [36]. The superstructure is designed to remain essentially elastic for the forces considered and thus expected to survive a design-level earthquake with no structural damage. Design standards for

seismic isolation were first introduced into building codes in the 1991 UBC [37], with subsequent revisions evolving towards more stringent design criteria. This is evident in the observed trend of more recent designs having a larger displacement capacity in the seismic isolation system [27]. Notably, one early implementation of seismic isolation has undergone a retrofit that included increasing the displacement capacity [38].

Current standards for the design of seismically isolated buildings have introduced more conservative requirements with ASCE 7-16 [31] providing the most recent significant changes. Evaluations of the minimum design standards for seismically isolated buildings in ASCE 7-16/22 [1] using the methodology proposed in FEMA P-695 [19] indicate they may not be sufficient and result in an unacceptable probability of collapse when subjected to MCE level shaking [26]. Considering evolving requirements, seismically isolated structures designed to earlier standards are likely to fare much worse. These recent probabilistic studies highlight a concern in seismically isolated buildings in that once a limit state is reached, the performance rapidly degrades. Yielding of the superstructure [7], exceedance of the moat clearance and consequent pounding [26], or failure of the bearings that support the structure [26] have all been considered indicative of imminent failure.

To further examine early applications of seismic isolation, a 3-story building with a 3-story tower in the city of Los Angeles, California, USA is subjected to a performance assessment. The building was designed in the late 1920s and later retrofitted with base isolation in the early 1990s following 1988 UBC [39]. These standards were intended for use in the design of new base isolated buildings but were extrapolated for retrofit applications in this case. The building in its current isolated state is evaluated using the latest standards for seismic evaluation and retrofit of existing buildings (ASCE41-17 [24]). ASCE41-17 defines Basic Performance

Objectives for Existing Buildings (BPOE) based on Risk Categories. For a Risk Category II building, as is the case for the subject building in this study, the Basic Seismic Performance is Life Safety for a Basic Safety Earthquake-1 (BSE-1E) event with a 20% probability of occurrence in 50 years and Collapse Prevention for a Basic Safety Earthquake-2 (BSE-2E) event with a 5% probability of occurrence in 50 years.

The initial phase of the study assesses the seismic performance of the building in its current condition based on ASCE41-17 using simplified models, with the purpose of identifying controlling limit states. Subsequently, the focus shifts towards improving the seismic performance, considering potential design space constraints and how the seismic isolation system properties affect performance. In the context of the structure examined, the limitation of the available moat wall clearance and the existing strength capacity of the superstructure are considered in terms of reducing the complexity of the retrofit solutions.

Evolving standards for seismic isolation

Prior to the seismic assessment of an early application of seismic isolation, it is worthwhile reviewing the evolving state of practice as dictated by design standards over the last decades. The focus here is on design standards [1,24] while the history and development of seismic isolation technology can be found elsewhere [40]. Two main factors have contributed towards more stringent design of isolated structures: updates to seismic hazard design maps and updates to design standards based on improved knowledge of seismicity and structural behavior, respectively. Considering the documented code requirements, the codified provisions for seismic isolation were first introduced into the 1991 UBC as an appendix to Chapter 23. These provisions were based on the work of the Structural Engineers Association of California (SEAOC [41]). ASCE 7-93 [42] later introduced a section on ‘Provisions for Seismically Isolated Structures’ within Chapter 9 (Earthquake Loads), and in 2005 [22] became Chapter 17 ‘Seismic

Design Requirements for Seismically Isolated Structures’. The ASCE 7-93 design standards sustained limited changes from its initial incorporation until substantial revision appeared in ASCE 7-16. Table 4.1 contains a summary of key base isolation design parameters for three distinct codes focusing on: (i) the required base shear for the structure including allowable strength reduction factors (R_I), (ii) superstructure drift limits, and (iii) seismic isolation design displacement.

Table 4.1: Changes within the code over the years

	UBC91	ASCE7-1993	ASCE7-16
DBE	10% 50yr	10% 50yr	10% 50yr
MCE	10% 250yr (2.1% in 50yr)	2% in 50yr	2% in 50yr
Superstructure design forces	DBE	DBE	MCE _R
R_{I,min}	R _{wl,min} =1.5	R _{I,min} =1.0	R _{I,min} =1.0
R_{I,max}	R _{wl,max} =3.0	R _{I,max} =2.0	R _{I,max} =2.0
Drift Limit - response spectrum analysis	0.015/R _{wl}	0.015hsx	0.015hsx
Drift Limit - response history analysis	0.020/R _{wl}	0.020hsx	0.020hsx
Bearings design	DBE	MCE	MCE
Bearing Properties	N/A	Kmin/Kmax	lambda factors

Table 1 reveals four major updates within the design of base-isolated structures. The first is the characterization of the seismic demand. In the early stages, as exemplified by the UBC

1927 [43], the seismic hazard was characterized as 'earthquake shaking', without any quantification of intensity or associated probability. Subsequently, classifications such as Minor, Moderate, and Major earthquakes were introduced in the SEAOC Blue Book, which later evolved with a more precise definition of "code ground shaking," as having a 10% probability of exceedance within a 50-year timeframe and labeled as Design Basis Earthquake (DBE). In 1997 the national seismic hazard mapping was introduced, addition a new term reflecting a 2% probability of exceedance within a 50-year period labeled as 'Maximum Considered Earthquake' (MCE) ground motion with the DBE demand defined as two-thirds of the MCE demand. In 2016, the Risk Targeted Maximum Considered Earthquake (MCE_R) ground motion maps were introduced to replace the MCE maps, to incorporate a risk-targeted approach to ensure uniform likelihood of collapse across varying seismic regions. In general, these changes have resulted in increased seismic demand.

The second major change is related to the design forces above the isolation level that is the superstructure minimum required base shear. The UBC 91 and ASCE 7-93 to ASCE7-10 use the same equation based on the resisting force of the isolation system at the DBE design displacement. In ASCE 7-16, the resisting force is obtained from the isolation system design displacement based on MCE_R demands. Additionally, ASCE7-16 incorporates additional factors such as the effective weight above the isolation interface and the total effective damping to estimate the minimum superstructure base shear.

The third major change is related to the strength reduction factor, R_I . In the UBC 91 code, the R_I values (called R_{wl}) were based on tables to characterize the structural system and lateral load-resisting mechanism, resulting in values ranging from 1.5 to 3.0. With ASCE 7-93 the

allowable R_1 is reduced to $2/3$ of the assigned Response Modification Factor (R) value for a structural system and limited between 1.0 and 2.0.

The fourth major change is related to bearing design requirements. Since ASCE 7-93, the design of the isolation system has been based on MCE seismic demands, while previously it was based on DBE. Potential variations in bearing properties from nominal were considered first by the maximum and minimum effective stiffness using the cyclic test data, often available after the design process. Property modification factors (λ factors) were introduced in ASCE 7-16 to better characterize the expected variability of the bearing properties. Upper and lower bound values for property modification factors consider the effects of the environment, aging, and uncertainty [44]. The required displacement capacity of the seismic isolation system and the superstructure design base shear are determined as the largest value for the range of bearing properties considered.

As shown, the code provisions for base-isolated structures have evolved towards more stringent design for the isolation system and the superstructure. Initially, the focus of base isolation was primarily on the decoupling of the superstructure from ground motion, with the intent to mitigate the transfer of seismic energy into the building and, consequently, reduce damage. However, as the field of seismic engineering has advanced, the understanding of base-isolated structures has deepened, leading to more stringent design requirements.

Description of Building

The building examined in this study was originally designed and constructed with a conventional base (i.e., conventional shallow foundation system consisting of spread and continuous concrete footings) according to the specifications of the 1927 UBC. An isometric view of the fixed base building in structural analysis software is shown in Figure 4.1. The superstructure has three full stories composed of three distinct structural systems: reinforced

concrete (RC) shear walls, unreinforced masonry (URM) shear walls, and reinforced concrete frames. A tower extends an additional three stories composed of unreinforced masonry (URM) shear walls and reinforced concrete frames, which leads to irregularities in vertical stiffness and strength.

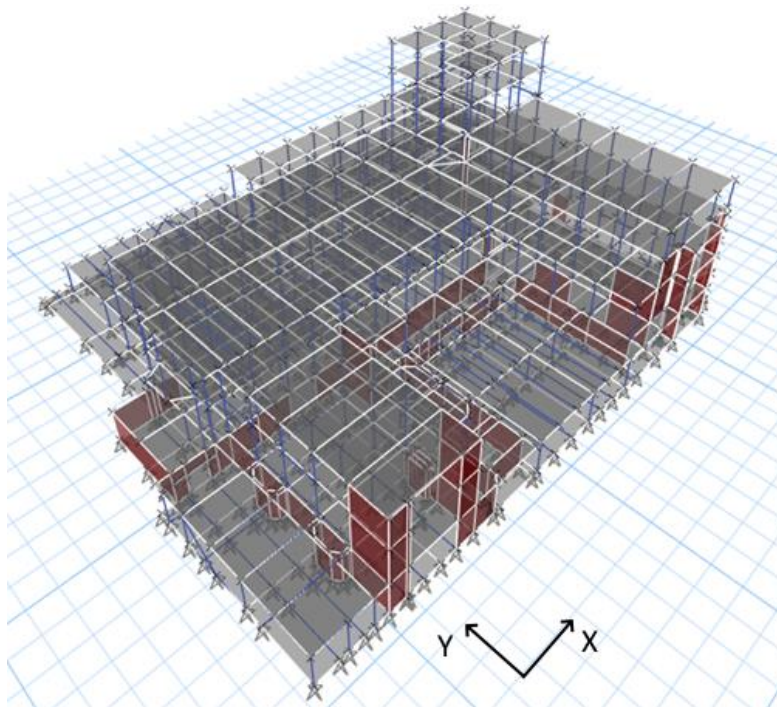


Figure 4.1: Isometric view of full building model

The fixed-based fundamental translational period (T_{fb}) in the x-direction was estimated at 0.93 sec and 0.56 sec in the y-direction, with a superstructure weight (W_s) of 65,140 kN. The building was retrofitted in 1994 using seismic isolation based on UBC 1988 guidelines. This retrofit consisted of 132 elastomeric bearings with and without lead cores installed at the basement level with a design displacement of 200 mm, an effective period (T_{eff}) of 2 sec, and a total weight (W_T) of 97,224 kN including the added mass. A significantly larger moat wall clearance of 457 mm was provided around the structure.

Development of simplified models

Model of seismic isolation system

The characterization of the isolation system is based on testing conducted as part of the retrofit to verify bearing properties under the expected vertical loads. Force-deflection plots were used to derive parameters for a smooth bilinear model (Bouc-Wen [18]) identified in Figure 4.2a. From this data, a linear model based on the effective stiffness and damping is also derived that is dependent on the peak displacement.

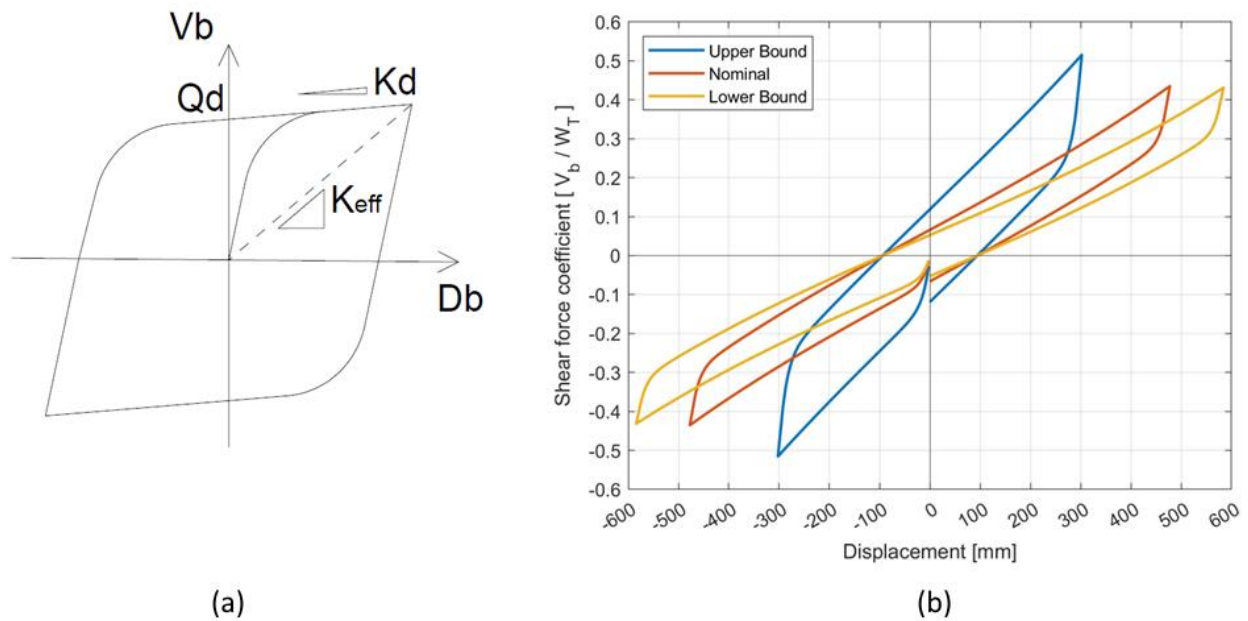


Figure 4.2: Models for the isolation level

The nonlinear model is characterized by: (i) the characteristic strength (Q_d) and (ii) the post-yield stiffness (K_d), for which the nominal values were obtained from the as-built drawings and testing report. The initial stiffness, K_1 , is not considered a critical parameter and set to $10K_d$. Given that the performance assessment is conducted on an existing building, the property modification factors from Table 14-1 of ASCE 41-17 are used to establish upper and lower bound limits of the bearing properties, with λ_{max} equal to 1.8 for Q_d and K_d , and λ_{min} equal to 0.8

for Q_d and K_d . The estimated system properties are shown in Table 4.2, where the isolation period (T_d) is shown instead of the post-yield stiffness K_d .

Table 4.2: Property modification factors for an existing system

	Lower Bound	Nominal	Upper Bound
Q_d/W_T [%]	5.2	6.6	11.8
T_d [s]	2.73	2.40	1.78

Figure 4.2b shows the hysteresis loops for the nominal, lower and upper bound properties of the isolation system. The plot highlights the range of behavior considered with the property modification factors and the resulting displacement and base shear values obtained under the same demand.

6DOF model of superstructure

A nonlinear model of the superstructure is first derived using backbone curves derived following ASCE41-17. The wall dimensions and detailing were obtained from available drawings of the building. Figure 4.3a shows the considered strength per unit length of the wall elements. The URM walls have a limited deformation capacity, reaching failure at 1% drift and providing minimal strength contribution. The RC walls are the main lateral force-resisting elements and provide a deformation capacity of up to 2% drift ratio. The moment-rotation behavior of the RC frame beam elements per story is shown in Figure 4.3b, with a sharp decline in capacity for the tower in stories 4-6. It is assumed that the walls are controlled by shear deformation while the frames are controlled by flexure.

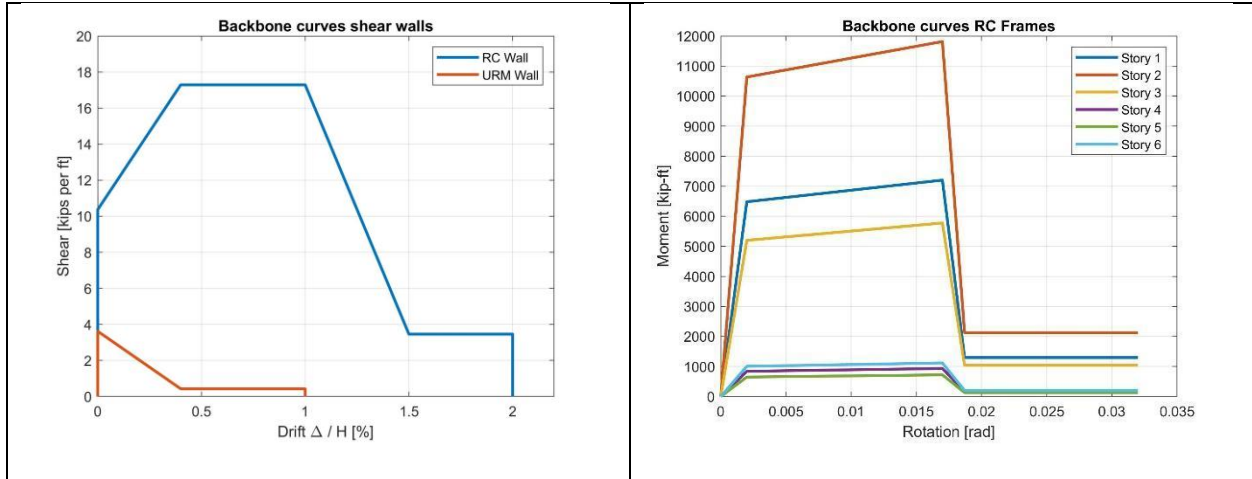


Figure 4.3: Backbone curves for (a) shear walls (b) frames

The reduced order nonlinear model (6DOF model) presented in Figure 4.4 is used to perform a seismic assessment of the building in its current state. While isolated buildings are generally expected to exhibit linear behavior, the model considers potential nonlinearities that may occur if the initial design capacities are surpassed.

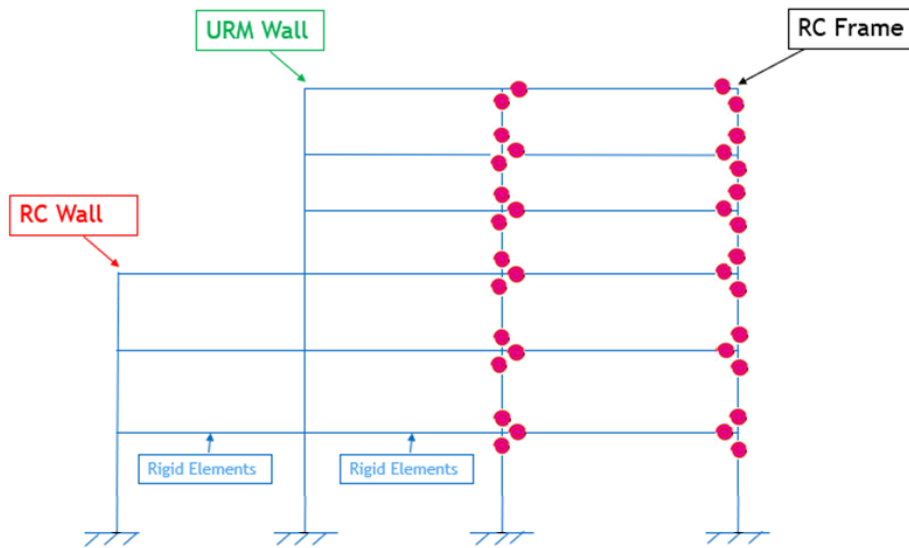


Figure 4.4: 6DOF model

The proposed model represents each structural system separately connected through rigid elements. The model includes a single column with shear springs for the wall elements (one RC

wall and one URM wall) and a single bay frame with beam-column elements including plastic hinges for the RC frame system. The discontinuity in horizontal stiffness due to the absence of RC walls on the top three levels is accounted for in the model. The base isolation layer is represented by four identical bearings, one under each column that sums to the equivalent system properties to the whole system.

Figure 4.5 shows the results of a pushover analysis performed using a mass equivalent load pattern applied to the shear frame shown in Figure 4.4. The load pattern recommended for isolated buildings in ASCE 41-17 resulted in an unrealistically low yield strength resulting from the stiffness irregularity of the superstructure and dominated by the tower. This decision was informed by prior knowledge of the expected behavior of the shear frame model under dynamic loading and is verified later by time history analysis.

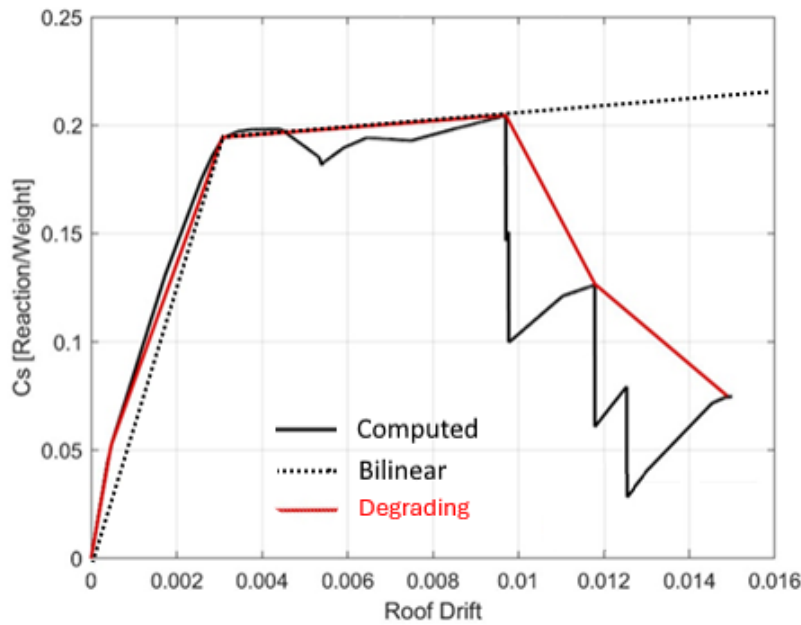


Figure 4.5: Superstructure capacity estimation: computed, bilinear, degrading

Reduction to 2DOF model

Simplified analysis models typically used in practice to provide estimates of seismic demands are examined. The simplest model used in the Equivalent Lateral Force (ELF)

procedure (ASCE 7-22) assumes a rigid superstructure on the isolation system modeled with the effective linear properties. The linear models utilize the effective linear stiffness and damping for the bearings that is dependent on the peak displacement. In the next level of complexity, the structural flexibility can be captured by a two-degree-of-freedom (2DOF) model representing the structure as a SDOF on top of the isolation system. Two types of superstructure models are considered: a linear model with the initial properties determined by the push over analysis and a bilinear model with a post-yield stiffness set to 3% of the linear elastic stiffness. The simplified model follows the pushover curve in Figure 4.5. Similarly, effective linear properties and bilinear models are considered for the seismic isolation system.

Performance Evaluation

Simplified models

A preliminary evaluation of the existing isolated structure is performed using simplified models under the corresponding ASCE 41-17 BSE-1E and BSE-2E seismic hazards. The ELF procedure is applied using the generated response spectrum for the site and Time History Analysis (THA) is conducted using eleven horizontal ground motion sets chosen and scaled for each hazard level through the PEER Ground Motion Database [45]. Figure 4.6 shows the calculated isolation system design displacement, D_b , for models of increasing complexity using lower-bound properties per ASCE-41. The displacement reported for THA is the average value of the eleven ground motions recorded using OpenSees [34]. The SDOF model includes the total weight on the isolation layer. The 2DOF model has the superstructure weight, W_s , at the top node and the isolation layer weight, W_b , at the lower free node.

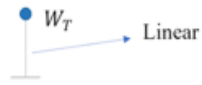
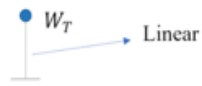
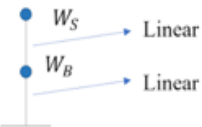
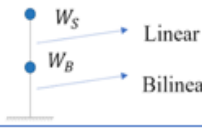
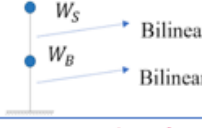

Model:	Analysis Type:	Model Approximation:	BSE-1E Result:	BSE-2E Result:
A	Seismic Response Spectral Analysis (SRSA)		$D_b = 183 \text{ mm}$	$D_b = 472 \text{ mm}$
B	Linear Time History Analysis (LTHA)		$D_b = 179 \text{ mm}$	$D_b = 434 \text{ mm}$
C	LTHA		$D_b = 171 \text{ mm}$	$D_b = 414 \text{ mm}$
D	Non-Linear Time History Analysis (NLTHA)		$D_b = 125 \text{ mm}$	$D_b = 330 \text{ mm}$
E	NLTHA		$D_b = 123 \text{ mm}$	$D_b = 297 \text{ mm}$
F	5DOF		$D_b = 122 \text{ mm}$	$D_b = 304 \text{ mm}$

Figure 4.6: Model Comparison Utilizing Isolation System Lower Bound Properties with BSE-1E and BSE-2E Hazard using Lower Bound Properties

Considering a SDOF model with rigid superstructure, Model A and B give the most conservative results and the similar outcome verifies the adequate scaling of ground motions. Only the Seismic Response Spectral Analysis (SRSA) computed displacement D_b exceeds the moat wall clearance of 457 mm under the updated seismic hazard with lower bound bearing properties. This indicates that the available moat wall clearance could be sufficient for the updated seismic hazard. Model C introduces the structure flexibility through the 2DOF linear model and shows a further reduction in bearing displacements as deformations are transferred to the building superstructure.

The use of a smooth bilinear hysteretic model is considered more accurate for the isolation system [46] and introduced in Model D with a linear superstructure and Model E with a

nonlinear superstructure. The use of nonlinear bearing models results in a significant reduction in displacements in the isolation system. The nonlinearity of the superstructure has a minor reduction in the isolation system displacement for BSE-1E shaking and is more pronounced as the superstructure yields for the BSE-2E hazard. Model F represents the most detailed model of the building considered. The displacement at the isolation interface for both seismic hazard intensities is comparable, suggesting that the results from Model E are adequate.

Overall, the more complex models show a decrease in the isolation system displacement, with a reduction of about 33% from the initial estimation for BSE-1E and 41% for BSE-2E. The fully nonlinear simplified model, Model E, estimates an average ductility demand of 5.3, greater than the expected ductility capacity shown in Figure 2. The response estimates provided by Model E and Model F considering the building capacity is further investigated in the next section.

Notably, the simpler models provide more conservative results and were likely used at the time of the original retrofit design of the isolation system. Considering the changes in design standards presented earlier, the simplified analysis may have provided additional conservatism to early design standards while THA has become more prevalent in more recent designs.

Comparison of the 2DOF model with the full 6DOF model

Previous studies have demonstrated the effectiveness of 2DOF models in capturing the dynamic response of base-isolated structures and insight into the dynamic interplay between the structure and the isolation system [6–8,10,11]. Analytical studies have leveraged simplified 2DOF models to explore inelastic superstructure demands, including ductility, under varying design parameters like superstructure stiffness, post-yield stiffness ratio, natural frequency, and ground motion characteristics. The use of a nonlinear 2DOF model to estimate the seismic response for the structure considered here is examined, including for damage states and post-

yield response, and compared to the 6DOF model to identify which parameters can be well estimated.

Figure 4.7 shows the resulting isolation system lateral displacement of both models when subjected to loading for each of the respective ground motions. The mean value of isolation displacements is within a 5% difference. In general, the 2DOF model results seems to overpredict for lower values of displacements and overpredict for records producing the larger displacements.

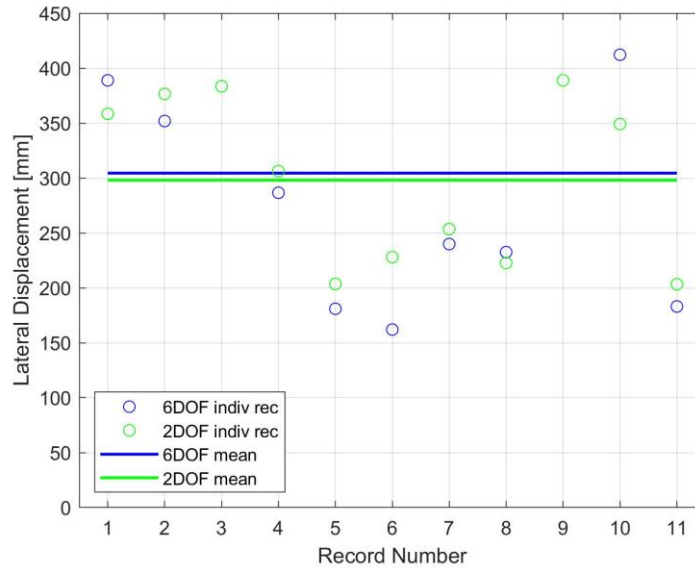


Figure 4.7: Isolation system lateral displacement using 6DOF and 2DOF model

Figure 4.8 compares the results obtained with the 6DOF and the 2DOF model, where the 6DOF model shows a mean IDR profile with a maximum drift at the fifth level, indicating a high likelihood of collapse of the tower. The response to the individual ground motions shows the variation in the building response with the shifting stories with large drifts. In contrast, the 2DOF model only provides an estimate of the global superstructure drift, which is a significant limitation for this irregular structure. In the simulations that follow, the reduced order nonlinear

model (6DOF model) is used to conduct comprehensive parametric analyses considering variations of the base isolation systems properties.

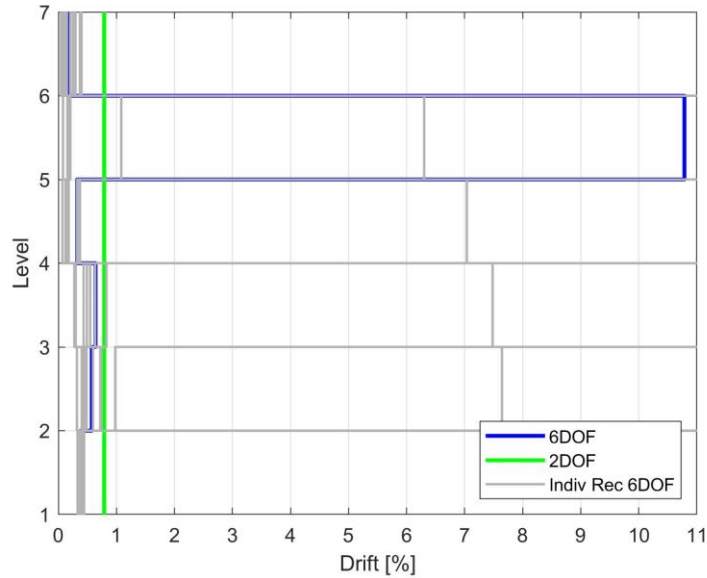


Figure 4.8: Interstory Drift using 6DOF and 2DOF model

Finally, the superstructure base shear coefficient for each record is compared, as shown in Figure 4.9. The 6DOF model shows an average shear coefficient of nearly 25%, whereas the 2DOF model has an average of 21%. The 6DOF model dynamic behavior shows a larger capacity compared to the static pushover analysis results using a mass equivalent load pattern, which is not the recommended load pattern for isolated buildings in ASCE 41-17, which resulted in an unrealistically low yield strength. The findings in Figure 4.9 prompted a reevaluation of the load pattern assumption, ultimately favoring the mass equivalent load pattern.

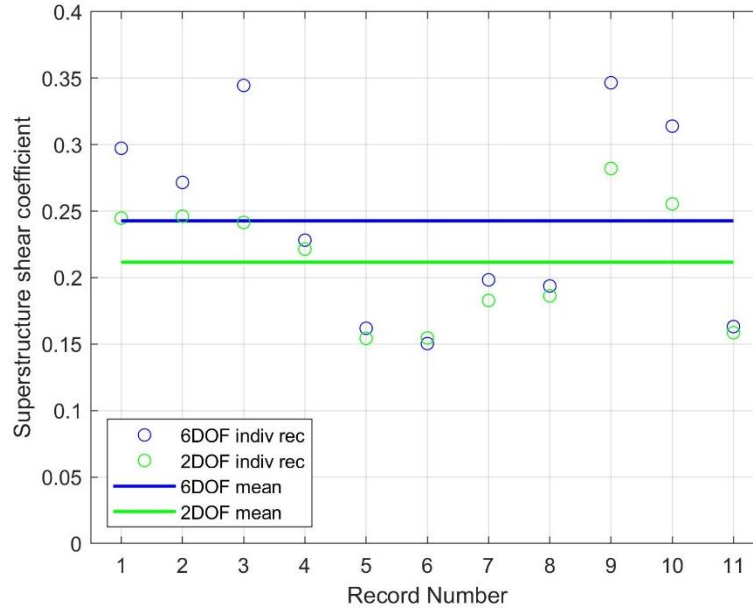


Figure 4.9: Superstructure shear coefficient using 6DOF and 2DOF model

Feasible Domain Analysis for the 6DOF Model

The minimum required seismic performance for the building under the BSE-2E hazard level is Collapse Prevention. To comply with this performance criteria, it is necessary to limit drifts in the superstructure. Initially, considering no modifications to the historic structure, the design space for the base isolation system is evaluated to examine effects on the superstructure. The seismic assessment is quantified using two normalized Engineering Demand Parameters (EDP): i) the isolation system lateral displacement normalized by the moat wall clearance of 457 mm, and ii) the peak Interstory Drift Ratio (IDR) normalized by the URM walls deformation capacity equal to 1%.

Dynamic analyses are conducted on the 6DOF model utilizing the eleven scaled ground motions for the BSE-2E hazard. The isolation system properties are characterized by the characteristic strength (Q_d) and the post-yield stiffness (K_d) considering nominal values. The considered range for parameter Q_d is between 3% and 10% of the total weight of the superstructure to ensure a reasonable activation force and effective damping value. Values of

$Q_d/W_T=10\%$ generate an effective damping of around 35%, which strongly influences the superstructure force distribution and leads to higher mode contributions [20]. The range for T_d is examined between 2.5 sec and 4.5 sec, with the lower bound close to the existing isolation system second slope period and the upper bound set to practice standard limits.

Figure 4.10a shows the surface representing normalized mean displacement of the isolation system, with displacements well beyond the moat wall clearance for lower Q_d and longer T_d values. Figure 4.10b shows the surface for the resulting normalized IDR, which is controlled by the response of the tower. The rapid increase in IDR is evident once yielding occurs in the superstructure, especially for decreasing T_d values. These two plots show the trade-offs between distribution of demands between the structure and isolation system for a given set of seismic isolation system parameters.

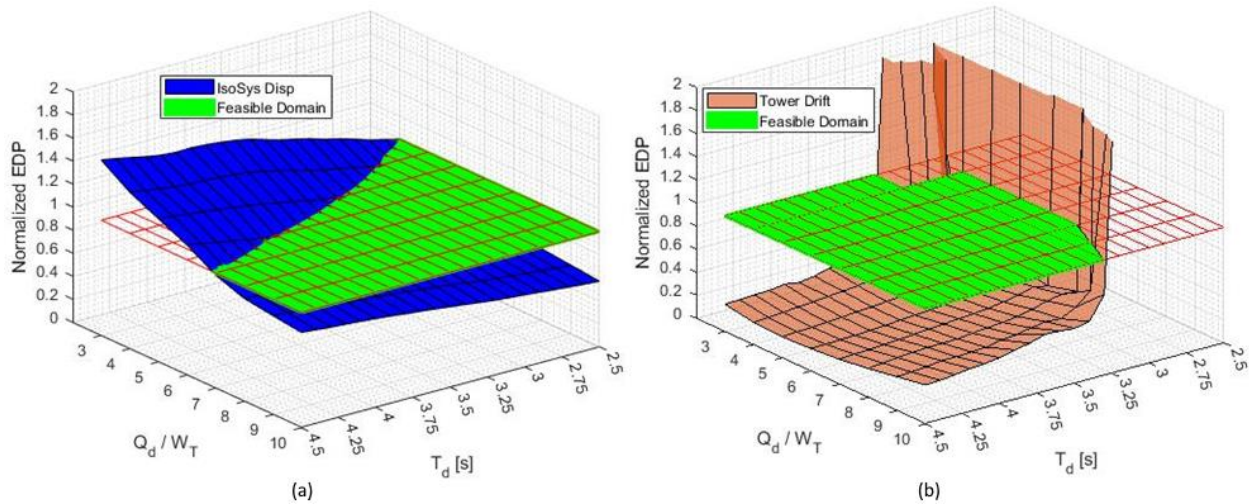


Figure 4.10: Feasible domain surface per EDP (a) Isolation System Lateral Displacement (b) Tower Drift

The results shown in Figure 4.10 can be combined to identify the feasible domain of isolation system properties that provide adequate balance of demands between the base isolation system and the superstructure. Figure 4.11 shows the intersection of both normalized EDP surfaces, for which the region with both EDP surfaces below a value of one represents the

feasible domain. The identified surface can provide preliminary design values to target for the isolation system.

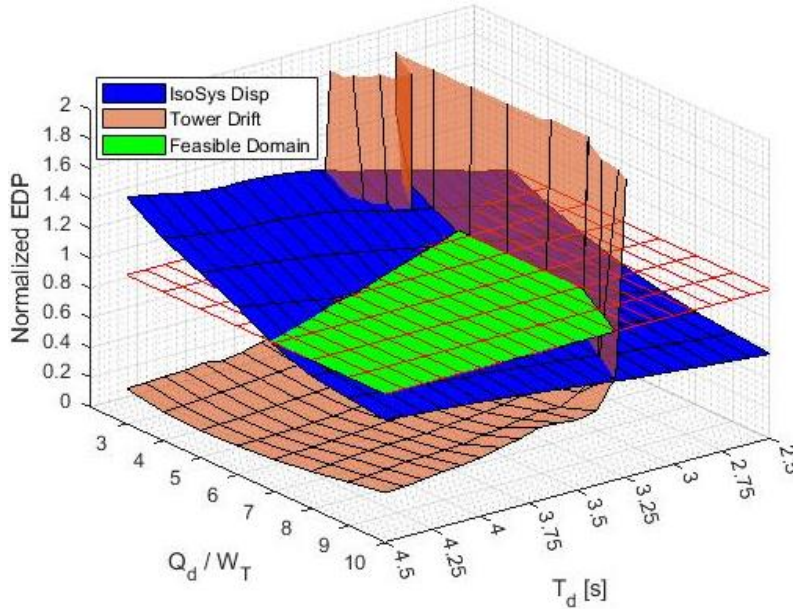


Figure 4.11: Design feasible domain for isolation system nominal properties

Moat wall pounding

Exceeding the moat wall clearance can result in impact between the base slab of the structure and the basement retaining wall. While the effects of moat wall impact are not typically considered in design, the resulting impact force can result in a substantial increase in accelerations and story drifts [3]. To quantify these effects, a gap material is added to the model using a uniaxial Hertz contact element [28] placed at the impact location, assuming a coefficient of restitution equal to 0.7.

Figure 4.12 shows an updated surface representation of the feasible domain considering the effects of impact for varying properties for the isolation system. The set of isolation parameters providing acceptable performance is shown to decrease especially for the lower values of Q_d . In contrast to Figure 4.11, the maximum average isolation displacement is limited

to a value of about 1.05, due to deformations in the moat wall. For the regions where pounding occurs, the superstructure drifts increased rapidly.

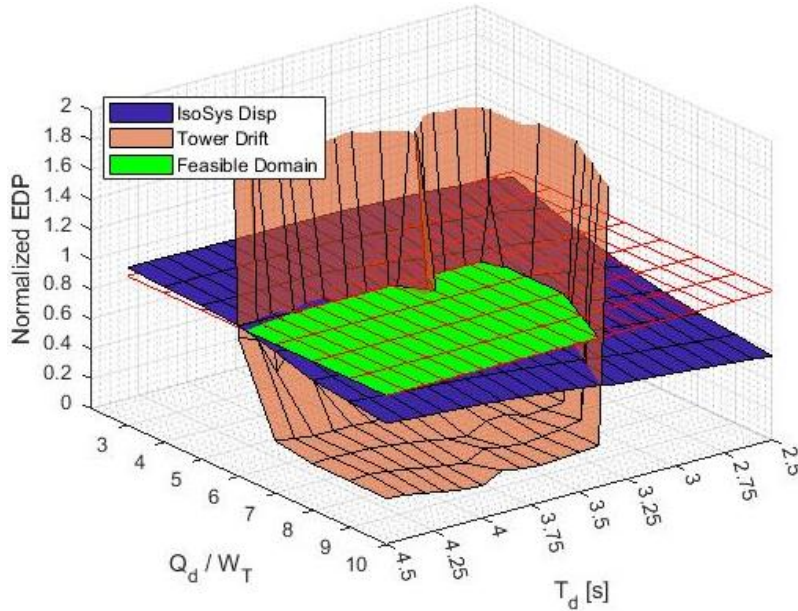


Figure 4.12: Design feasible domain for isolation system nominal properties

These findings emphasize the potential influence of pounding effects in seismic performance assessment of seismically isolated structures. These results are in agreement with previous studies that identify the potential collapse risk associated with pounding and/or yielding in isolated structures [26]. Excluding pounding effects may not adequately capture the expected average response of the structure under the selected ground motions. Standard commercial software does not readily include capabilities for impact modeling, which remains a challenge in practice.

Consideration of property modification factors

Given that a new base isolation system is explored, the property modification factors set by ASCE 7-22 are used to establish upper and lower bound limits of the bearing properties, with λ_{\max} equal to 1.5 for Q_d and 1.3 for K_d , and λ_{\min} equal to 0.8 for Q_d and K_d :

Figure 4.13 shows the resulting feasible domain accounting for the range of bearing properties with property modification factors and moat wall pounding effects. The subplots are divided by stories for the IDR, with the feasible domain mostly limited by the maximum drift in the tower (Figure 4.13d). The feasible domain is limited to a narrow region around $Q_d/W_T=8\%$ and $T_d=4.0$ sec, where the effective damping is around 35% using the property modification factors and resulting in a more stringent feasible domain than the one shown in Figure 4.12 and Figure 4.13.

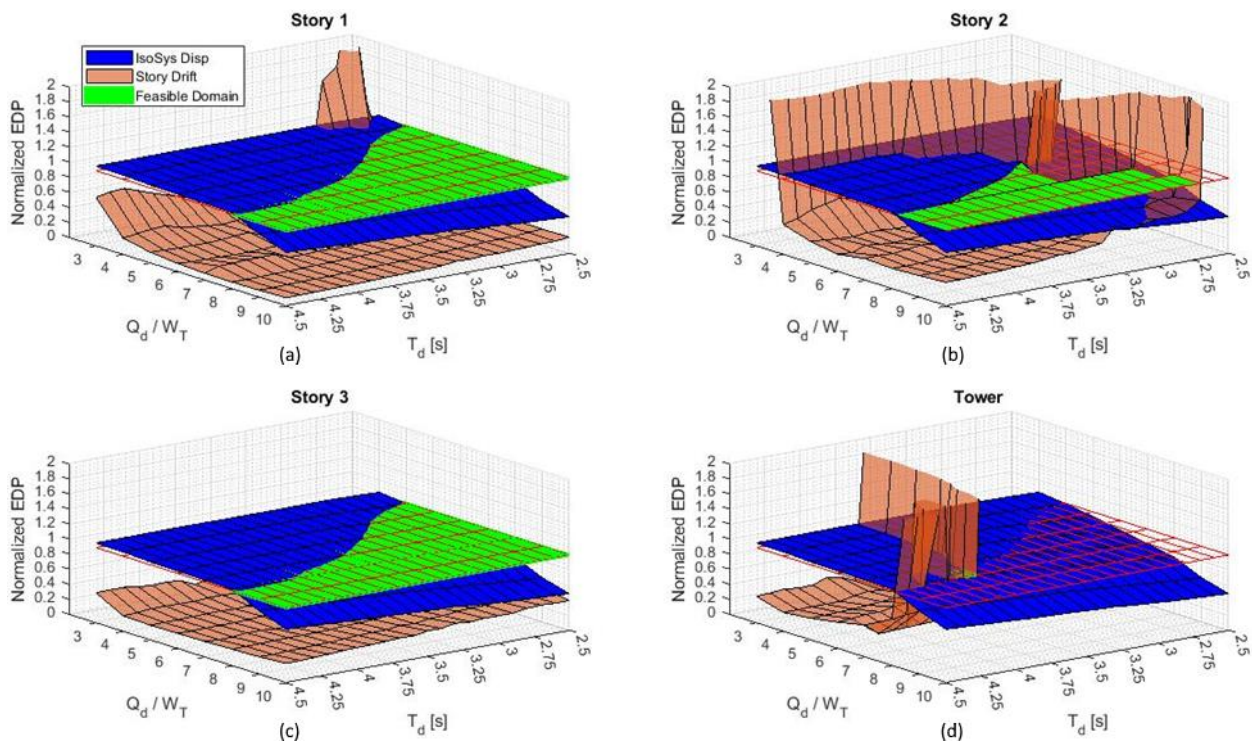


Figure 4.13: Feasible domain design for the isolation system using lower and upper bound properties considering IDR at various levels

To better visualize the controlling performance measures in more detail, the surfaces are subdivided in Figure 4.14, showing the contour line as a function of Q_d and T_d parameters. The tower drift limits control for the majority of the design space considered. This highlights the limited options for modifying the isolation system properties to comply with the Collapse

Prevention performance criteria due to a significant vertical stiffness irregularity and limited strength in the tower.

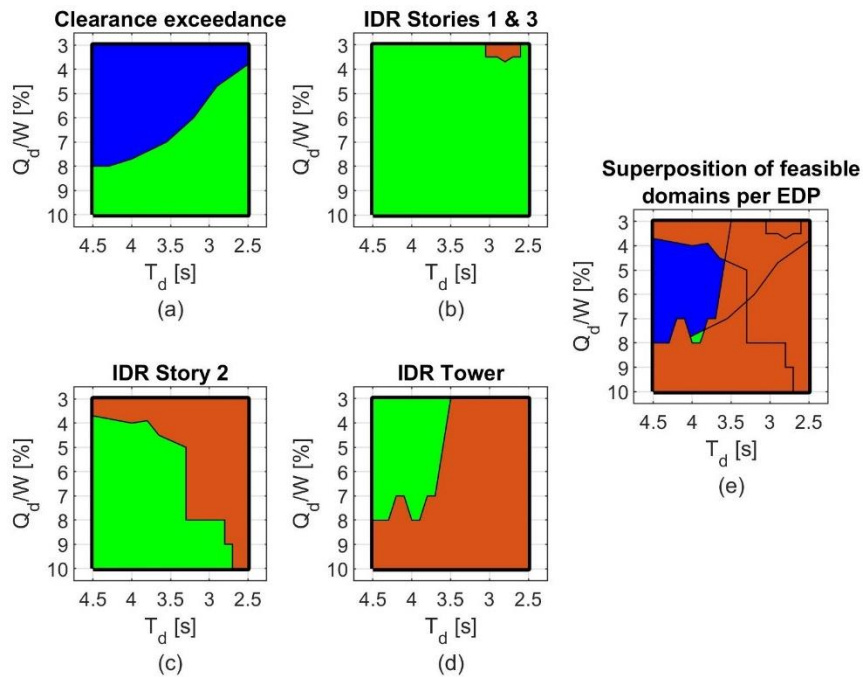


Figure 4.14: Feasible domain per EDP (a) moat wall clearance (b) IDR Stories 1 & 3 (c) IDR Story 2 (d) IDR Tower and (e) overall feasible domain.

Figure 4.14 also provides insights into the performance metric defined by the average isolation system lateral displacement. Over half of the considered domain is not feasible because the average lateral displacement exceeds the moat wall clearance. Furthermore, by exceeding the clearance, the interstory drifts are affected since moat wall pounding transfers large forces into the system. These findings underscore the substantial increase in seismic demand over the years. Initially, the design estimated a design displacement of approximately 200 mm, prompting the provision of a moat wall clearance significantly exceeding this requirement, at 450 mm. Despite these precautions, the clearance seems not sufficient for the retrofit.

Influence of the tower on the feasible domain

The current model of the building including the tower limits the overall building response and solutions for the seismic isolation system. Assuming the tower can be strengthened as necessary, and analysis of the building system is conducted with the tower remaining linear.

Figure 4.15 updates the feasible domain considering a linear elastic tower, and considering both the property modifications factors and an impact element to capture the effects of moat wall pounding. In contrast to the results shown in Figure 4.14 the linear tower shifts the controlling story from the Tower to Story 2 and increases the isolation system feasible domain. In particular, the feasible domain increases for Q_d/W_T in the range between 8% to 10%. Considering both Figure 4.14 and Figure 4.15, the isolation system lateral displacement remains a limiting parameters.

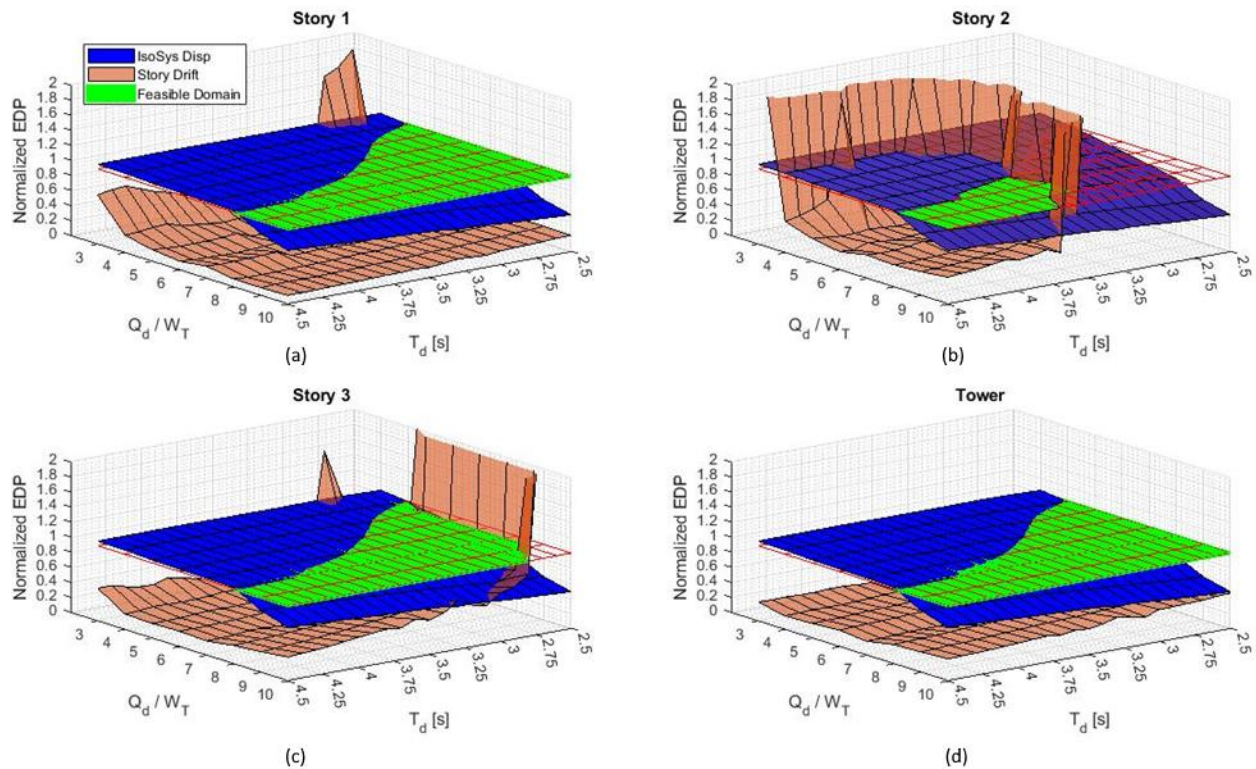


Figure 4.15: Feasible domain design assuming a linear Tower for (a) Story 1 (b) Story 2 (c) Story 3 and (d) Tower

Supplemental damping

Supplemental viscous damping is considered to reduce displacements of the isolation system while minimizing the increase in base shear. Linear viscous damping is considered to add additional damping of 5%, 10%, 15%, and 20%. The building model considers both the superstructure with nonlinear tower behavior and with using a linear model for the tower to examine if the demands on the tower could be reduced sufficiently.

Figure 4.16 shows the feasible domain for the four levels of damping, with the IDR surface corresponding to the maximum drift considering all stories. The supplemental damping increases the feasible domain for all damping ratios considered, with the higher damping showing the most gains. The most significant influence of adding viscous dampers is reducing the isolation system lateral displacement and the potential for pounding. However, the structural drifts increase as the damping increases and noted by the shift of the surface edges moving towards lower values of Q_d and T_d .

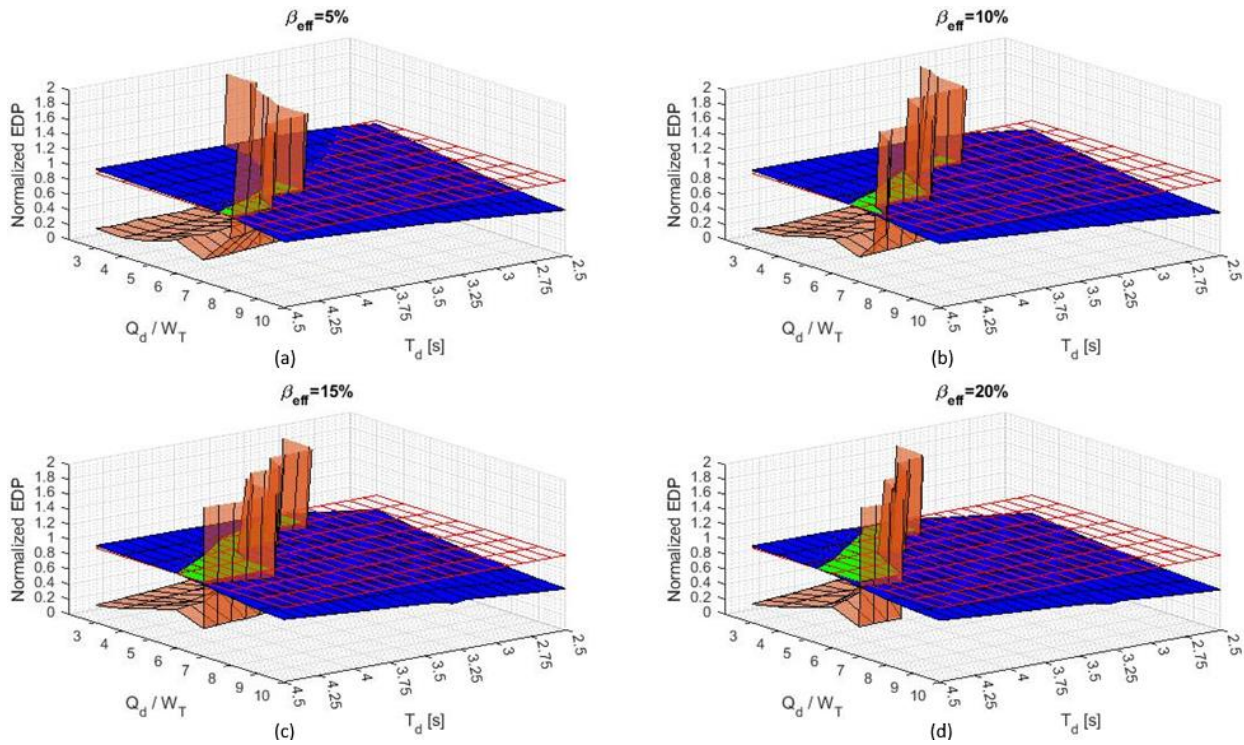


Figure 4.16: Feasible domain with superstructure as is adding viscous damping a) 5% b) 10% c) 15% d) 20%

The results considering the linear behavior of the tower in Figure 4.17 show a significant increase in the feasible domain when compared to its nonlinear counterpart. However, as the effective damping increases, the IDR surface corresponding to larger Q_d values begins to approach and surpass the 1% interstory drift threshold. This is attributed to the increased base shear transferred to the building structure with the supplemental dampers.

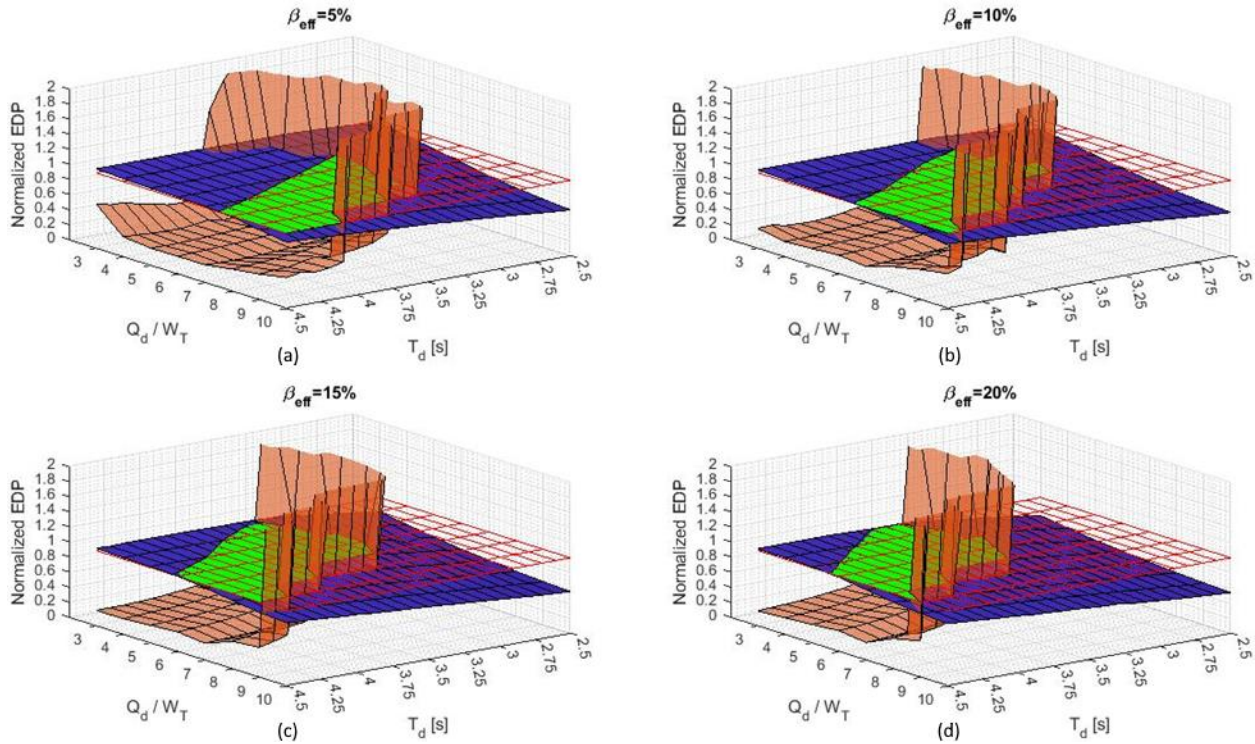


Figure 4.17: Feasible domain with linear tower adding viscous damping for a) 5% b) 10% c) 15% d) 20%

To clearly compare the feasible domains obtained by the different amounts of viscous damping, Figure 4.18 shows an overlapped graphic for both models of the tower. Each colored area represents a range of possible outcomes for different levels of damping. For example, the 20% viscous damping (labeled as 20% VD) area shows where the structure would perform feasibly with this level of added damping. As the viscous damping percentage decreases, the size and position of the feasible domains change, indicating how different levels of added viscous damping influence the seismic response of the structure. The feasible solution considering the nonlinear tower in Figure 4.18a shows a significant increase in the domain, even for small levels of added viscous damping. The feasible domain shifts to lower values of Q_d with increasing viscous damping. The upper boundary moves up as the isolation displacements are reduced. The lower boundary follows upward as the increasing damping results in increased superstructure drifts. The lower values T_d also produces a higher effective stiffness of the isolation system and

transfer larger forces, which increases when adding viscous dampers. It should be noted that the feasible domains show sharp breaks on the contour lines. This stepped contour is primarily attributed to the discretization process applied to the Q_d/W_T axis, which differs from the discretization used for the T_d axis.

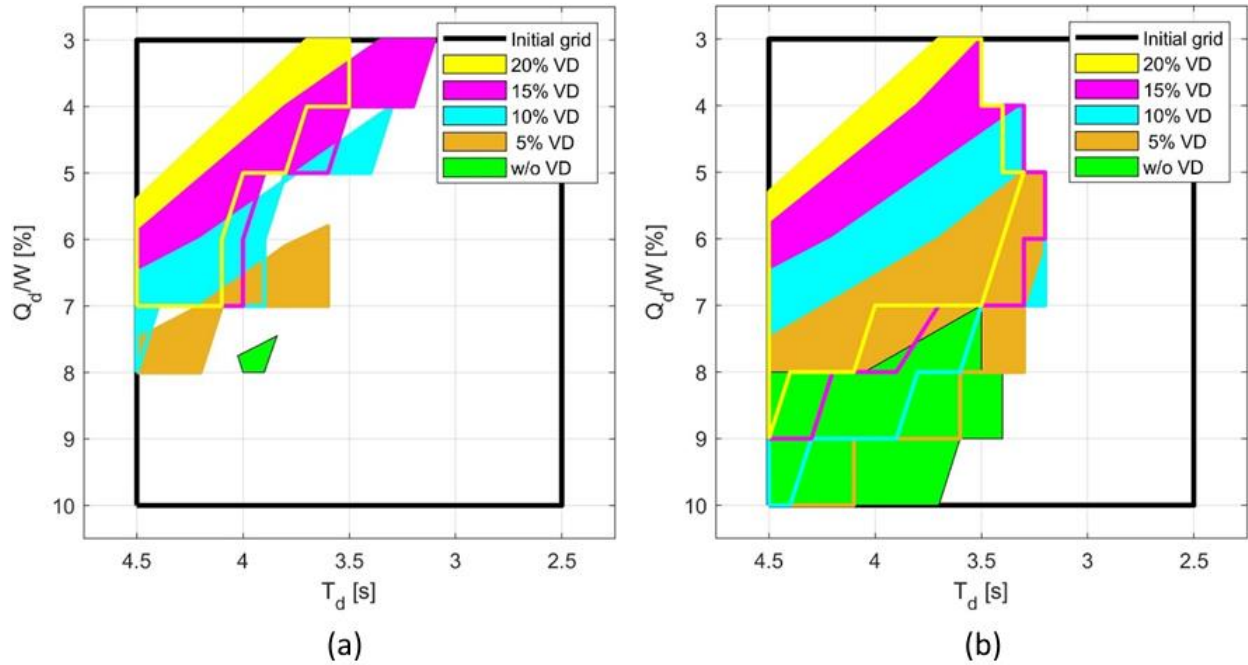


Figure 4.18: Feasible domain for a) superstructure with nonlinear tower, b) superstructure with the linear tower.

Figure 4.18b shows the effects of adding viscous dampers without considering the larger drifts in the tower produced by the nonlinear model. The upper boundary of the feasible domain is similar when compared with Figure 4.18a, but the lower boundary is much lower due to the reduced drifts without considering the tower. The overall areas of each feasible domain in Figure 4.18b remain similar when viscous damping is added, while the areas shift positions towards a larger second slope period and lower activation forces. The results show a disadvantage of increasing the viscous damping when the inherent damping provided by the bearings is already

large, around 25% to 30%, reflected in Figure 4.18a by the removal of feasibility at values characterizing $Q_d/W_T=0.08$ and shown in terms of damping in Figure 4.19a.

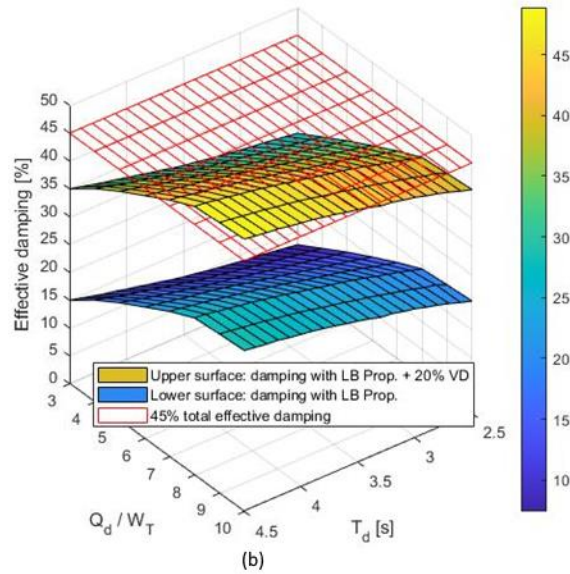


Figure 4.19: Effective damping using Lower Bound Properties with and without adding viscous damping for a) superstructure with nonlinear tower, b) superstructure with a linear tower

These limitations on the contribution of added supplemental damping also arise for the case with a linear tower when reaching a total effective damping values around 45%, as shown Figure 4.19b. Furthermore, the incorporation of supplemental linear viscous damping beyond 15 percent of critical shows limited benefits, since for both the superstructure with the nonlinear and linear tower, the feasible domain surface does not increase, but translates. The translation is the result of lesser lateral displacement by the additional viscous damping on one side of the surface, while the opposite side translates towards the same direction given the increase in superstructure shear forces leading to larger interstory drifts.

Conclusions

This paper addresses the potential challenges of retrofitting early seismic isolation designs to meet modern hazard levels and design criteria. The case study assesses the seismic

performance of a non-ductile 6-story building retrofitted with base isolation using early design standards. The assessment shows that achieving the seismic performance involves a trade-off between the isolation system lateral displacement and the interstory drift ratio. Reaching limit states such as superstructure yielding or moat wall pounding resulted in a rapid increase in superstructure drift demands. The study concludes that the design space for the seismic isolation system retrofit is very limited without altering the superstructure.

A comprehensive set of 1DOF and 2DOF models were considered to quickly assess the current seismic performance of the building. The results showed that the superstructure would require a ductile behavior given the seismic demand, concluding that any retrofit strategy requires a reduction of the shear forces transferred to the superstructure by the isolation system. Given the limited deformation capacity and stiffness irregularity of the superstructure, a nonlinear plane frame model was developed, acknowledging that the superstructure may exhibit nonlinear behavior.

A detailed seismic assessment evaluation using the detailed nonlinear model was performed, which resulted in a narrow viable range of options to achieve the Collapse Prevention criterion. However, this viable region is deemed too narrow to be reliable for design purposes, as even minor variations in the properties of the superstructure could lead to performance that falls short of the target.

Although superstructure alterations are not desirable, an enhancement of the tower response was considered in light of the findings, assuming it would remain linear and elastic. This assumption expanded the feasible domain space, highlighting the constraints defined the tower to achieve the seismic retrofit of the building.

The analyses show that the existing moat wall clearance and superstructure strength limits the retrofit options. A practical solution to reduce the isolation system lateral displacement is the incorporation of viscous dampers at the isolation interface, reducing the lateral displacement and the impact velocity (hence mitigating the moat wall pounding effects). The analysis highlights that by maintaining the tower in its existing condition, the feasible domain is effectively broadened, and this domain is further expanded when considering enhancements to the tower structural behavior, ensuring it remains within the linear elastic range. Nevertheless, limitations on its contribution arise when reaching a total effective damping values above 50%.

This case study highlights the sensitivity of a retrofit design to superstructure characteristics, particularly in existing buildings designed with significant stiffness irregularities. This paper provides insights into the complexities and challenges of retrofitting early seismic isolation designs. It offers a comprehensive understanding of the trade-offs and considerations necessary to develop feasible retrofit solutions that comply with modern seismic hazard levels and design criteria. The findings presented can inform engineers and practitioners in effectively retrofitting existing base-isolated structures for enhanced seismic performance.

Acknowledgements

Chapter 4 is currently being prepared for submission for publication, coauthored with Erler, Kayla; Sepulveda, Claudio; Mosqueda, Gilberto; Del Carpio, Maikol; Lopez, Joshua; and Elwood, Kenneth, J. The dissertation author was the primary researcher and author of this material. I extend sincere appreciation to everyone involved for their invaluable contributions and unwavering support throughout the development of this paper.

Chapter 5 ENHANCED SEISMIC PROTECTION SYSTEM FOR AN EMERGENCY DIESEL GENERATOR UNIT

Abstract

Nuclear Power Plants are required to maintain operation after an earthquake, leading to a safe shutdown if necessary. In the case of a Loss of Offsite Power, the onsite Emergency Diesel Generator is critical to ensure procedural operations of the Nuclear Power Plant. As a means to reduce the overall seismic risk, a three-dimensional seismic protection system is proposed to enhance the seismic performance of the Emergency Diesel Generator. The proposed seismic isolation system decouples the horizontal and vertical components of shaking and considers available hardware to achieve an effective isolation solution over the range of excitation frequencies considered. Numerical analysis of the proposed system demonstrates a reduction in seismic demands on the Emergency Diesel Generator and provides a higher safety margin than conventional base installation procedures. Umbilical lines that cross the isolation plane are considered and impose additional constraints on the displacement capacity of the isolation system. However, increasing the displacement capacity of these components can significantly increase the safety margin against failure. The seismic protection system can be customized depending on the seismic hazard and application to different seismic regions.

Introduction

The application of base isolation to equipment and nonstructural components has been studied for almost three decades [47–51]. Many proposed systems are adapted versions of non-seismic vibration isolation systems designed to limit the lateral travel of equipment. Most previous systems studied are composed of vertical coil springs with viscous dampers or restrainers in multiple directions. Nuclear Power Plants (NPPs) have several nonstructural

components and equipment with different sizes, weights, and stiffnesses. Therefore, no unique and customizable three-dimensional (3D) isolation device was studied that could simultaneously satisfy the seismic design requirements for the various medium-weight equipment and their sensitivity to base shaking.

Several studies have examined 3D seismic protection systems in NPPs [51–57]. Base isolation has been typically used to reduce the horizontal seismic demand, successfully applying it at the component level or for the whole structure to reduce acceleration. Different approaches have been used for the vertical seismic demand, ranging from springs to dampers and a combination of both. The type of approach depends on how the horizontal isolation is considered. Najafijozani et al. [51] studied adaptive vertical isolation of light-weight acceleration-sensitive equipment for a base-isolated NPP. Using a combination of springs and dampers, they achieve a reduction of the acceleration to meet the seismic capacity of the equipment. They focus solely on the vertical movement of the equipment, assuming the base isolation system of the NPP reduces the horizontal acceleration and suppresses any rocking. Medel-Vera and Ji [53] concluded that horizontally isolated structures with vertical isolation at the equipment level avoid issues with the rocking motion and that it is more feasible to isolate lighter components vertically.

The Emergency Diesel Generator (EDG) unit is typically located outside the NPP buildings, so any seismic protection system should isolate the unit horizontally and vertically. In a shake table test, Choun et al. [58] studied the EDG performance supported by a coil spring–damper unit under two different types of ground motion. They found that the performance varied significantly with each ground motion set. The effectiveness depended on the natural frequency resulting from the coil springs and the ground motion frequency content. Nawrotzki and Siepe

[57] studied the performance of helical springs and viscous dampers to implement a 3D protection system. Combining both allows to lower the fundamental frequencies and increase the structural damping.

This study focuses on the seismic protection of an Emergency Diesel Generator, for which functionality is critical for the safe operation of NPP in a Loss of Offsite Power (LOOP) event [59]. The proposed system is based on a combination of previously studied and widely applied devices such as Lead Rubber Bearings (LRB) and vertical coil springs and dampers, merging their advantages to meet operational and seismic requirements. Notably, past experimental studies of LRB alone have indicated their effectiveness for horizontal motion isolation with the potential for amplification of vertical vibrations, including for NPPs [52]. The proposed 3D isolation system for the EDG comprises lead rubber bearings (LRB) to isolate the horizontal ground shaking. A spring and damper vibration isolation layer is included as a second isolation layer on top of the LRB system to mitigate the effect of vertical shaking. A similar approach has been proposed to isolate lightweight equipment in NPPs [51] and for building structures [60,61].

The proposed 3D isolation system is designed for a generic medium-weight EDG, and seismic probabilistic risk analysis (SPRA) is performed. An Incremental Dynamic Analysis (IDA) [25] is performed to obtain fragility curves [62] for two distinct engineering demand parameters (EDP). The common EDP for a non-isolated EDG unit is acceleration [58]. In contrast, an additional EDP is required to control the isolation system lateral displacement for an isolated EDG unit. This study considers two displacement-based failure criteria: the bearings lateral deformation and the umbilical lines deformation capacity crossing the isolation interface. The SPRA as applied in this study is limited to a few ground motions, focusing on demonstrating

the feasibility of the design. Rocking is not allowed in the numerical model. It is assumed an adequate frictionless rocking restraint system with vertical guides is provided following commercially available 3D Isolation Systems [63].

The proposed seismic protection system can be customized for different sizes, weights, and seismic hazards. Fragility functions characterize the current system and identify the high confidence low probability of failure of key components.

Seismic hazard and expected seismic performance

The proposed design of the EDG is based on a set of synthetic seismic input ground motions compatible with a Uniform Hazard Spectra (UHS). Five three-dimensional ground motion sets are generated based on the UHS (10⁻⁴/year) for Ulsan, South Korea with a PGA=0.273g [64,65]. Figure 5.1 shows the target Pseudo Spectral Acceleration for the horizontal and vertical directions with the individual ground motions shown in a lighter shade. The artificial motions provided closely follow the target spectra, showing low variability among them.

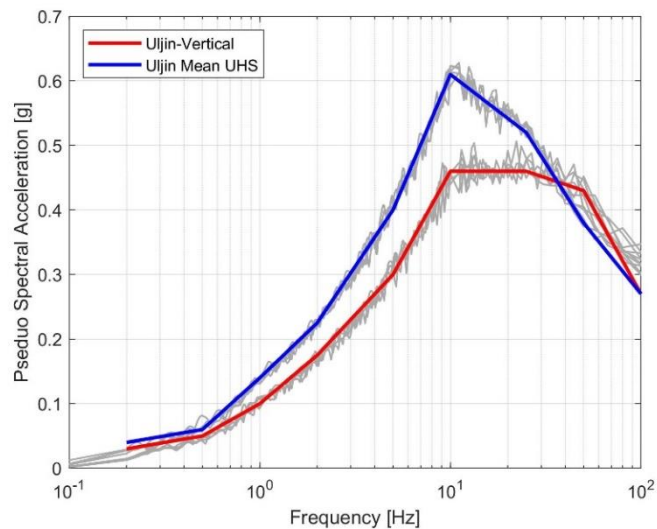


Figure 5.1: Ground motion pseudo spectral acceleration

The Hazard Exceedance Probability (HD) for the ground motions as provided is equivalent to a Seismic Design Category 5 (SDC-5) according to ASCE/SEI-43-05 [66]. This probability of exceedance has a qualitative goal related to acceptable structural behavior or Limit State (LS). The Limit States are specified from LS-A when large deformation and significant damage are accepted to LS-D, when no damage and elastic behavior are expected. For this study, the limit state considered is LS-D, i.e., no damage and linear behavior are expected.

The selected limit state LS-D can be related to a pre-failure mode of the primary components of an EDG system. Structural failure modes can result from the equipment frame, the anchorage system, or the umbilical lines. The seismic probabilistic assessment is based on fragility curves following NUREG [67,68]. The safety margin is obtained after expressing the capacity in terms of the High Confidence Low Probability of Failure (HCLPF), defined as "the acceleration value for which we have approximately 95% confidence that the probability of failure is less than about 5%" [67]. This HCLPF value represents the equipment or component capacity that corresponds to the earthquake level at which it is unlikely that failure will occur. The earthquake level is typically expressed in terms of the peak ground acceleration (PGA), defined as the average of the two horizontal peak components of free-field ground-surface acceleration.

The seismic performance of the equipment is evaluated using two Engineering Demand Parameter (EDP). The probability of failure of the EDG unit can be characterized by the acceleration experienced by the unit, while the base isolation system and the umbilicals crossing the isolation plane are characterized by their displacement capacity. Therefore, two different types of HCLPF capacities are examined, the first based on the isolation system lateral deformation and the second based on the EDG acceleration. Previous studies [53–57,69] have

provided the parameters to estimate the HCLPF value for the EDG unit, the anchorage, and the umbilical lines attached to the EDG. Parameters reported include the median capacity and the randomness and uncertainty standard deviations. Table 5.1 summarizes the HCLPF values per EDP found in the literature.

Table 5.1: Limit States and HCLPF values per EDP

EDP	Label	Limit State	Value	Reference
EDG Acceleration	DS1-A	EDG LS1	0.40g	[70]
Isolation	DS1-D	Pipeline LS1	127mm	[71]
Lateral	DS2-D	Bearing LS2	320mm ($\gamma_s=250\%$)	[72]
Displacement	DS3-D	Bearing LS3	576mm ($\gamma_s=450\%$)	[72]

The HCLPF values for the EDG isolation lateral displacement limit states are defined for two components. One component is the pipeline attached to the EDG that crosses the isolation interface. In a standard piping system, seismic demands lead to plastic deformation and potential failure in the elbows of the piping system [73,74]. Jeon et al. [71] provide seismic fragility curves for elbows in piping systems expressed in terms of the maximum relative displacement between the ground and the isolated floor. This displacement is defined as 1D in an analysis that does not consider the vertical ground motion and uses a standard pipeline system. Due to limited data on 3D base-isolated NPP piping systems, the 1D relative displacement is considered in this study, using the 127mm value for the horizontal relative displacement. A flexible pipeline designed to accommodate the relative displacement could provide a larger deformation capacity.

The second component of the Isolation Lateral Displacement EDP is the bearings. The bearing limit state is expressed in terms of the shear strain deformation. The bearing vertical load capacity is assumed to be checked in the design process.

The HCLPF value for the EDG acceleration limit state is based on the PGA for non-isolated EDG unit studies. The value chosen to represent the EDG Acceleration EDP characterizes the functional and structural failure of the non-isolated EDG unit [70]. Structural failure refers to anchor bolt failure, breakout, tension, or shear failure. Choun and Kim [75] reported that the expected failure mode of an EDG is due to concrete coning with an HCLPF equal to 0.38g. The acceleration used to characterize the HCLPF is for the ground level and does not necessarily equal to the acceleration experienced by the EDG unit. Kawakami et al. [76] reports a 1.2 amplification factor from the PGA to the EDG acceleration.

Placing the EDG unit on 3-D seismic isolation can reduce the accelerations experienced by the EDG and increase the limit state value in terms of PGA. In this study, a conservative approach is taken by considering the allowable acceleration on the EDG unit equal the previously reported PGA values for HCLPF. It should be noted that experimental studies on isolated and conventionally supported EDGs are limited to better characterize the level of amplification in both cases. Further, there are no reports of limit state for vertical excitation of EDG within the literature. It is assumed that the EDG unit can withstand the vertical seismic demands if the 3-D isolation system can reduce the transmissibility of accelerations from the ground to the EDG.

Design of Seismic Protection System

For the design of the 3-D seismic isolation system, a simplified model of the EDG is considered. The EDG is assumed to have a weight equal to 150 Tf and a primary vibration frequency of 34 Hz following [77]. The analyses models consider the EDG as a single degree of freedom with lumped mass at mid-height of the EDG unit.

Different seismic protection configurations were examined. The proposed seismic protection presented here can reduce the EDG acceleration and limit the lateral displacement. The layout is based on two physical levels of isolation. The bottom level (IsoH) consists of 6 lead rubber bearings (LRBs), while the top level (IsoV) consists of 12 coil springs and viscous dampers units. A rigid frame is considered between the two isolation levels. Figure 5.2 shows the proposed configuration.

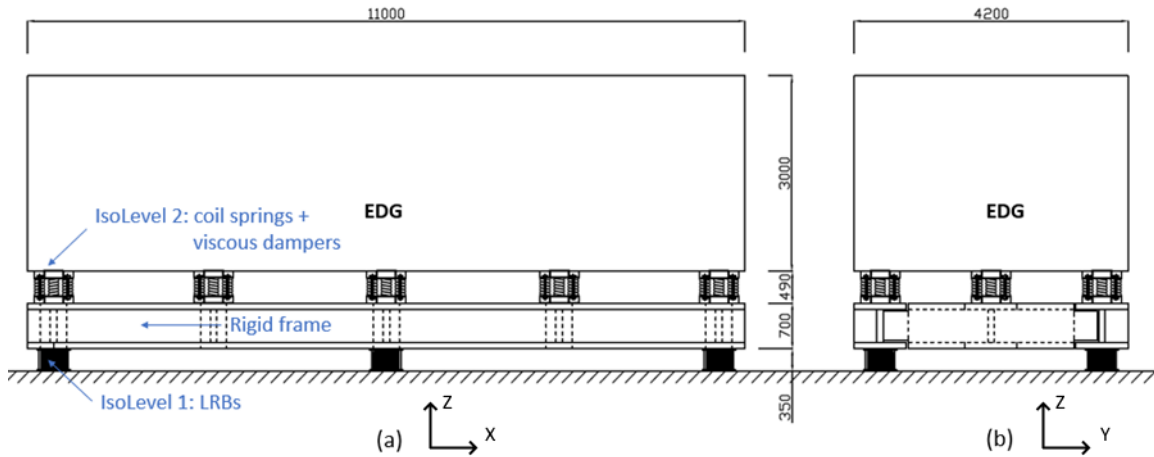


Figure 5.2: Proposed seismic protection configuration; (a) side elevation view; (b) front elevation view. Dimensions in millimeters

Each isolation level targets the reduction of the seismic demand in a particular direction. IsoH focuses solely on the horizontal plane, while IsoV is on the vertical axis. The de-coupling allows for customization of the devices based on the seismic hazard, including the frequency content. This feature could enable simple adjustments to standardize its use for different seismic regions.

The frequency content of the seismic hazard considered shows a peak around 11Hz for the horizontal plane and a plateau between 8Hz and 20Hz for the vertical component. This information is used to define the properties of both isolation levels, such that the primary vibration frequency of each level is below the peak frequencies of the seismic hazard.

Lead rubber bearings are considered and sized to define the IsoH frequencies. Lead rubber bearings typically result in a lower natural vibration frequency in the horizontal plane, typically around 0.25Hz to 1.0Hz, and a higher frequency in the vertical axis of about 10Hz and higher. The IsoV frequencies are defined by the coil springs. The vibration control performance defines restrictions for the vertical natural frequency of the coil spring [77]. Providing a low natural vertical frequency is beneficial for the seismic demand but sets the spring static deflection to be large which is detrimental during operation. The performance during normal operation is critical hence the static deflection defines the vertical frequency. Following [77], the coil spring vertical frequency is set to 2.0Hz which defines a static deflection equal to 62mm. Table 5.2 summarizes the required vibration frequencies upon the primary frequency content of the ground motions.

Table 5.2: Frequencies dependent properties of both isolation levels

Isolation Level	Horizontal vibration frequency [Hz]	Vertical vibration frequency [Hz]	Primary horizontal frequency [Hz]
[0.25-4.0]	[0.25-4.0]	>10	11
-	-	~2.0	[8-20]

The design of the horizontal isolation system considers a tradeoff between the transfer of shear forces related to the accelerations experienced by the EDG and the displacement demand for a given hazard level. This is demonstrated for the EDG and the considered seismic hazard following the Equivalent Lateral Force procedure in FEMA P-751 [78], as shown in Figure 5.3.

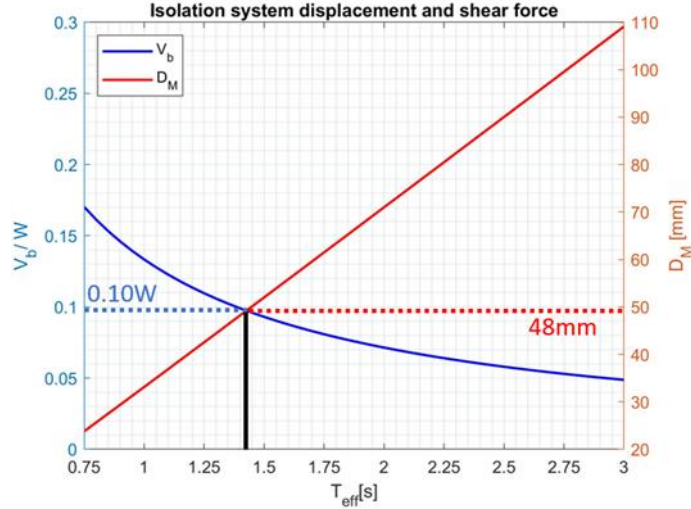


Figure 5.3: FEMA P-751 equivalent lateral force procedure results

The effective period of the isolation systems is based on the linearization of the stiffness and damping of the inherently nonlinear bearings. The value chosen is the intersection of the base shear and the lateral displacement. This was found to be a reasonable compromise to provide reduced base shear while limiting the horizontal displacement at a vibration frequency of 0.7Hz (period of 1.40s). To verify the feasibility of this design, the required bearings are sized with dimensions and resulting bearing properties for IsoH shown in Table 5.3.

Table 5.3: Properties of LRB and resulting isolation system properties

Type	Diameter [mm]	Lead core [mm]	Rubber thickness [mm]	Shear modulus [MPa]	Rubber layers []	f_H [Hz]	f_v [Hz]
Lead Rubber	405	40	8	0.4	16	0.7	13.8

The equations and assumptions to obtain the horizontal and vertical effective properties of the LRB system are described considering a bilinear model for the bearings. The ratio between the horizontal elastic stiffness (k_1) and the post-yield stiffness (k_2) is 10. The post-yield stiffness of the laminated rubber bearings is expressed as:

$$k_1 = 10k_2 \quad (\text{Eq. 7})$$

$$k_2 = \frac{G_{eff} \cdot (A_e - A_i)}{n_r \cdot t_r} \quad (\text{Eq. 8})$$

The yield force (F_y) and yield displacement (D_y) are obtained based on the characteristic strength of the lead (Q) and the horizontal elastic stiffness (k_1) and the post-yield stiffness (k_2).

$$F_y = \frac{Q \cdot k_1}{k_1 - k_2} \quad (\text{Eq. 9})$$

$$D_y = \frac{F_y}{k_1} \quad (\text{Eq. 10})$$

The energy dissipated (W_{eff}) can be expressed as:

$$W_{eff} = 4 \cdot Q \cdot (D - D_y) \quad (\text{Eq. 11})$$

The effective horizontal stiffness ($k_{eff,H}$) and vertical stiffness ($k_{eff,V}$) values are obtained based on the lateral displacement (D), the effective rubber shear modulus (G), the external isolator area (A_e), internal area (A_i), the number of rubber layers (n_r), the rubber thickness for each layer (t_r) and the shim thickness (t_s) as [2,79]:

$$k_{eff,H} = \frac{Q}{D_{isp}} + \frac{G_{eff} \cdot (A_e - A_i)}{n_r \cdot t_r} \quad (\text{Eq. 12})$$

$$k_{eff,V} = \frac{(A_e - A_i) \cdot E_c}{n_r \cdot t_r + (n_r - 1) \cdot t_s} \quad (\text{Eq. 13})$$

With the compressive modulus (E_c) and shape factor (S) expressed as:

$$E_c^{-1} = \frac{1}{6G_{eff} \cdot S^2} + \frac{4}{3 \cdot K} \quad (\text{Eq. 14})$$

$$S = \frac{D_e^2 - D_i^2}{4 \cdot D_e \cdot t_r} \quad (\text{Eq. 15})$$

The coil springs in the IsoV level are sized for two conditions: the operational vibration (including vertical static deflection) and the primary vertical frequency content of the ground motion. The target is to achieve a primary vertical frequency less than 2Hz, satisfying both conditions. The dampers are sized based upon a parametric study of a feasible range of sizes while targeting the reduction of the ground acceleration. A linear viscous damper with force proportional to velocity is used with the system properties shown in Table 5.4 including the % of critical damping.

Table 5.4: IsoV properties

Type	Direction	Value	f [Hz]	Damping [%]
Stiffness	Horizontal	16.4 [kN/mm]	2.5	-
	Vertical	28.4 [kN/mm]	2.0	-
Damping coefficient	Horizontal	1.55 [kN s/mm]	-	12.0
	Vertical	5.37 [kN s/mm]	-	11.0

The vertical stiffness is defined using the targeted vertical frequency:

$$K_{ISOV} = 4\pi^2 \cdot m \cdot f_v^2 \quad (\text{Eq. 16})$$

The static deflection can be obtained as:

$$\delta_0 = \frac{g}{4\pi^2 \cdot f_v^2} \quad (\text{Eq. 17})$$

A lumped mass is added to the numerical model to account for the rigid frame, and the IsoV weight is estimated as 30 [Tf]. No rocking is allowed in the numerical model, assuming an adequate rocking restraint system with vertical guides for the IsoV layer. The analytical model is developed in OpenSees [34] structural analysis software.

Results

Nonlinear time-history analyses were conducted to examine the performance of the EDG under the five ground motion sets considered. The results are first presented for an individual ground motion to understand the isolation system's behavior and the EDG's response. Record 4 is

selected since it is most representative of the average response of the five records. The record is applied at two scale factors, including the unscaled record with a PGA of 0.273g and scaled to a horizontal PGA of 0.925g. The higher amplitude was selected as this is when the first potential limit state is reached as shown in Table 5.1.

Response for target seismic hazard intensity

The unscaled Record 4 with a PGA of 0.273g is used to demonstrate the performance of the 3-D isolated EDG under the target UHS. The acceleration of each isolation level and the EDG unit are compared, both in the horizontal and vertical directions in Figure 5.4 and Figure 5.5.

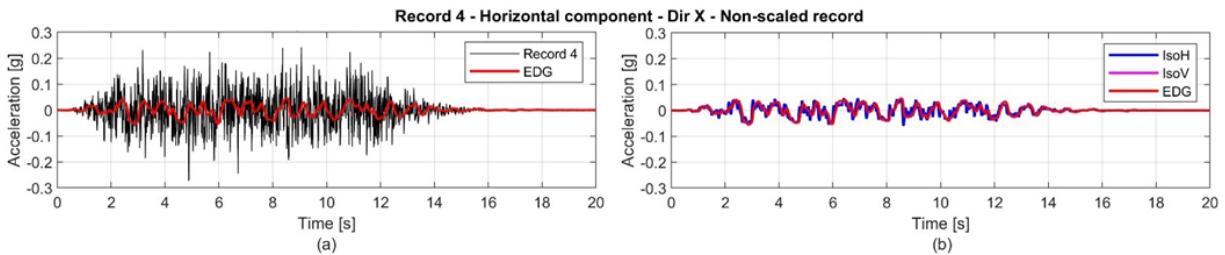


Figure 5.4: Horizontal acceleration time history results for non-scaled Record 4 – Direction ‘X’
 (a) Record and EDG response comparison (b) System response by isolation level

The horizontal acceleration time histories in the 'X' direction are shown in Figure 5.4a. An amplification factor from the PGA to the EDG acceleration is used to quantify the proposed seismic protection system performance after Kawakami et al. [76], who reports a factor of 1.20 for the 2D ground motion, not providing a factor for the 3D ground motion. Considering only the 2D horizontal acceleration, a factor of 0.22 times the PGA is obtained, while a factor of 0.50 times the PGA is obtained for the 3D ground motion. Including the vertical ground motion reduces the effectiveness of the proposed seismic protection system, although still reducing the EDG acceleration for the unscaled ground motion set. The EDG acceleration time history shows that the proposed seismic protection system can filter the high-frequency content of the horizontal shaking. The acceleration time histories immediately above each isolation level and

the EDG unit are shown in Figure 5.4b. Notably, the IsoV level further reduced the high-frequency content experienced above the IsoH level due to the additional contribution of the low horizontal stiffness provided by the coil springs. The EDG behaves as a rigid body, and thus its response is identical to the IsoV time histories, which is why the IsoV line is not visible.

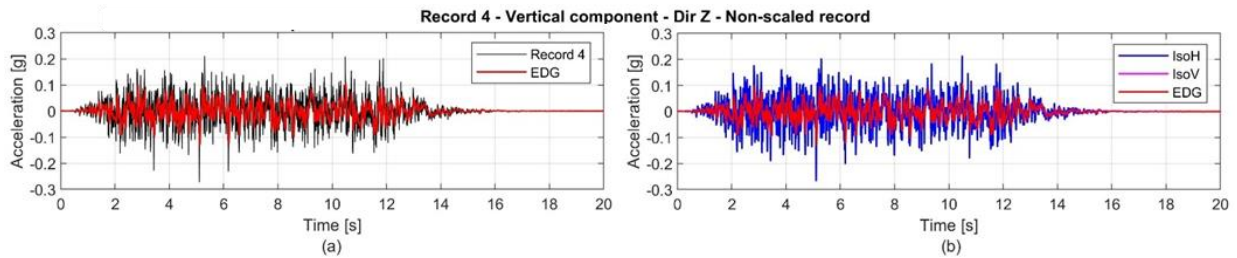


Figure 5.5: Vertical acceleration time history results for non-scaled Record 4 – Direction ‘Z’ (a) Record and EDG response comparison (b) System response by isolation level

The vertical input ground motion is compared to the EDG vertical acceleration in Figure 5.5a, indicating a reduction factor of about two while still transmitting the high-frequency content. The vertical vibration frequencies of both isolation levels are close to the dominant range of the input ground motion, transmitting some of the high frequency shaking into the EDG unit. Figure 5.5b shows the effects of the IsoV level defined by the coil springs in reducing the acceleration experienced by the EDG unit. The acceleration of the IsoH level is about the same as the vertical ground motion showing that the LRB alone would not reduce the vertical response.

Figure 5.6 compares the Pseudo Spectral Acceleration (PSA) corresponding to 5% of critical damping for the ground record, the EDG, and above each isolation level for the horizontal and vertical directions. The horizontal PSA in Figure 5.6a has a marker to indicate the EDG unit natural frequency of 34Hz corresponding to $PSA=0.056g$ with the isolation system. The reduction in PSA is clearly shown above each isolation level. Figure 5.6a also confirms that the IsoV level further reduces the higher frequency vibration between 3-30 Hz, although it

causes slight amplification in lower frequencies. The vertical PSA in Figure 5.6b indicates that IsoH amplifies the vertical ground motion across the LRB, a concept that has previously been raised for horizontal isolations systems [52] while IsoV effectively reduces the vertical excitation above 5 Hz.

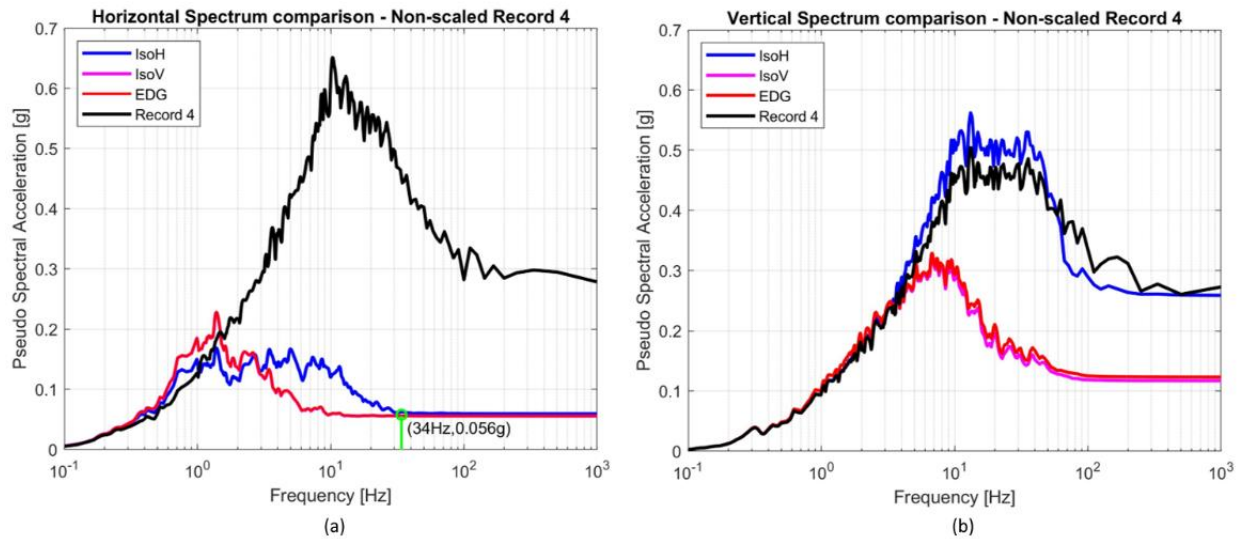


Figure 5.6: Spectral acceleration results for non-scaled record 4 (a) horizontal direction ‘X’ (b) vertical direction ‘Z’

The results for Record 4 shown here are representative of the average response for the five considered records. These detailed results show the effectiveness of the proposed seismic protection system in reducing the seismic demands for a given seismic hazard as specified by the UHS.

The second EDP considered is the isolation system lateral displacement. The base isolation system and the umbilicals crossing the isolation plane are characterized by their displacement capacity. For the unscaled Record 4, the isolation system lateral displacement is about 15mm, with the horizontal acceleration transferred to the base of the EDG reduced by a factor of 4.5 and the vertical acceleration reduced by a factor of 2. The small lateral displacement is expected for this seismic hazard with a high-frequency content. Different results are expected for seismic hazards with lower primary frequencies, which are considered in the next section.

Scaled ground motion records

To observe the response of the seismically isolated EDG at a higher intensity, record 4 is scaled to a horizontal PGA of 0.925g, at which the isolation system lateral displacement reaches the first limit state (LS1-D), corresponding to 127mm at which the piping systems crossing the isolation plane reaches its deformation capacity of. The results in Figure 5.7 show a similar performance to the non-scaled record in Figure 5.4. In Figure 5.7a, the EDG horizontal acceleration is significantly reduced in amplitude while Figure 5.7b shows that the EDG unit experiences a 0.166g acceleration with an isolation system lateral displacement equal to 127mm for this scaled seismic hazard. A 2D horizontal acceleration factor of 0.18 times the PGA is obtained, while a factor of 0.48 times the PGA is obtained for the 3D ground motion. Notably, the reduced horizontal seismic demands are conditional on the deformation capacity of the pipeline crossing the isolation interface. The vertical isolation response shown in Figure 5.8 shows the same response observed for the non-scaled record. This type of response is expected since the vertical isolation is linear.

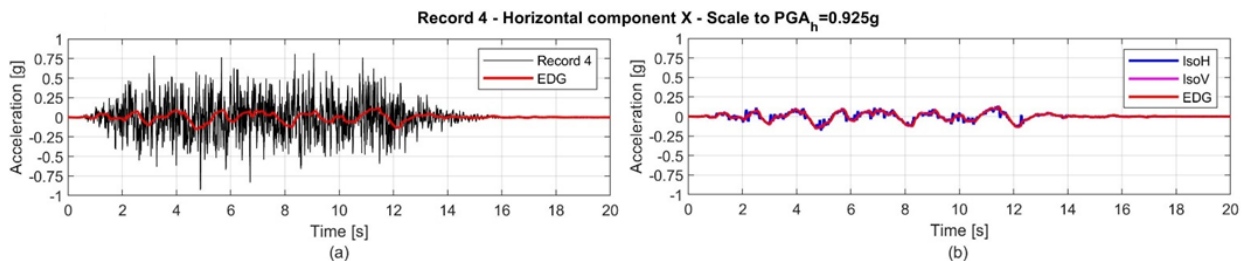


Figure 5.7: Horizontal acceleration time history results for the Record 4 with PGA = 0.925g – Direction ‘X’ (a) Record and EDG response comparison (b) System response by isolation level

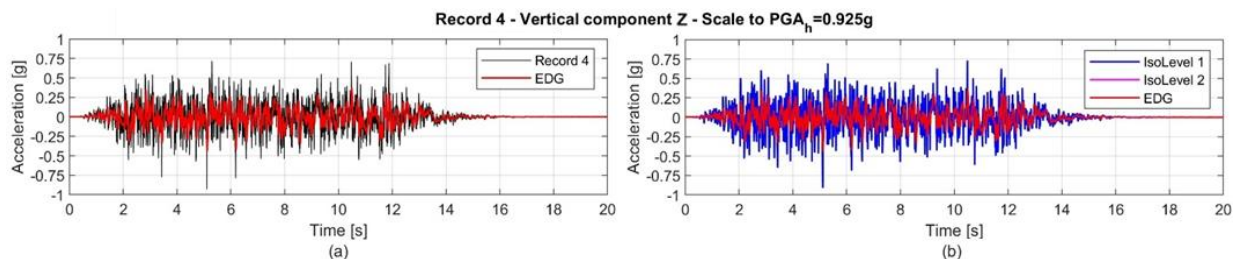


Figure 5.8: Vertical acceleration time history results for the Record 4 with PGA = 0.925g – Direction ‘Z’ (a) Record and EDG response comparison (b) System response by isolation level

The results shown in Figure 5.9 are similar to the results in Figure 5.6. The horizontal PSA in Figure 5.9a is significantly reduced for all isolation levels. The vertical PSA in Figure 5.9b shows a reduction of the EDG acceleration and amplification for the IsoH level. For this scaled record intensity there is no amplitude dependence.

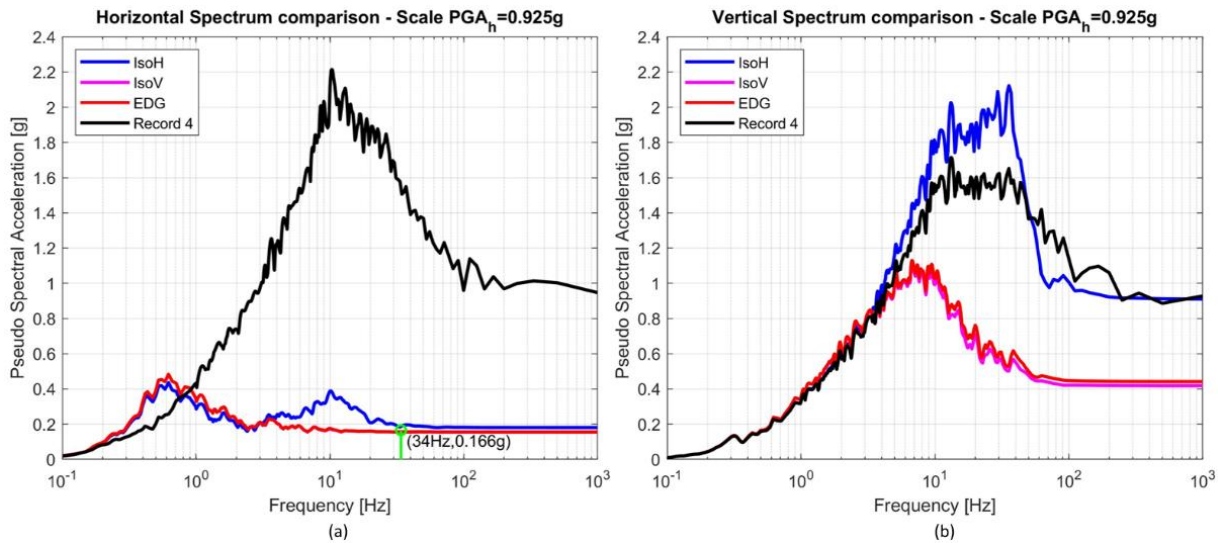


Figure 5.9: PSA results for scaled Record 4 (a) horizontal direction ‘X’ (b) vertical direction ‘Z’

The behavior of the isolation systems is shown in Figure 5.10 for both horizontal and vertical directions. The individual force-displacement hysteretic behavior of levels IsoV and IsoH shows that most of the lateral deformation is captured by the LRB. The LRB bearings have a lower effective stiffness and dissipate energy through hysteretic action of the lead core while the coil springs have added linear viscous dampers to dissipate energy. The force-displacement behavior in the vertical direction of the IsoV demonstrates that the response is dominated by the viscous dampers with small oscillations around the static deflection equal to 63mm. The IsoH level, in Figure 5.10d shows that the behavior of the bearing in the vertical direction is model as a linear spring with 2% damping not shown.

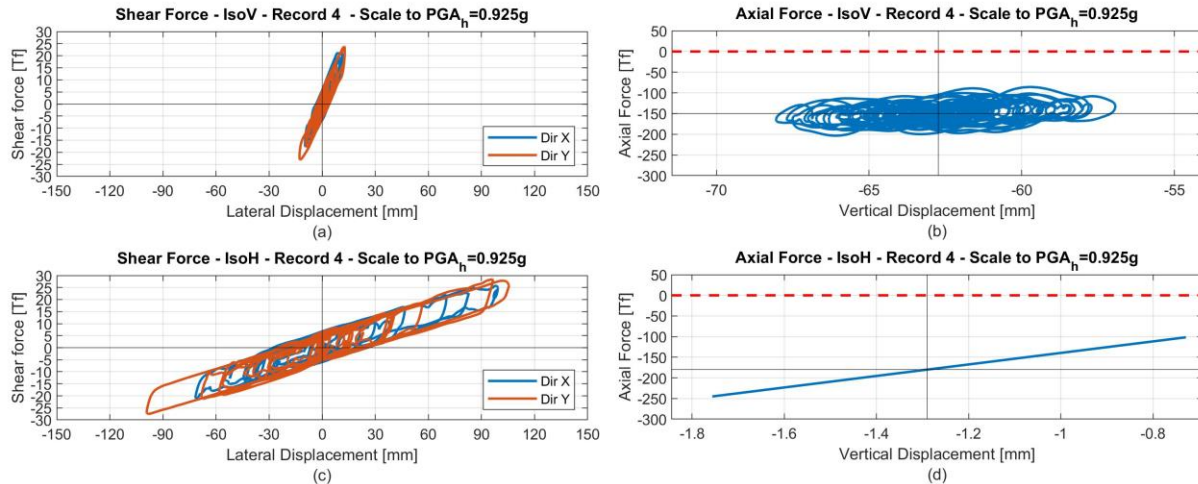


Figure 5.10: Force-displacement hysteresis for the Scaled Record 4 (a) IsoV horizontal direction 'X' response (b) IsoV vertical direction 'Z' response (c) IsoH horizontal direction 'X' response (d) IsoH vertical direction 'Z' response

The time-history analysis for a single ground motion provides insight into the behavior of the isolation system. A more thorough probabilistic analysis is necessary to quantify the ground motion intensity at which there is a High Confidence of a Low Probability of Failure (HCLPF) as described in the next section.

Incremental Dynamic Analysis

An Incremental Dynamic Analysis (IDA) is a nonlinear dynamic analysis method that correlates the seismic demand and the capacity estimation using single or multiple ground motion records incrementally scaled in magnitude. The IDA is performed to derive Fragility Curves for two Engineering Demand Parameters, including displacements at the isolation level and accelerations in the EDG. The Limit States considered for each EDP are described in Table 5.1. The five ground motion triplets are used to account for seismic hazard randomness (β_r), while an uncertainty standard deviation (β_u) equal to 0.30 is assumed. The records are scaled from 0.1 to 10 times the original PGA in increments of 0.1g.

Base isolation system lateral displacement

Figure 5.11 shows the IDA result for each ground motion's isolation system lateral displacement with the displacement Limit State considered indicated by vertical dashed lines. The horizontal axis is presented by the rubber bearings shear deformation, and one at the bottom is expressed in terms of the maximum lateral deformation.

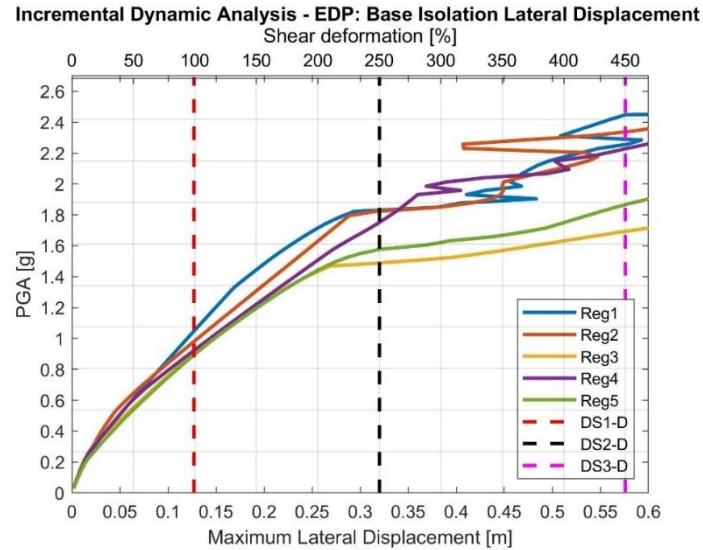


Figure 5.11: IDA for Lateral Displacement EDP

Table 5.5 contains the median PGA and the randomness standard deviation value for each Limit State. The resulting β_r values are relatively small, providing little variation in response between the ground motions. This is likely the result of the scaling method used for the ground motion to closely match the desired spectrum.

Table 5.5: IDA results for the Lateral Displacement EDP

EDP	Label	Limit State	Value [mm]	Median PGA [g]	β_r []
Isolation Lateral Displacement	DS1-D	Pipeline LS1	127	0.94	0.07
	DS2-D	Bearing LS2	320	1.75	0.10
	DS3-D	Bearing LS3	576	2.23	0.17

EDG Acceleration

The results for the EDG acceleration Limit State are provided in a similar format in Figure 5.12. The values in Table 5.6 contain the median PGA and the randomness standard deviation value for EDG acceleration Limit State.

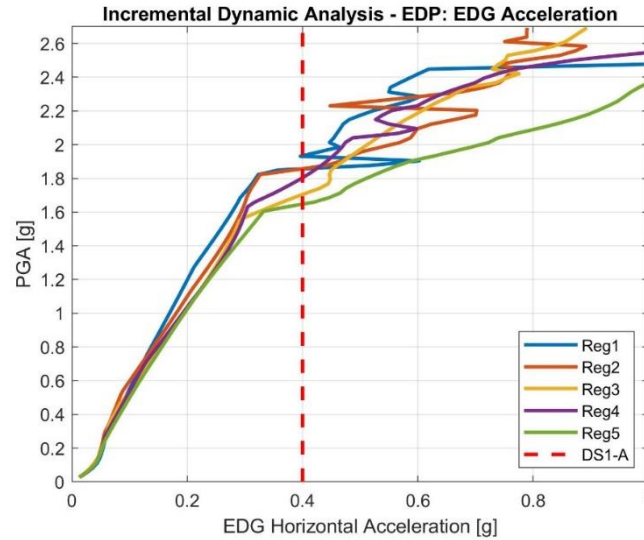


Figure 5.12: IDA for EDG Acceleration EDP

Table 5.6: IDA results for the EDG acceleration EDP

EDP	Label	Limit State	Value [g]	Median PGA [g]	β_r []
Acceleration	DS1-A	EDG LS1	0.40	1.80	0.07

Fragility Curves

Fragility curves estimate the probability of obtaining damage levels or grades as a function of each the seismic hazard intensity. The application of fragility curves on nonstructural elements [80,81] and other fields [82] is extensive. The fragility curves considered are used to calculate the probability of exceeding a specific Limit State for a given ground motion PGA. The median fragility curve is obtained directly from the IDA data, while the 95% curve is the 95%

confidence that the median capacity exceeds the PGA level. The HCLPF value is obtained at a 5% failure probability of the 95% confidence probability distribution.

The fragility curves are based on three parameters including the median capacity and the logarithmic standard deviation representing random uncertainty obtained directly from the IDA and listed in Table 5.5 and Table 5.6. The third parameter is the uncertainty logarithmic standard deviation (β_u), representing systematic or modeling uncertainty. The value assumed for all cases is $\beta_u=0.30$.

Base isolation system lateral displacement

The median and 95% confidence probability distribution curves for all the displacement-based Limit States are plotted in Figure 5.13. For the first displacement-based limit state, i.e., the Pipeline LS1 in Figure 5.13a, the HCLPF value is 0.50g, represented by the blue dashed line. The EDG unit could experience a ground motion similar to the UHS described with a 5% probability of failure. This failure comes from the assumption of exceeding the lateral deformation capacity of the pipeline crossing the isolation interface. Figure 5.13b shows the HCLPF value for the Bearing LS2 is 0.91g. This particular limit state is related to the bearing reaching a shear deformation of 250%, which is defined as a limit for the bearing's linear behavior [72]. Exceeding this shear deformation threshold does not imply a bearing failure; rather highly nonlinear behavior is expected in the rubber that could include stiffening. Figure 5.13c shows the HCLPF value for the Bearing LS3 is 1.03g. This lateral deformation is equivalent to a 450% bearing shear strain, defined as a fracture limit [72]. Changes in the bearing design can lead to higher lateral displacements by changing the bearing diameter, the number, and the thickness of the rubber layers.

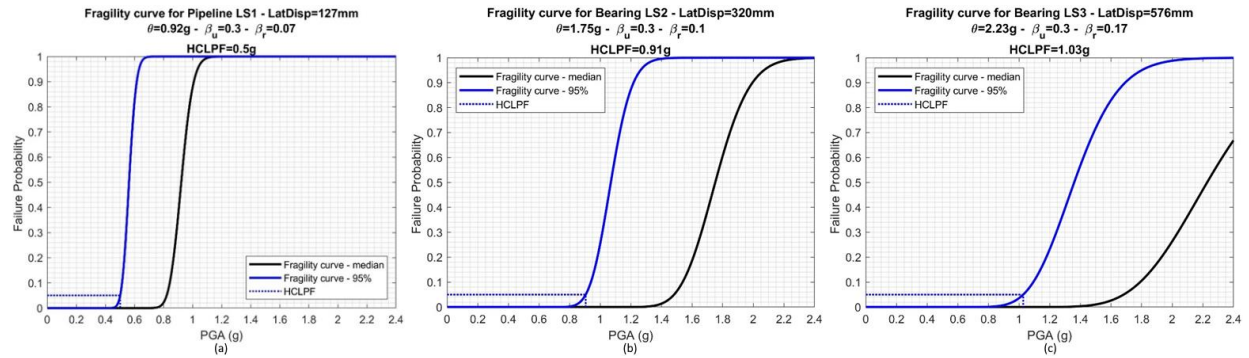


Figure 5.13: Fragility curve for (a) Pipeline LS1 (b) Bearing LS2 – LatDisp=320mm (c) Bearing LS3 – LatDisp=576mm

The fragility curves for the base isolation system lateral displacement EDP show a significant difference in the deformation capacity of the components crossing the isolation interface. The bearings can sustain a larger deformation than the pipeline before exhibiting damage. To take advantage of the bearing’s deformation capacity, umbilicals crossing the isolation interface can be designed to accommodate larger deformations as is typically done in buildings. This would enhance the system's performance and allow it to sustain higher seismic demands.

EDG Acceleration

The values in Table 5.6 are used to develop the fragility curves for the three acceleration limit states. These Limit States are based on reported values of non-isolated EDG units, specifically to the failure modes these units experience. The conservative assumption made here is that since the EDG unit is assumed to be rigid, the reported PGA should be similar to the EDG acceleration [76]. The behavior of an isolated EDG unit is unknown, and it is believed that some failure modes will not appear in the isolated unit. Experimental testing on an isolated EDG unit will provide helpful insight into characterizing its failure modes.

Three acceleration-based limit states are used in a narrow acceleration range of [0.30g-0.50g]. The first limit state, EDG LS1, is the lower bound value of any possible EDG failure

mode found in the literature [67–69,75,83,84]. The consensus is that a fix-based EDG unit should have at least an HCLPF equal to a PGA=0.30g.

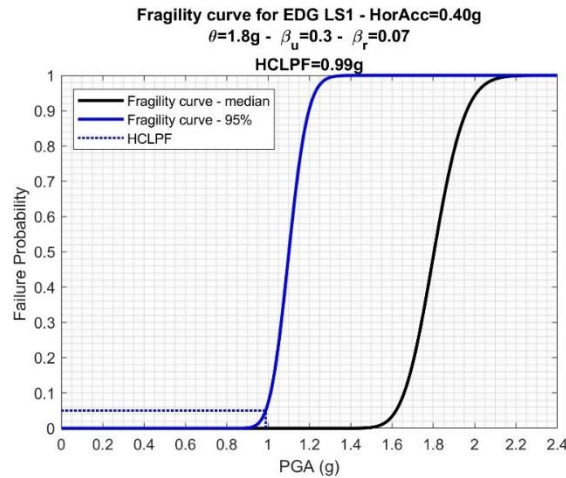


Figure 5.14: Fragility curve for EDG LS1 – Acc=0.40g

Figure 5.14 shows the fragility curves for EDG LS1. The HCLPF value for the acceleration-based limit state is 0.99g, represented by the blue dashed line. This result shows a 5% probability of failure given a horizontal PGA=0.99g. This failure is characterized by the lowest bound value of a fix-based EDG unit.

Results

Figure 5.15 presents the HCLPF in terms of the ground motion PGA for all Limit States, including displacement and acceleration based EDPs. As shown previously, different HCLPF values were presented. These values were obtained assuming an uncertainty logarithmic standard deviation of $\beta_u=0.30$ and varying values for the randomness logarithmic standard deviation of β_r . This parameter comes from the five ground motion triplets for each limit state with values ranging from 0.06 to 0.17. These values are recognized to be small for the ground motion set considered and increased to $\beta_r=0.20$ to determine the HCLPF for every Limit State.

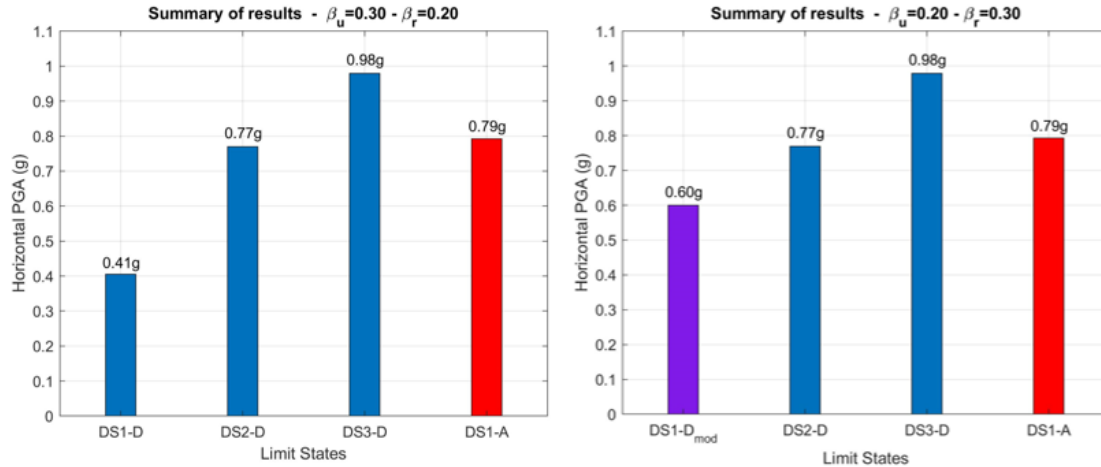


Figure 5.15: Fragility Curves results for both Limit States

Figure 5.15a shows that the pipeline LS (DS1-D) limits the seismic protection system's performance. All other LS are above a PGA=0.77g, while the DS1-D is reached at PGA=0.41g. This PGA value would be the maximum horizontal PGA that the seismic protection system could experience with a 95% confidence of not exceeding the 5% probability of failure with no damage and linear behavior expected, as required by Design Category 5 (SDC-5) with an LS-D according to ASCE/SEI-43-05 [66]. Figure 5.15b shows the results by modifying the pipeline LS (DS1-D_{mod}) at a limit equal to 224mm, which represents a moderate damage state (equivalent to damage of broken meshes) [85]. The seismic protection system could perform at 146% of the previously defined maximum PGA. Locations with a horizontal PGA up to 0.60g could use the seismic protection system while complying with ASCE/SEI-43-05 [66] if the deformation capacity of the pipeline is 224mm.

To equal the PGA required to reach the second displacement-based Limit State (DS2-D), the pipeline's HCLPF should be 320mm. This would allow the seismic protection system to satisfy the performance of places with a seismic hazard equal to PGA=0.77g (188% of the original maximum PGA). Providing a pipeline with a higher deformation capacity to cross the isolation interface with limited damage would enhance the system's performance.

Discussion

The proposed seismic isolation system satisfies the SDC-5 for the seismic hazard considered according to ASCE/SEI-43-05 [66], assuming a limit state LS-D, i.e. when no damage and elastic behavior is expected. The seismic hazard, characterized by the PGA that the system could handle under the LS-D is 0.41g. This is similar to a non-seismically isolated EDG and is based on having conventional pipelines. Detailing the pipelines to accommodate larger displacements is necessary to gain benefit from the isolation system. Conservative assumptions are made to be aligned and comply with the NPP safety standards. Experimental testing would provide a deeper insight into the EDG behavior when base-isolated, particularly the controlling failure mode and the behavior in the vertical di-rection. The minimum non-isolated EDG HCLPF was used for acceleration, which is a conservative assumption. Even under this assumption, the proposed system can withhold a $PGA=0.79g$ assuming the scaled seismic hazard maintains its frequency content range used for design.

The probabilistic approach outcome shows its inherent conservatism compared to the deterministic approach. The same base isolation average lateral displacement of 127mm, equivalent to the Pipeline LSD-1, is used to compare the approaches. For the probabilistic approach, the PGA is 0.41g for HCLPF, while the deterministic approach only considers the mean response with the PGA of 0.925g. The probabilistic approach explicitly quantifies the failure probability, a feature the deterministic approach does not capture.

Including the vertical ground motion reduces the effectiveness of the proposed seismic protection system but still reduces the EDG acceleration. Quantifying the reduction in terms of the PGA shows an amplification around 0.20 time the PGA for the EDG acceleration when considering only the 2D horizontal acceleration. When using the 3D ground motion acceleration, a factor of 0.50 times the PGA is obtained.

This analysis shows that the pipeline deformation capacity is the controlling limit state. To be aligned with the LS-D criteria [66], the pipeline must be designed to accommodate the system lateral deformation under a controlled damage level. The metric required to characterize the pipeline deformation needs to be expressed as an HCLPF value for consistency. Experimental testing on flexible pipelines crossing the isolation interface would provide the necessary data to extend the proposed seismic protection system to areas with higher seismic hazards than $PGA=0.41g$.

Further studies are required to validate the proposed system under different seismic hazards and also consider the performance under operational loads not considered here. The two isolation levels need to be designed considering the local seismic hazard including expected frequency content for effective isolation performance.

Conclusions

The EDG seismic performance is critical to the operations of a NPP in the case of a loss of off-site power. The proposed seismic protection system can significantly increase safety margin compared to standard EDG support installation. Incorporating two isolation levels with distinct properties defined according to a specific seismic hazard allows the base isolated EDG to perform at a higher seismic demand, expressed in terms of PGA, with significant confidence of a low probability of failure and elastic behavior. The pipe-line deformation capacity that crosses the isolation interface needs to be designed accordingly for the system to function effectively in larger seismic hazard regions, i.e., larger horizontal PGAs.

Experimental testing on both a pipeline designed to accommodate the required lateral deformation and the isolated EDG unit failure modes are critical to validate the proposed seismic protection system.

The innovation of the proposed seismic protection system is in the use of two isolation levels to decouple the seismic demand and enables designers to combine existing and proven seismic protection devices. One isolation level focuses solely on the reduction of the horizontal component demand, while the second isolation level handles the vertical component. This approach maximizes the seismic reduction capabilities of each device. The enhanced seismic protection system can be tailored to specific seismic demands by changing a few parameters only for a decouple seismic demand. The low probability of failure that this design adds to the standard EDG support solution could be a step forward to standardizing an EDG seismic protection system.

Acknowledgements

Chapter 5, in full, is a reprint of the material as it appears in *Energies*, MDPI, 2022. The dissertation author was the primary investigator and author of this paper. I am profoundly grateful to Minkyu Kim and Gilberto Mosqueda for their invaluable guidance and support, which significantly enriched the quality and depth of this dissertation. Their expertise, mentorship, and encouragement have been instrumental in shaping the direction and outcomes of this research endeavor.

Chapter 6 SUMMARY AND CONCLUSIONS

Summary

Base isolated buildings have been shown to achieve functional performance within their design range, but there are concerns once this design capacity is exceeded. Given that base-isolated buildings are typically surrounded by a moat wall or the building could yield at large bearing displacements, unrestricted travel of the isolation layer is limited. This makes the isolation system design capacity a critical parameter for design and retrofit applications.

Worldwide, there is a large stock of base-isolated buildings designed using early standards with less stringent design criteria than used for new base isolated buildings today. Many buildings adopted this technology as a retrofit in early applications and may not satisfy current assessment standards. Furthermore, there are no explicit guidelines for engineers to assess the limit states of isolated buildings, which are generally considered beyond design and intended to be avoided in building design codes.

This dissertation examined the nonlinear behavior of the superstructure to understand the role of ductility and strength degradation in the performance of base-isolated superstructures. While isolated buildings are assumed to remain essentially elastic in conventional design (e.g. ASCE 7), large displacement at the isolation level with increased shear force or moat wall pounding can result in yielding of the superstructure. For base-isolated systems designed to early standards, large seismic events can pose a significant risk considering that smaller displacement capacities were used and the structure could have limited ductility. This research focuses on two limit states which may lead to damage in the superstructure of base isolated buildings: 1) yielding of the superstructure at large isolation displacements, and 2) moat wall impact and

effects on superstructure response. This thesis does not address limit states of the isolation system itself such as bearing stability or shear failure.

The chapters of this dissertation build towards the development and evaluation of simplified methods of assessment. A simplified two-degree-of-freedom (2DOF) model was used to characterize a base-isolated building, with one DOF representing the isolation system and another DOF characterizing the superstructure. The range of application of the 2DOF model under beyond design loads was examined to determine how accurately the 2DOF model can capture the behavior of the superstructure after superstructure yielding and following moat wall pounding. These studies provide insight for assessing the effectiveness of the 2DOF model as a rapid assessment tool in predicting structural responses under extreme loading conditions.

The 2DOF model was validated by a direct comparison to a full nonlinear superstructure model. Based on these studies, the isolation system lateral displacement can be reliably estimated, even under demands that are twice the average of when the superstructure begins to yield. Given its reliable estimation, this parameter can also be used to assess the potential for moat wall pounding. In the event of moat wall pounding, the superstructure drift estimation provided by the 2DOF model is conservative. The simplicity of 2DOF models makes it a useful tool for preliminary analysis, providing a reliable estimation of isolation system lateral displacement and the potential for pounding. However, these models tend to overestimate roof drifts and underestimate roof accelerations and individual story drifts due to the limited contribution of higher modes and force redistribution post-yielding. On moat wall pounding, relying on small increases in moat wall clearances to reduce or prevent pounding may not be an effective approach. The impact velocity-trajectory relationship shows large variability across records, although further validation with a larger set of models is required.

Recognizing the limitations of the 2DOF model to study beyond design-basis events, an investigation of various superstructure archetypes was analyzed using the 2DOF model. The analysis allowed for a close examination of the deformation capacity effects in the overall behavior and performance of the superstructure. The results show that the ductility capacity changes the performance the most when compared to the post-yielding stiffness ratio and the failure slope ratio, regardless of whether the system is very ductile or has limited ductility. At a system level, the results show that ductile systems can sustain larger demands while keeping the drift ratios constrained below collapse limit states, while limited ductility systems exhibit sudden increases in drift beyond collapse limit states rapidly after the onset of yielding. Increasing the strength of the superstructure of limited ductility system shows to be an effective way to sustain larger demands but does not change the nonlinear performance once yielding occurs.

A case study of an early application of seismic isolation was examined. The seismic assessment of the building following current standards and evaluation of retrofit options offers valuable insights into the practical challenges to satisfy current seismic criteria. The retrofit options evaluated a range of properties for the isolation system and demonstrated a trade-off between i) increasing isolation system lateral displacement and potential for pounding when reducing the effective stiffness of the isolation system, and ii) superstructure yielding for increased effective stiffness of the isolation system. In either case, when limit states such as superstructure yielding or moat wall pounding are reached, there is a rapid increase in superstructure drift demands. The study concludes that the design space for the isolation system parameters that provide adequate performance can be limited, particularly in existing buildings with limited moat clearance and with significant stiffness irregularities.

These series of studies provide insight in the performance of base isolated structures beyond design considerations. These studies show that the performance after superstructure yielding or moat wall pounding rapidly degrades and provides a high level of uncertainty in predicting expected performance. This uncertainty needs to be accounted for in the assessment of performance of existing buildings with base isolation.

Discussion of Results

Understanding the seismic performance of seismically isolated buildings beyond design considerations is important for making informed decisions about building safety. These assessments can inform building owners and users about the vulnerabilities of the structure, identifying necessary strengthening or increased capacity to improve the resilience over time. Current tools and guidelines to support practicing engineers in addressing issues such as the nonlinear behavior of the superstructure and the potential for moat wall pounding are lacking.

In the US, ASCE41-17 provides guidance for the seismic evaluation and retrofit of existing buildings. The standard acknowledges the potential for nonlinear behavior in the superstructure by requiring that seismically isolated buildings be represented using a three-dimensional model for nonlinear dynamic procedures, unless the structure above the isolation system exhibits essentially linearly elastic behavior. Regarding the exceedance of the available moat wall clearance, ASCE 41-17 defines that the required building separation shall be not less than the total displacement computed at the largest hazard level considered. The intent is to avoid pounding and does not address the potential for pounding in the presence of limited moat wall clearance.

In New Zealand, recently proposed guidelines for the design of seismic isolation systems [4], provide a framework for assessing moat wall pounding. In circumstances where pounding is

deemed unavoidable, the designer must communicate this decision and its potential impacts to the client. This acknowledgment inherently limits the percentage of current code demands that the isolated building can meet, similar to how current assessment procedures determine compliance. Even though the Guidelines acknowledges the issue of pounding, it does not provide specific modeling recommendations for the contact elements nor criteria on how to address these cases. This omission leaves designers without clear guidance, potentially impacting the reliability of seismic performance assessments.

Following New Zealand guidelines, the risk of moat wall pounding can be represented utilizing a percentage of New Building Standard (%NBS) to rate the seismic performance of an existing building relative to that of a new building. Considering this approach, the findings of this dissertation suggest that the rating for an existing base isolated structure should involve two metrics: the isolation system lateral displacement capacity and the strength and ductility of the superstructure. The first metric, based on the isolation system lateral displacement, quantifies the capacity of the system to accommodate the lateral displacements. The second metric, based on superstructure strength, evaluates the structural resilience of the superstructure in the event of yielding.

The rating for the first metric, the isolation system lateral displacement, can be correlated to the exceedance of the moat wall clearance, resulting in pounding, or to bearings instability due to large displacements. The estimation of isolation system lateral displacement can be obtained using the simplified 2DOF model, which this research shows provides a reliable estimation, for demand levels up to twice the expected yielding of the superstructure. Once the lateral displacement is determined, the potential for moat wall pounding can be assessed. Moat wall pounding transfers significant inertia to the structure, increasing both accelerations and interstory

drift ratios. The effects of pounding on the superstructure can be correlated to the impact velocity. This research shows that a velocity threshold can be defined, at which the effects of pounding does not cause significant amplification of the interstory drifts beyond those expected without pounding. For this research, the threshold observed was approximately 0.5m/s, at which the pounding effects were localized mostly at the first story. Given the limited scope of models and ground motions considered in this dissertation, further studies with a larger database are recommended to verify the impact velocity threshold. This research did not examine the case where the displacement of the isolation system is limited by the bearing capacity rather than the moat wall clearance, and this needs further investigation.

The second metric, the superstructure strength, is related to the superstructure ductility and the ratio between the yield strength and the MCE lateral seismic design force. Yielding of the superstructure may occur in base-isolated buildings with increased shear resistance in the bearing or from moat wall pounding. The results of this dissertation highlight that once the superstructure yields, the superstructure performance depends on the ductility and rate of strength degradation. After the onset of yielding in systems with limited ductility, the results show a rapid increase in drifts, quickly reaching collapse limit states. Variations of 50% in the backbone parameters of the limited ductility systems do not alter their overall brittle behavior, while delaying yielding in less ductile systems is more effective to improve seismic performance. The results show that ductile systems have the potential to achieve life-safety performance up to 1.4 times the demand level expected to yield superstructure (see Incremental Dynamic Analysis Section on Chapter 3). For systems with limited ductility, this factor should be one, reflecting the dependence only on the superstructure strength. Considering the limited data and analysis used in this scope of work, the values of the factors related to the superstructure ductility should be

further investigated based on rated ductility for a particular type of building and the design overstrength.

This approach can lead to a standardized metric for evaluating the relative safety and resilience of buildings under seismic conditions. This would allow building owners and users to readily interpret building performance and make informed decisions regarding necessary improvements to the isolation system, the structure, or both.

Limitations and future research work

Several analyses were conducted to understand the implications of superstructure yielding and moat wall pounding. However, there are additional analyses that can be carried out. Some of these aspects are mentioned below:

- Inclusion of the wall flexibility and soil models to characterize their influence on the superstructure response. Their omission provides a conservative estimation of the pounding effects.
- The use of more detailed bearing models, which may capture other potential failure modes of the isolation system.
- The incorporation of bidirectional models to account for torsional effects and their influence on the moat wall pounding effects and isolation system orbital displacement.
- Comparison between full nonlinear and 2DOF models between various structural archetypes, to further validate the results obtained in this research
- A probabilistic approach on the velocity-trajectory path of the isolation system orbital displacement, that could help quantify impact velocities that have minimal effects on the superstructure deformation.

- Using representative building prototypes, refine a rating system to enhance the seismic assessment for scenarios beyond design-basis events. This approach will ensure a more accurate evaluation of building performance under extreme seismic conditions, providing a robust framework for assessing the resilience and safety of structures when subjected to forces exceeding standard design expectations. The refined rating system will help in identifying critical weaknesses and informing necessary design adjustments to improve overall seismic performance

REFERENCES

1. ASCE7-22. Minimum Design Loads and Associated Criteria for Buildings and Other Structures. 2022.
2. Christopoulos C, Filiatrault A. Principles of Passive Supplemental Damping and Seismic Isolation. Vol. 133, IUSS Press. 2006. p. 1192.
3. Masroor A, Mosqueda G. Seismic response of base isolated buildings considering pounding to moat walls. Civil, Structural and Environmental Engineering. 2012.
4. NZSEE. Guideline for the Design of Seismic Isolation Systems for Buildings. 2019;(June).
5. Ordoñez D, Foti D, Bozzo L. Comparative study of the inelastic response of base isolated buildings. Earthq Eng Struct Dyn. 2003;
6. Kikuchi, M., Black, C.J., & Aiken ID. On the response of yielding seismically isolated structures. Earthq Eng Struct Dyn. 2007;21(056):1–6.
7. Thiravechyan P, Kasai K, Morgan TA. Response of Base Isolated Structures Considering Inelastic Behavior of Superstructure. 15th World Conf Earthq Eng. 2012;9.
8. Vassiliou MF, Tsiavos A, Stojadinović B. Dynamics of inelastic base-isolated structures subjected to analytical pulse ground motions. Earthq Eng Struct Dyn. 2013;
9. Tsiavos A, Stojadinovic B, Mackie K. Dynamics of inelastic isolated bridges subjected to analytical pulse ground motions. NCEE 2014 - 10th US Natl Conf Earthq Eng Front Earthq Eng. 2014;(October 2016).
10. Bao Y, Becker TC. Inelastic response of base-isolated structures subjected to impact. Eng Struct [Internet]. 2018;171(April):86–93. Available from: <https://doi.org/10.1016/j.engstruct.2018.05.091>
11. Tsiavos A, Markić T, Schlatter D, Stojadinović B. Inelastic Response Modes of Seismically Isolated Structures: Failure of the Isolators or Damage in the Isolated Structure? 8th Int Conf Comput Methods Struct Dyn Earthq Eng Methods Struct Dyn Earthq Eng. 2021;(June):4100–10.
12. Buckle IG, Mayes RL. Seismic Isolation: History, Application, and Performance—A World View. Earthq Spectra [Internet]. 1990 May 27;6(2):161–201. Available from: <http://journals.sagepub.com/doi/10.1193/1.1585564>
13. Sasaki T, Sato E, Ryan KL, Mahin SA. NEES / E-Defense Base-Isolation Tests : Effectiveness of Friction Pendulum and Lead-Rubber Bearings Systems. 15th World Conf Earthq Eng Lisbon Port. 2012;

14. Okazaki T. NEES/E-Defense Base-Isolation Tests: Interaction of Horizontal and Vertical Response. 15th World Conf Earthq Eng. 2012;(2000).
15. Ordonez D, Foti D, Bozzo L. Comparative study of the inelastic response of base isolated buildings. *Earthq Eng Struct Dyn*. 2003;32(1):151–64.
16. Tsiavos A, Mackie KR, Vassiliou MF, Stojadinović B. Dynamics of inelastic base-isolated structures subjected to recorded ground motions. *Bull Earthq Eng*. 2017;15(4):1807–30.
17. NEHRP Consultants Joint Venture. Evaluation of the FEMA P-695 Methodology for Quantification of Building Seismic Performance Factors (NIST GCR 10-917-8) [Internet]. National Institute of Standards and Technology, 2010. Available from: <http://scholar.google.com/scholar?hl=en&btnG=Search&q=intitle:Evaluation+of+the+FEMA+P-695+Methodology+for+Quantification+of+Building+Seismic+Performance+Factors#0>
18. Wen YK. Method for Random Vibration of Hysteretic Systems. *J Eng Mech Div* [Internet]. 1976 Apr;102(2):249–63. Available from: <https://ascelibrary.org/doi/10.1061/JMCEA3.0002106>
19. ATC. Quantification of building seismic performance factors. Fema P695. 2009.
20. York K, Ryan KL. Distribution of lateral forces in base-isolated buildings considering isolation system nonlinearity. *J Earthq Eng*. 2008;12(7):1185–204.
21. Institute AC. Building code requirements for structural concrete (ACI 318-08) and commentary. 2008.
22. ASCE7-05. Minimum Design Loads and Associated Criteria for Buildings and Other Structures. 2005.
23. AISC. ANSI/AISC 341-05: Seismic Provisions for Structural Steel Buildings. 2005.
24. ASCE41-17. Seismic evaluation and retrofit of existing buildings. 2017.
25. Vamvatsikos D, Allin Cornell C. Incremental dynamic analysis. *Earthq Eng Struct Dyn*. 2002;31(3):491–514.
26. Kitayama S, Constantinou MC. Collapse performance of seismically isolated buildings designed by the procedures of ASCE/SEI 7. *Eng Struct* [Internet]. 2018;164(December 2017):243–58. Available from: <https://doi.org/10.1016/j.engstruct.2018.03.008>
27. Bustamante R, Mosqueda G, Elwood KJ. Moat Wall Pounding Analysis for a Prototype Base-Isolated Building in Wellington New Zealand. *Struct Eng Soc New Zeal*. 2021;
28. Hughes PJ, Mosqueda G. Evaluation of uniaxial contact models for moat wall pounding simulations. *Earthq Eng Struct Dyn* [Internet]. 2020 Oct 10;49(12):1197–215. Available

from: <https://onlinelibrary.wiley.com/doi/10.1002/eqe.3285>

29. Bao Y, Becker T. Three-dimensional double friction pendulum bearing model including uplift and impact behavior: Formulation and numerical example. *Eng Struct* [Internet]. 2019 Nov;199:109579. Available from: <https://linkinghub.elsevier.com/retrieve/pii/S014102961930896X>
30. ASCE7-10. Minimum Design Loads and Associated Criteria for Buildings and Other Structures [Internet]. Reston, VA: American Society of Civil Engineers; 2010. Available from: <https://ascelibrary.org/doi/book/10.1061/9780784415788>
31. ASCE7-16. Minimum Design Loads and Associated Criteria for Buildings and Other Structures. 2016.
32. Guan X, Burton H, Shokrabadi M. A database of seismic designs, nonlinear models, and seismic responses for steel moment-resisting frame buildings. *Earthq Spectra*. 2021;37(2):1199–222.
33. FEMA P-2012. Assessing Seismic Performance of Buildings with Configuration Irregularities: Calibrating Current Standards and Practices [Internet]. 2018. Available from: www.ATCouncil.org
34. PEER. OpenSees: a framework for earthquake engineering simulation. 2020.
35. Ibarra LF, Medina RA, Krawinkler H. Hysteretic models that incorporate strength and stiffness deterioration. *Earthq Eng Struct Dyn* [Internet]. 2005 Oct;34(12):1489–511. Available from: <https://onlinelibrary.wiley.com/doi/10.1002/eqe.495>
36. Naeim F, Kelly JM. Design of Seismic Isolated Structures: From Theory to Practice. John Wiley & Sons. 1999.
37. IBC. Uniform Building Code: UBC-91. 1991.
38. Makris N. Seismic isolation: Early history. *Earthq Eng Struct Dyn* [Internet]. 2019 Feb 23;48(2):269–83. Available from: <https://onlinelibrary.wiley.com/doi/10.1002/eqe.3124>
39. IBC. Uniform Building Code: UBC-88. 1988.
40. Warn GP, Ryan KL. A Review of Seismic Isolation for Buildings: Historical Development and Research Needs. *Buildings* [Internet]. 2012 Aug 3;2(3):300–25. Available from: <http://www.mdpi.com/2075-5309/2/3/300>
41. SEAOC. SEAOC Blue Book. International CODE Council; 2009.
42. ASCE7-93. Minimum Design Loads and Associated Criteria for Buildings and Other Structures. 1993.
43. IBC. Uniform Building Code: UBC-27. 1927.

44. McVitty W, Constantinou MC. Property Modification Factors for Seismic Isolators: Design Guidance for Buildings. MCEER-15-0005. 2015.
45. PEER. PEER Ground Motion Database [Internet]. 2022. Available from: <https://ngawest2.berkeley.edu/>
46. Mosqueda G, Whittaker AS, Fenves GL. Characterization and Modeling of Friction Pendulum Bearings Subjected to Multiple Components of Excitation. *J Struct Eng* [Internet]. 2004 Mar;130(3):433–42. Available from: <https://ascelibrary.org/doi/10.1061/%28ASCE%290733-9445%282004%29130%3A3%28433%29>
47. Ebisawa K, Ando K, Shibata K. Progress of a research program on seismic base isolation of nuclear components. *Nucl Eng Des*. 2000 May 2;198(1):61–74.
48. JAERI. Characteristics and Dynamic Response Analysis of 3-D Component Base Isolation System Using Ball Bearings and Air Springs. 2000.
49. Choun YS, Kim MK, Ohtori Y. The use of a base isolation system for an emergency diesel generator to reduce the core damage frequency caused by a seismic event. *SMiRT*. 2007;19:1–8.
50. Furukawa S, Sato E, Shi Y, Becker T, Nakashima M. Full-scale shaking table test of a base-isolated medical facility subjected to vertical motions. *Earthq Eng Struct Dyn*. 2013;42(13):1931–49.
51. Najafijozani M, Becker TC, Konstantinidis D. Evaluating adaptive vertical seismic isolation for equipment in nuclear power plants. *Nucl Eng Des*. 2020;358.
52. Kumar M, Whittaker AS, Constantinou MC. Seismic isolation of nuclear power plants. MCEER-15-0008. University at Buffalo, USA. 2015.
53. Medel-Vera C, Ji T. Seismic protection technology for nuclear power plants: A systematic review [Internet]. Vol. 52, *Journal of Nuclear Science and Technology*. Taylor & Francis; 2015. p. 607–32. Available from: <http://dx.doi.org/10.1080/00223131.2014.980347>
54. Tsutsumi H, Ebisawa K, Suzuki M, Yamada H, Fujimoto S. Development of the Methodology for Evaluating the Probability of Failure of Seismic Isolation System for Nuclear Components. 2007.
55. Inoue K, Fushimi M, Moro S, Morishita M, Kitamura S, Fujita T. Development of Three-Dimensional Seismic Isolation System for Next Generation Nuclear Power Plant. In: 13th World Conference on Earthquake Engineering. 2004.
56. Suhara J, Tamura T, Ohta K, Okada Y, Moro S. Research on 3-D Base Isolation System Applied to New Power Reactor 3-D Seismic Isolation Device with Rolling Seal Type Air Spring : Part 1. In: Transactions of the 17 th International Conference on Structural Mechanics in Reactor Technology (SMiRT 17). 2003. p. 1–6.

57. Nawrotzki P, Siepe D. Structural challenges of power plants in high seismic areas. In: Second European Conference on Earthquake Engineering and Seismology, Istanbul, Aug. 2014. p. 25–9.
58. Choun Y sun, Kim M kyu, Seo J moon. Seismic and Vibration Isolation of an Emergency Diesel Generator by Using a Spring-Viscous Damper System. 2006;8.
59. Kančev D, Duchac A, European Commission. Joint Research Centre. Institute for Energy and Transport. European clearinghouse : events related to emergency diesel generators. Publications Office; 2013.
60. Gregory N, Simon R, Branden D, Kermin C. Practical Implementation of ASCE-41 and NLRHA Procedures for the Design of the LLUMC Replacement Hospital. 2017 Seaoc Conf Proc. 2017;1–8.
61. Tomizawa T, Takahashi O, Suhara J, Okada K, Tsuyuki Y, Fujita T. Vibration test in a building named “ Chisuikan” using three-dimensional seismic isolation system. In: ISEC 2013 - 7th International Structural Engineering and Construction Conference: New Developments in Structural Engineering and Construction. 2013. p. 791–6.
62. Budnitz RJ. Current status of methodologies for seismic probabilistic safety analysis. Reliab Eng Syst Saf. 1998;62(1–2):71–88.
63. DIS. DIS 3D Isolation System [Internet]. Available from: http://dis-inc.com/pdf_files/DIS_3D_Isolation_Systems.pdf
64. KAERI. Generation of Input Ground Acceleration for Analysis of Nuclear Plant Structures Reflecting Site Characteristics in Korea. 2018.
65. Choi IK, Nakajima M, Choun YS, Ohtori Y. Development of the site-specific uniform hazard spectra for Korean nuclear power plant sites. Nucl Eng Des. 2009;239(4):790–9.
66. ASCE43-05. Seismic Design Criteria for Structures, System , and Components in Nuclear Facilities. 2006.
67. U.S. Nuclear Regulatory Commission. NUREG/CR-4334 - An approach to the quantification of seismic margins in nuclear power plants. 1985;
68. U.S. Nuclear Regulatory Commission. Risk Assessment Standardization Project (RASP) Handbook -External Events: Seismic Event Modeling and Seismic Risk Quantification Seismic Event Modeling and Seismic Risk Quantification. 2017.
69. Liu W, Aziz TS. Seismic Capacity of Emergency Power Supply Diesel Generator Set for Candu 6. 2007;1–8.
70. Jeong YS, Baek ER, Jeon BG, Chang SJ, Park DU. Seismic performance of emergency diesel generator for high frequency motions. Nucl Eng Technol. 2019;51(5):1470–6.

71. Jeon B gyu, Choi H suk, Hahm D gi, Kim N sik. Seismic Fragility Estimation of Piping System of Base-. 2015;(2007).
72. JNES. Proposal of Technical Review Guidelines for Structures with Seismic Isolation. 2013.
73. Touboul F, Sollogoub P, Blay N. Seismic behaviour of piping systems with and without defects: Experimental and numerical evaluations. Nucl Eng Des. 1999;192(2):243–60.
74. Zhang T, Brust FW, Wilkowski G, Shim DJ, Nie J, Hofmayer CH, Ali SA. Analysis of JNES seismic tests on degraded piping. Vol. 8, American Society of Mechanical Engineers, Pressure Vessels and Piping Division (Publication) PVP. 2010.
75. Choun YS, Kim MK. A performance assessment of a base isolation system for an emergency diesel generator in a nuclear power plant. Nucl Eng Technol. 2008;40(4):285–98.
76. Kawakami, S.; Hara, F.; Shibata, H.; Ohno, T.; Horimizu, Y.; Ichimashi, I.; Uchiyama, Y.; Niino, T.; Takayanagi, M.; Kajimura, Y.; Maeda K. Seismic Proving Test of Emergency Diesel Generator System. SMiRT. 1993;
77. Kim MK, Choun YS, Seo JM. Demonstration of the vibration control performance of coil spring-viscous damper systems by measuring the vibration of an emergency diesel generator. JVC/Journal Vib Control. 2010;16(2):207–29.
78. Fema. FEMA P-751: 2009 NEHRP Recommended Seismic Provisions: Design Examples. 2012;(September).
79. Kelly JM, Konstantinidis DA. Mechanics of Rubber Bearings for Seismic and Vibration Isolation. Mechanics of Rubber Bearings for Seismic and Vibration Isolation. 2011.
80. Kafali C, Grigoriu M. Seismic fragility analysis: Application to simple linear and nonlinear systems. Earthq Eng Struct Dyn. 2007;(36):1885–900.
81. Zhao C, Yu N, Peng T. Probabilistic seismic fragility assessment of isolated nuclear power plant structure using IDA and MSA methods. Structures. 2021;34(March):1300–11.
82. Pang R, Xu B, Zhou Y, Song L. Seismic time-history response and system reliability analysis of slopes considering uncertainty of multi-parameters and earthquake excitations. Comput Geotech [Internet]. 2021;136(September 2020):104245. Available from: <https://doi.org/10.1016/j.compgeo.2021.104245>
83. Jeong YS, Baek ER, Jeon BG, Chang SJ, Park DU. Seismic performance of emergency diesel generator for high frequency motions. Nucl Eng Technol. 2019 Aug 1;51(5):1470–6.
84. Laboratory LLN. Seismic Margin Review of the Maine Yankee Atomic Power Station. Vol. 1. 1987.

85. Shang Q, Wang T, Li J. Seismic fragility of flexible pipeline connections in a base isolated medical building. *Earthq Eng Eng Vib*. 2019;18(4):903–16.